

ISTANBUL TECHNICAL UNIVERSITY ★ GRADUATE SCHOOL OF SCIENCE
ENGINEERING AND TECHNOLOGY

**THE COMPARISON OF EFFECTS OF TORREFACTION AND
CARBONIZATION TREATMENTS ON BIOMASS**

M.Sc. THESIS by

Ezgi BİLGİÇ

Department of Chemical Engineering
Chemical Engineering Programme

JUNE 2014

ISTANBUL TECHNICAL UNIVERSITY ★ GRADUATE SCHOOL OF SCIENCE
ENGINEERING AND TECHNOLOGY

**THE COMPARISON OF EFFECTS OF TORREFACTION AND
CARBONIZATION TREATMENTS ON BIOMASS**

M.Sc. THESIS

Ezgi BİLGİÇ

(506121014)

Department of Chemical Engineering

Chemical Engineering Programme

Thesis Advisor: Prof. Dr. Serdar YAMAN

JUNE 2014

İSTANBUL TEKNİK ÜNİVERSİTESİ ★ FEN BİLİMLERİ ENSTİTÜSÜ

**TORREFAKSİYON VE KARBONİZASYON İŞLEMLERİNİN BİYOKÜTLEYE
ETKİLERİNİN KARŞILAŞTIRILMASI**

YÜKSEK LİSANS TEZİ

**Ezgi BİLGİÇ
(506121014)**

**Kimya Mühendisliği Ana Bilim Dalı
Kimya Mühendisliği Programı**

Tez Danışmanı: Prof. Dr. Serdar YAMAN

HAZİRAN 2014

Ezgi Bilgiç, a M.Sc. student of ITU **Graduate School of Science Engineering and Technology** student ID **506121014**, successfully defended the **thesis/dissertation** entitled “**THE COMPARISON OF EFFECTS OF TORREFACTION AND CARBONIZATION TREATMENTS ON BIOMASS**”, which she prepared after fulfilling the requirements specified in the associated legislations, before the jury whose signatures are below.

Thesis Advisor : **Prof. Dr. Serdar YAMAN**

Istanbul Technical University

Jury Members : **Prof. Dr. Ayşegül MERİÇBOYU**

Istanbul Technical University

Assist. Prof. Dr. Didem ÖZÇİMEN

Yildiz Technical University

Date of Submission : 5 May 2014

Date of Defense : 2 June 2014

To my family,

FOREWORD

I would like to express my deepest gratitude to my thesis advisor Prof. Dr. Serdar YAMAN for giving a chance to study in his great laboratory group and for his excellent guidance, caring, patience, and endless contribution in the process of making this study.

I would also like to present my special thanks to Prof. Dr. Hanzade HAYKIRI AÇMA for her great guidance, help and support during this thesis.

I would like to thank to Ayşen AKTÜRK for her great laboratory guidance, friendship and providing me with an excellent atmosphere for doing research.

I would also like to thank to Dr. Hasan GÖKÇE for XRD, SEM and particle size analyzes, and valuable help throughout the experimental studies.

I would also like to thank to Gizem Muazzez YILMAZ for her great friendship and endless support during this study.

Son olarak ve en önemlisi, hayatta ne yaparsam yapayım beni her zaman destekleyen, cesaretlendiren, sonsuz sabır, hoşgörü ve sevgi gösteren aileme teşekkür etmek istiyorum (Finally, and the most importantly, I would like to thank my parents for their endless support, encouragement, patience, tolerance and love whatever I do in the life).

June 2014

Ezgi BİLGİÇ
Chemical Engineer

TABLE OF CONTENTS

	<u>Page</u>
FOREWORD	IX
ABBREVIATIONS	XIII
LIST OF TABLES	XV
LIST OF FIGURES	XVII
1. INTRODUCTION	1
1.1 Energy Resources in the World.....	1
1.2 Biomass.....	2
1.2.1 Biomass types	6
1.2.2 Biomass advantages and disadvantages	6
1.2.3 Biomass properties	7
1.2.4 Structure of biomass.....	10
1.2.5 Biomass potential in Turkey.....	13
1.3 Physical Processes	15
1.3.1 Pelletizing and briquetting.....	15
1.3.2 Dewatering and drying	16
1.4 Thermal Pretreatment Processes	17
1.4.1 Torrefaction	17
1.4.2 Pyrolysis	20
1.4.3 Gasification.....	22
1.4.4 Carbonization.....	24
1.5 Biomass Pyrolysis Kinetics.....	26
1.5.1 Kinetic expressions for biomass thermal decomposition.....	26
1.5.2 Coats-Redfern method.....	28
2. MATERIALS AND METHODS	31
2.1 Experimental Studies	31
2.2 Sample Preparation.....	32
2.3 Macromolecular Ingredients Analysis.....	32
2.4 The Thermal Analyses (TGA, DTG, DTA, DSC)	32

2.5 The Torrefaction and Carbonization Experiments in a Horizontal Tube Furnace	33
2.6 Characterization of Samples	34
2.6.1 Proximate analysis	34
2.6.2 Calorific value analysis	34
2.6.3 Particle size analysis	35
2.6.4 Scanning electron microscopy (SEM) analyses	35
2.6.5 Ultimate analysis	36
2.6.6 X-ray diffraction (XRD) analysis	37
2.6.7 Fourier transform infrared (FTIR) spectroscopy analysis	37
3. RESULTS AND DISCUSSION	39
3.1 Characterization of Main Samples	39
3.1.1 Proximate analysis results	39
3.1.2 Macromolecular analysis results	41
3.2 Effects of Torrefaction and Carbonization Processes	41
3.2.1 Effects on sample characteristics and fuel quality	41
3.2.2 Ultimate analysis results	45
3.2.3 Effects on burning characteristics	46
3.3 Particle Size Analysis Results	69
3.4 SEM Results	70
3.5 XRD Results	73
3.6 FTIR Analysis Results	74
3.7 Kinetic Analysis of Burning Profiles	79
4. CONCLUSION AND RECOMMENDATIONS	91
REFERENCES	95
CURRICULUM VITAE	103

ABBREVIATIONS

A : Frequency factor (s^{-1})

α : Degree of conversion

ASTM : American Society for Testing and Materials

BET : Brauner-Emmet-Teller

β : heating rate ($^{\circ}C s^{-1}$)

Btu : British thermal unit

CAM : Crassulacean Acid Metabolism

db : Dry basis

DTA : Differential Thermal Analysis

DTG : Derivative Thermogravimetry

DSC : Differential Scanning Calorimetry

E_a : Apparent activation energy ($kJ mol^{-1}$)

$f(\alpha)$: Reaction model (function expressing the dependence of the reaction rate on the conversion)

FTIR : Fluorescence Transform Infrared

$g(\alpha)$: Integrated reaction model

HHV : Higher Heating Value

HS : Hazelnut shells

IEA : International Energy Agency

k : Reaction rate constant (s^{-1})

$k(T)$: Temperature-dependent rate constant (s^{-1})

Mtoe : Million Tonnes of Oil Equivalent

MWm : MegaWatt Mechanic

n : Reaction order

R : Universal gas constant ($8.3144 \times 10^{-3} kJ mol^{-1} K^{-1}$)

SEM : Scanning Electron Microscopy

SSS : Sunflower seed shells

t : Time (s)

T : Absolute temperature (K)

TG : Thermogravimetry

TGA : Thermogravimetric Analysis

UNFCCC : United Nations Framework Convention on Climate Change

v : Volatile mass at time t

w : substrate mass at time t

XRD : X-ray Diffraction

LIST OF TABLES

	<u>Page</u>
Table 1.1 : The changes in various types of plant weight for two CO ₂ concentrations.....	4
Table 1.2 : The biomass sources.....	5
Table 1.3 : The biomass groups.....	6
Table 1.4 : The heats of combustion of different substances	9
Table 1.5 : The renewable energy supply in Turkey.....	14
Table 1.6 : The potential agricultural plantation and residues in Turkey	15
Table 1.7 : The biomass characteristics and improvements through torrefaction. ..	18
Table 1.8 : The properties of various kinds of solid fuels.....	19
Table 1.9 : Different types of pyrolysis and conditions	21
Table 1.10 : The syngas composition under different gasifying agents.....	23
Table 1.11 : Proximate analysis of char produced from bagasse (moisture free basis)	25
Table 1.12 : The most common reaction models in solid state reactions	28
Table 3.1 : The proximate analysis and HHV results.	40
Table 3.2 : Macromolecular analysis results of the main samples (on dry basis). ..	41
Table 3.3 : Proximate analysis and HHV results on dry basis.	44
Table 3.4 : Ultimate analysis results (on dry basis).....	45
Table 3.5 : The results from DTG and DTA of the main samples under dry air.....	50
Table 3.6 : The results from DTG and DTA of the main samples with pure oxygen.	54
Table 3.7 : The results from DTG and DTA of the torrefied biochars with dry air.....	58
Table 3.8 : The results from DTG and DTA of torrefied biochars under pure oxygen.....	62
Table 3.9 : The results from DTG and DTA of carbonized biochars under dry air.	65
Table 3.10 : The DTG and DTA results of carbonized biochars under pure oxygen.	69
Table 3.11 : The results of specific surface area and mean diameter.	69
Table 3.12 : The mineral phases.....	73
Table 3.13 : Wavenumbers and corresponding functional groups	75
Table 3.14 : The activation energies and frequency factors of sunflower seed shells.	80
Table 3.15 : The activation energies and frequency factors of torrefied sunflower seed shells biochar at 300 °C.....	82
Table 3.16 : The activation energies and frequency factors of carbonized sunflower seed shells biochar at 600 °C.....	83

Table 3.17 : The activation energies and frequency factors of hazelnut shells.....	85
Table 3.18 : The activation energies and frequency factors of torrefied hazelnut shells biochar at 300 °C.	87
Table 3.19 : The activation energies and frequency factors of carbonized hazelnut shells biochar at 600 °C.	88

LIST OF FIGURES

	<u>Page</u>
Figure 1.1 : The world energy consumption between 1990 and 2040.....	1
Figure 1.2 : Van Krevelen diagram for various solid fuels.....	8
Figure 1.3 : The structure of cellulose	11
Figure 1.4 : Hemicellulose structure.....	11
Figure 1.5 : The structure of monolignols and subunits of lignin	12
Figure 1.6 : The structure of lignin	13
Figure 1.7 : Pyrolysis in a biomass particle	20
Figure 2.1 : The flowchart of experimental studies.....	31
Figure 2.2 : TA instruments, model SDT Q600.....	33
Figure 2.3 : Horizontal tube furnace.....	34
Figure 2.4 : IKA C2000 Basic Calorimeter Bomb.....	35
Figure 2.5 : Malvern Instruments™ Mastersizer 2000 particle sizing instrument.	35
Figure 2.6 : Leco TruSpec® CHN model elemental analysis instrument.....	36
Figure 3.1 : The proximate analysis TGA profile of SSS.....	39
Figure 3.2 : The proximate analysis TGA profile of HS.....	40
Figure 3.3 : The proximate analysis TGA profile of SSS biochar at 300 °C.....	42
Figure 3.4 : The proximate analysis TGA profile of HS biochar at 300 °C.....	42
Figure 3.5 : The proximate analysis TGA profile of SSS biochar at 600 °C.....	43
Figure 3.6 : The proximate analysis TGA profile of HS biochar at 600 °C.....	43
Figure 3.7 : The burning DTG profile of SSS main sample under dry air.....	46
Figure 3.8 : The burning DTA profile of SSS main sample under dry air.....	47
Figure 3.9 : The burning DSC profile of SSS main sample under dry air.....	47
Figure 3.10 : The burning DTG profile of HS main sample under dry air.....	48
Figure 3.11 : The burning DTA profile of HS main sample under dry air.....	49
Figure 3.12 : The burning DSC profile of HS main sample under dry air.....	50
Figure 3.13 : The burning DTG curve of SSS under pure oxygen.....	51
Figure 3.14 : The burning DTA curve of SSS under pure oxygen condition.....	51
Figure 3.15 : The burning DSC curve of SSS under pure oxygen condition.....	52
Figure 3.16 : The burning DTG profile of HS under pure oxygen condition.....	52
Figure 3.17 : The burning DTA profile of HS under pure oxygen condition.....	53
Figure 3.18 : The burning DSC profile of HS under pure oxygen condition.....	54
Figure 3.19 : The burning DTG curve of the torrefied SSS under dry air.....	55
Figure 3.20 : The burning DTA curve of the torrefied SSS under dry air.....	56
Figure 3.21 : The burning DSC curve of the torrefied SSS under dry air.....	56
Figure 3.22 : The burning DTG curve of the torrefied HS under dry air condition.....	57

Figure 3.23 : The burning DTA curve of the torrefied HS under dry air.	57
Figure 3.24 : The burning DSC profile of the torrefied HS under dry air.	58
Figure 3.25 : The burning DTG profile of torrefied SSS under pure oxygen.	59
Figure 3.26 : The burning DTA profile of torrefied SSS under pure oxygen.	59
Figure 3.27 : The burning DSC profile of torrefied SSS under pure oxygen.	60
Figure 3.28 : The burning DTG profile of torrefied HS under pure oxygen.	60
Figure 3.29 : The burning DTA profile of torrefied HS under pure oxygen.	61
Figure 3.30 : The burning DSC profile of biochar from HS under pure oxygen.	61
Figure 3.31 : The burning DTG profile of carbonized SSS under dry air.	62
Figure 3.32 : The burning DTA profile of carbonized SSS under dry air.	63
Figure 3.33 : The burning DSC profile of carbonized SSS under dry air.	63
Figure 3.34 : The burning DTG profile of carbonized HS under dry air.	64
Figure 3.35 : The burning DTA profile of carbonized HS under dry air.	64
Figure 3.36 : The burning DSC profile of carbonized HS under dry air.	65
Figure 3.37 : The burning DTG curve of carbonized SSS with pure oxygen.	66
Figure 3.38 : The burning DTA curve of carbonized SSS with pure oxygen.	66
Figure 3.39 : The burning DSC curve of carbonized SSS with pure oxygen.	67
Figure 3.40 : The burning DTG profile of carbonized HS under pure oxygen.	67
Figure 3.41 : The burning DTA profile of carbonized HS under pure oxygen.	68
Figure 3.42 : The burning DSC profile of carbonized HS under pure oxygen.	68
Figure 3.43 : SEM micrographs of the samples derived from sunflower seed shells.	71
Figure 3.44 : SEM micrographs of the samples derived from hazelnut shells.	72
Figure 3.45 : The FTIR spectra for sunflower seed shell main sample and its derivatives.	76
Figure 3.46 : The FTIR spectra for hazelnut seed shell main sample and its derivatives.	77

THE COMPARISON OF EFFECTS OF TORREFACTION AND CARBONIZATION TREATMENTS ON BIOMASS

SUMMARY

The sources of fossil fuels have been gradually consumed; therefore, biomass which has a great potential has been used as a renewable energy source in the world. The biomass sources can be classified as agricultural, forestry, municipal solid waste, energy crops and biological waste. The total primary use of biomass energy was around 10% of total primary energy in the world. The biomass is an important renewable energy source due to the largest energy source in the world, having great potential, low ash content and zero CO₂ effect. In contrast, biomass has some drawbacks compared to fossil fuels such as low calorific value and density, high moisture and volatile matter contents, high oxygen to carbon ratio. Some pretreatments are carried out to biomass to produce higher quality fuels by minimizing these undesirable properties. Performed treatments are generally thermal such as torrefaction, pyrolysis and carbonization. As a consequence of these treatments, there is a decrease in the moisture and volatile matter contents of biomass, a considerable fall in oxygen to carbon ratio and an increase in the calorific value of biomass.

Turkey depends on outside sources in spite of having a great unused biomass potential. In this study, sunflower seed shells and hazelnut shells in which grown our country were evaluated as a waste biomass source. The purpose of this study is improvement of their physical and chemical properties to produce higher quality solid fuels. From this point of view, each biomass sample was subjected to thermal decomposition in a horizontal tube furnace at 300 °C and 600 °C under nitrogen atmosphere to perform torrefaction and carbonization thermal treatments, respectively. The thermal decomposition of biomass was happened during these experiments due to the nitrogen atmosphere condition. After these treatments, produced biochars were compared with untreated biomass samples in different ways. The changes of biomass properties of interest were determined with regard to both of thermal treatments. In this study, the effects of torrefaction and carbonization treatments on physical and chemical characteristics of fuel were investigated with regard to proximate analysis (moisture, volatile matter, ash and fixed carbon content), ultimate analysis (C, H, N, S, O), higher heating value, macromolecular component analysis (holocellulose, lignin and extractive-free substance), functional group analysis via FTIR technique, electron microscope images via SEM technique, mineralogical structure via XRD technique. In addition, particle size analysis was carried out to determine physical structures of samples. The effect of thermal treatments on the burning mechanism of torrefied and carbonized samples as compared with original samples. From this point of view, the kinetic study was done with regard to TGA and DTG profiles which obtained from dry air and pure oxygen burning conditions in the thermal analysis system.

TORREFAKSİYON VE KARBONİZASYON İŞLEMLERİNİN BİYOKÜTLEYE ETKİLERİNİN KARŞILAŞTIRILMASI

ÖZET

Dünyadaki enerji kaynakları yenilenebilir (güneş ışığı, hidrolik güç, jeotermal, dalga enerjisi ve biyokütle) ve yenilenemez (kömür, petrol, doğalgaz ve nükleer enerji) olmaz üzere ikiye ayrılır. Dünyadaki toplam enerji tüketiminin yaklaşık %80'inin 2040 yılına kadar fosil yakıtlardan sağlanacağı tahmin edilmektedir. Bu nedenle dünyada fosil enerji kaynakları hızla tükenmektedir. Gelişmiş ülkeler, büyük bir potansiyele sahip olan biyokütleyle yönelerek, alternatif yenilenebilir enerji kaynağı olarak kullanmaya başlamışlardır. Bundan dolayı biyokütle günümüzde giderek artan bir öneme sahiptir.

Biyokütle kaynakları; tarımsal, ormansal ve kentsel atıklar, endüstriyel atıklar, enerji bitkileri ve biyolojik atıklar olmak üzere sınıflandırılabilir. Dünyada toplam kullanılan birincil enerjinin %10'u biyokütleden sağlanmaktadır. Biyokütle; her yerde kolayca bulunabilmesi, büyük bir potansiyele sahip olması, karbondioksit emisyonu açısından nötral bir yakıt olması, kömüre göre daha düşük kül, kükürt ve azot içeriğine sahip olması, atık biyokütlenin kullanılabilmesinden dolayı ucuz enerji kaynağı gibi özelliklerinden ötürü önemli bir yenilenebilir enerji kaynağı durumundadır. Ancak, biyokütlenin düşük ısıl değer, yüksek nem ve uçucu madde içerikleri, düşük yoğunluğu ve yüksek oksijen/karbon oranı nedeniyle kömür gibi fosil yakıtlara göre dezavantajları söz konusudur. Bu olumsuzlukları en aza indirmek amacıyla biyokütleyle bir takım işlemler uygulanarak daha kaliteli yakıtların elde edilmesine çalışılmaktadır. Uygulanan yöntemler genellikle torrefaksiyon, piroliz veya karbonizasyon gibi termal yöntemlerdir. Bu yöntemlerin uygulanması sonucunda biyokütlenin nem ve uçucu madde içerikleri azalmakta, oksijen/karbon oranı önemli ölçüde düşmekte ve ısıl değeri yükselmektedir. Ayrıca biyokütlenin temel bileşenleri hemiselüloz, selüloz ve lignindir. Bu nedenle uygulanan termal işlemlerin çalışma sıcaklığı aralığı bu bileşenlerin bozunma sıcaklıkları göz önünde bulundurularak seçilmelidir.

Torrefaksiyon, biyokütleden daha yüksek kaliteli yakıt üretilmesini sağlayan termal bir ön işlemdir. Temel amacı; biyokütlerdeki oksijeni uzaklaştırarak içeriğindeki karbon oranını arttırmaktır. Bu işlem 200-300 °C sıcaklıkları arasında düşük ısıtma hızında ve inert gaz atmosferi altında uygulanmaktadır. Torrefaksiyon işlemi sonucunda ana kütlein %70'i katı ürün olarak geriye kalırken %90'ından fazla başlangıçtaki enerjiyi içerir. Torrefaksiyon işlemi biyokütlenin bazı özelliklerini geliştirdiği için termal işlemler arasında giderek önemi artmaktadır. Geliştirilen özellikler arasında sabit karbon oranının artması, daha yüksek ısıl değere sahip ürün elde edilmesi, hidrofilik özelliğinin azalması, göreceli olarak daha homojen karakterli yakıt olması, oksijen ve uçucu bileşen içeriklerinin azalmasından dolayı yakma işlemi sırasında daha az emisyon üretmesi, daha kolay öğütülebilmesi (torrefaksiyon işlemi

sırasında lifli yapıların giderek bozunması) ve düşük nem içeriğinden dolayı biyobozunmaya uğramaması gibi özellikler yer almaktadır.

Karbonizasyon ise katı yakıttan uçucu bileşenleri (CO, CO₂), hafif hidrokarbonları ve hidrojeni reaksiyona girmeyen bir gaz atmosferi altında uzaklaştırarak içeriğindeki karbon oranını arttıran bir termal işlemdir. Elde edilen ürüne yarı kok denilir. Düşük ısıtma hızları, uzun bekletme süresi ve düşük son sıcaklık elde edilen yarı kok miktarını arttırmaktadır. Karbonizasyon sürecinde biyokütlenin ana yapısını oluşturan hemiselüloz, selüloz ve lignin yapısı sırasıyla bozunmaya uğrar. Üretilen yarı kok temel olarak ligninin bozunmasından meydana gelmektedir. Bu nedenle uygulanacak karbonizasyon işleminde ligninin bozunma özelliklerine dikkat edilmelidir.

Türkiye’de yenilenebilir enerji kaynağı olarak rüzgar gücü, hidrolik güç ve biyokütle kullanılmaktadır. Ülkemiz enerjide dışa bağımlı olup, kullanılmayan çok büyük bir biyokütle potansiyeline sahiptir. Biyokütle atıkları arasında ormansal, endüstriyel ve tarımsal atıklar genel olarak kullanılmaktadır. Ülkemizde ayçekirdeği, pamuk, fındık, muz ve zeytin atığı tarımsal atıklar arasında çok büyük bir potansiyele sahiptir. Fındık yaygın olarak Doğu Karadeniz Bölgesi’nde üretilmektedir. Bunun dışında, ayçekirdeği tarımı daha çok Trakya-Marmara Bölgesi’nde yapılmaktadır. Bu nedenle, çalışmada ülkemizde yetiştirilen ayçekirdeği ve fındık kabuklarının atık biyokütle kaynağı olarak değerlendirilmesi planlanmıştır. Bu çalışmanın amacı söz konusu biyokütlelerin fiziksel ve kimyasal özelliklerinin geliştirilerek yüksek kaliteli katı yakıt üretmektir. Bu amaçla, her bir biyokütle örneğine yatay boru fırında, azot gazı atmosferi altında 300 °C’de torrefaksiyon ve 600 °C’de karbonizasyon işlemleri uygulandı. Bu deneyler azot atmosferi altında yapıldığı için biyokütlelerde termal bozunma meydana gelmektedir. Bu işlemler sonunda ele geçen yarı koklar (char yapıları) işlem görmemiş biyokütle ile çeşitli açılardan karşılaştırılmıştır. Uygulanan her iki termal işlemin biyokütle özelliklerinde meydana getireceği değişimler belirlenmiştir.

Bu çalışmada, her bir ana numuneye ve yarı koka kısa analiz uygulanmıştır. Bunun sonucunda, nem, uçucu madde, kül ve sabit karbon içerikleri hesaplanarak uygulanan termal işlemlerle ilgili karşılaştırmalar yapılmıştır. Bu işlemler sonucunda elde edilen yarı kokların sabit karbon/uçucu bileşen oranı arttırılarak kömürün özelliklerine yaklaştığı görülmüştür. Ana biyokütle örneklerinin ve yarıkokların bozunma özelliklerini belirleyebilmek için termal işlemler uygulanmıştır. Termal analiz sisteminde her bir örnek kuru hava ve saf oksijen ortamlarında ayrı ayrı yakılmıştır. Elde edilen TGA, DTG, DTA ve DSC profillerine göre yanma özelliklerine karar verilmiştir. TGA profiline bakılarak her bir örneğin stokiyometrik bozunması ve reaksiyonun gerçekleştiği sıcaklık aralığı belirlenmiştir. DTG profilinden maksimum bozunma hızı ve buna bağlı olarak gerçekleştiği sıcaklık bulunmuştur. DTA grafiklerindeki pik alanlarından meydana gelen entalpi değişimlerine bakılmıştır. DSC profillerinden ise faz geçişlerine bağlı olarak ısı akışlarına bakılarak endotermik ya da ekzotermik karakter gösteren bölgeler belirlenmiştir. Bundan dolayı, ana biyokütle örnekleri ile yarı kokların kuru hava ve oksijen gazları altında yanma özelliklerine karar verilmiştir.

Her bir işlem görmemiş ana numuneye ve üretilen yarı koka elementel analiz uygulanmıştır. Bu analiz sonuçlarına göre C, H, N, S ve O içerikleri belirlenmiştir. Böylece, orijinal numune ve yarı koklar yakıldıklarında çevreye verecekleri emisyonların içeriği belirlenebilmektedir. Bunun dışında, üst ısıl değer analizi yapılarak elde edilen sonuçlardan içerdikleri enerjinin ne kadar arttırıldığı

incelenmiştir. ASTM standartları göz önünde bulundurularak yapılan makromoleküler bileşen analizleriyle işlem görmemiş biyokütlelerin holoselüloz (toplam hemiselüloz ve selüloz içeriği), lignin ve ekstraktif madde oranları belirlenmiştir. Holoselüloz içerdiği zayıf eter bağları nedeniyle lignine göre daha reaktif bir karaktere sahiptir. Bunun sonucunda daha yüksek holoselüloz/lignin oranına sahip olan ayçekirdeğinin daha reaktif özellik gösterdiğine karar verilmiştir.

Yapılan termal analiz işlemlerinden elde edilen TGA ve DTG grafikleri de bu sonucu desteklemektedir. Her bir ana numune, yarı kok ve makromoleküler bileşenine fonksiyonel grup analizi FTIR tekniği kullanılarak yapılmıştır. Böylece, yapılarındaki kimyasal bağlara karar verilmiştir. Bunun dışında, elektron mikroskop görüntüleri, SEM tekniği ile elde edilerek her bir numunenin fiziksel özelliklerinin nasıl olduğuna karar verilmiştir. Bu analiz sonucuna göre torrefaksiyon ve karbonizasyon işlemleri sonucunda elde edilen yarı koklarda daha fazla parlak bölgeler bulunmuştur. Bunun nedeni, termal işlemler sırasında uçucu bileşenlerin giderek azalarak inorganik bileşen içeren külün oranının artmasıdır. Ayrıca, mineralojik yapıları XRD tekniği ile belirlenmiştir. Literatür araştırmasına göre biyokütle temel olarak silisyum bileşenlerinden oluşmaktadır. Yapılan XRD analizine göre termal işlem görmemiş ayçekirdeği ve fındık kabuklarının silisyum içerdiği belirlenerek literatür verisi ile uygunluk gösterdiği belirlenmiştir. Ayrıca fındık kabuğu ana numunesi potasyum bileşenlerini içermektedir. Literatürde potasyum bileşenlerinin külün ergime sıcaklığını düşürerek termal işlemler sırasında cüruf oluşturma ve çeşitli kirlenmelere sebep olacağı bilgisi yer almaktadır. Bu nedenle, fındık kabuğu biyokütle kaynağı olarak kullanıldığı zaman uygulanacak termal işlemler bu özelliğine dikkat edilerek yapılmalıdır. Her bir numuneye partikül boyut analizleri uygulanarak özgül yüzey alanları ve ortalama çapları bulunarak fiziksel yapısına karar verilmiştir. Holoselülozun en yüksek özgül yüzey alanına ve en küçük ortalama çapa sahip olduğu görülmüştür. Ligninin ise bunun tersi bir fiziksel yapıya sahip olduğu belirlenmiştir. Böylece yapılan boyut analizleri holoselülozun lignine göre daha reaktif bir karaktere sahip olması bilgisini desteklemektedir.

Biyokütlelerin ve elde edilen yarı kokların yanma kinetiği analizi TGA ve DTG profilleri kullanılarak yapılmıştır. Bu amaçla reaksiyon merteye, difüzyon, faz sınır kontrolü tepkimesi ve çekirdeklenme olmak üzere dört farklı reaksiyon modeli uygulanmıştır. DTG profillerine göre ayçekirdeği kabuğu ve fındık kabuğu ana numuneleri ile torrefaksiyon sonucu elde edilen yarı koklarda iki farklı yanma bölgesi görülmüştür. Bunlardan birinci bölge, pirolitik bozunma ve ardından uçucu bileşenlerin homojen yanma reaksiyonunu göstermektedir. İkinci bölge ise, uçucu bileşenlerin yanmasından sonra geriye kalan gözenekli katının heterojen fazda yanmasını belirtmektedir. Bu nedenle, kinetik çalışma sırasında bu iki bölge ayrı ayrı göz önünde bulundurularak gerekli hesaplamalar yapılmıştır. Yapılan kinetik çalışmadan her bir ana biyokütle ve yarıkok örnekleri için kinetik değişkenler (aktivasyon enerjisi (E_a) ve frekans çarpanı (A)), Coats-Redfern integrasyon yöntemiyle hesaplanmıştır. Elde edilen grafikler sonucunda, birinci merteye reaksiyon kinetiği, 3-D Ginstling-Brounshtein difüzyon modeli ve faz sınır kontrolü tepkimesi (etkileşim geometrisi küresel simetride) reaksiyon modellerinin en uygun olduğuna karar verilmiştir. En yüksek aktivasyon enerjisi 3-D Ginstling-Brounshtein difüzyon modeli kullanılarak hesaplanmıştır. Bunun nedeni oksijen gözenekli yapıya doğru transfer olurken difüzyon ve kütle transferi gibi sorunlarla karşılaşmasıdır. Literatürde birinci merteye reaksiyon modelinin genel olarak biyokütlelerin yanma kinetiğine uygunluğu yer almaktadır. Bu çalışma aynı zamanda bu bilgiyi de desteklemektedir.

1. INTRODUCTION

1.1 Energy Resources in the World

According to World Energy Council, the energy resources are divided into renewable (hydro power, wind, solar power, geothermal, marine energies, bioenergy and wastes) and nonrenewable (coal, oil, natural gas, nuclear and peat) [1]. The world energy consumption will gradually increase by 56% between 2010 and 2040. That is to say; the total world energy consumption increases from 524 quadrillion Btu in 2010 to 820 quadrillion Btu in 2040. The world energy use by various fuel types is shown in Figure 1.1 [2].

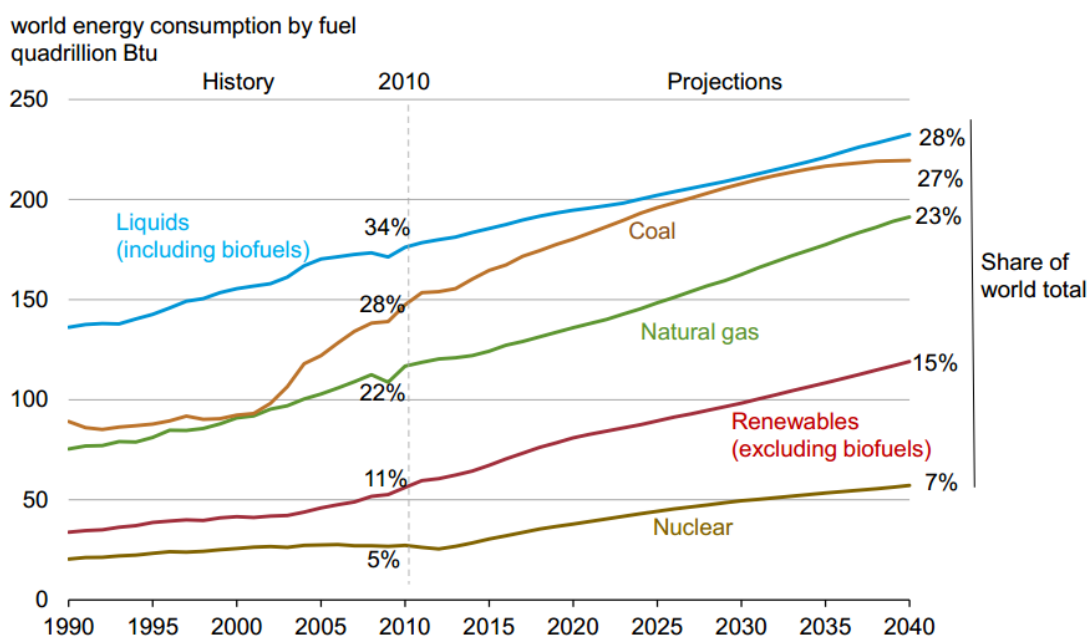


Figure 1.1 : The world energy consumption between 1990 and 2040 [2].

Renewable energy and nuclear energy have been grown 2.5% per year, making them the fastest growing energy sources. On the other hand, fossil fuels will be supplied about 80% of world total energy consumption by 2040. The energy-related carbon dioxide emissions are predicted to increase considerably at 40 billion metric tons in 2040; in other words, it has grown 46% by 2040 [2]. As a consequence, renewable energy sources such as biomass are preferred in order to mitigate CO₂ emissions.

According to IEA, the total primary use of biomass energy was 52 EJ which was around 10% of total primary energy in the world in 2009 [3]. Approximately two thirds of energy of biomass was used in residential area such as heating and cooking in developing countries. Moreover, the remaining biomass was used in industrial applications such as heating, power production and transportation [3].

In spite of the fact that biomass supply scenarios point out that potential of biomass would be between 200 and 500 EJ/yr, and forestry and agricultural residues and organic wastes would supply between 50 and 150 EJ/yr, the technical potential for biomass is forecasted as 1500 EJ/yr by 2050 [1]. The consumption of biomass is estimated to increase from 825 Mtoe in 1995 to 1071 Mtoe in 2020 [4].

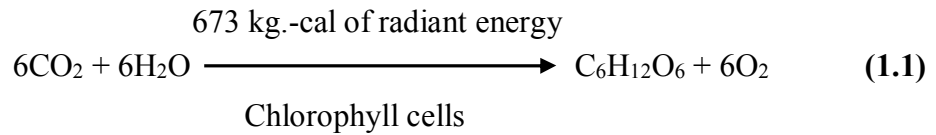
Most of the developing countries tend to use biomass as a renewable energy source to produce power due to the having low carbon emission to the atmosphere. For instance; in Sweden, the carbon tax had been risen from 30 EUR/ton CO₂ in the early 1990s to 101 EUR/ton CO₂ in 2007 resulted in a shift away from fossil fuels to biomass. Furthermore, before the 1990s, heat was mainly generated from coal or oil in Swedish cities. On the other hand, commercial heat was produced from biomass, renewable MSW (municipal solid waste), and solar thermal and heat pumps with 44%, 9% and 2%, respectively in 2007 [4].

1.2 Biomass

Biomass is any plant- or animal- derived material that originates from carbohydrates formed from CO₂, water and sunlight via photosynthesis reaction. As a result of this, in case of burning biomass does not contribute to total CO₂ in the atmosphere; in other words, it plays an important role in decline of greenhouse gas emissions [5]. According to the United Nations Framework Convention on Climate Change (UNFCCC), biomass is defined as:

“non-fossilized and biodegradable organic material originating from plants, animals and micro-organisms. This shall also include products, by-products, residues and waste from agriculture, forestry and related industries as well as the non-fossilized and biodegradable organic fractions of industrial and municipal wastes” [6].

Photosynthesis is a process to synthesize carbohydrates and oxygen from carbon dioxide and water via chlorophyll cells in plants in the presence of sun light. The overall equation of photosynthesis could be written as Equation 1.1 [7].



The value of 673 kcal is required for synthesis of 1 mole of glucose. On the other hand, the energy necessity is almost the same for per CH₂O group such as any synthesis of hexose or disaccharide, polysaccharide derived from hexoses [7].

The organic constituents in biomass are formed during the dark reactions of photosynthesis. The biochemical pathways of dark reactions mainly divided into the Calvin-Benson pathway, C₄ cycle and Crassulacean Acid Metabolism (CAM), which play an important role for reduction of CO₂ to sugars. That is to say, the molecular events in plant growth and differentiation between different plants species can be clarified [8].

The Calvin or Calvin-Benson cycle contains three carbon intermediate 3-phosphoglyceric acid. Plant biomass species which use this cycle called as C₃ plants. The C₃ plants show lower rates of photosynthesis at light saturation, low light saturation points, sensitivity to oxygen concentration, rapid photorespiration and high CO₂ compensation points such as around 50 ppm. In case of environmental CO₂ concentration below this compensation point, the plant respire more CO₂ to atmosphere compared to fixed CO₂ via photosynthesis. The typical C₃ plants are alfalfa, barley, cotton, Eucalyptus, peas, potato, rice, soybean, spinach, sugar beet, sunflower, tobacco, and wheat [8].

In the C₄ cycle, the four carbon dicarboxylic acids, malic or aspartic acids are formed from CO₂. The C₄ plants exhibit higher rates of photosynthesis at high light saturation points, insensitivity to atmospheric oxygen concentrations less than 21 mol%, low levels of respiration, low CO₂ compensation points and higher efficiency of water usage. The typical C₄ plants are corn, sugarcane, sorghum, tropical grasses etc. [8].

The other pathway is the crassulacean acid metabolism (CAM) which synthesizes free malic acid from fixing CO₂ via phosphoenolpyruvate carboxylase in dark reactions. The CAM plants can live in arid environments, and they have low photosynthesis rates

and high efficiency of water usage. The less water losses during the initial CO₂ fixation in dark reactions in CAM compared to C₃ and C₄ pathways. Furthermore, the optimum temperature is between 12 and 17 °C for CO₂ fixation in the dark. The stomates in CAM plants just open at night to minimize water loss; therefore, CO₂ passes through the stomates at night. The sugars are formed from carboxylic acids in the presence of daylight. The CAM plant species are cactus and succulents such as pineapple [8].

The plant biomass growth depends on CO₂ fixation. The type of plant affects the rate of photosynthesis. For instance, C₃ and C₄ plants respond photosynthesis in different ways which affect plant growth. The percentage of plant growth for various C₃ and C₄ plant species at different CO₂ concentrations for 28 days is shown in Table 1.1 [9].

Table 1.1 : The changes in various types of plant weight for two CO₂ concentrations [9].

Species	Biomass increase in %	
	600 ppm	1200 ppm
C ₃ plants		
<i>Datura stramonium</i> (1) (Jimson weed or thorn apple)	74	115
<i>Datura stramonium</i> (2)	60	107
<i>Chenopodium album</i> (lamb's quarters)	76	140
<i>Polygonum pensylvanicum</i>	48	100
<i>Abutilon theophrasti</i> (Velvetleaf)	38	65
<i>Ambrosia artemisiifolia</i> (Common ragweed)	68	112
<i>Acer saccharium</i>	32	63
<i>Populus deltoides</i> (Eastern cottonwood)	29	20
<i>Platanus occidentalis</i> (American sycamore)	33	33
<i>Glycine max</i> (Soybean)	47	100
<i>Helianthus annuus</i> (Sunflower)	40	55
C ₄ plants		
<i>Setaria faberi</i> (the Giant foxtail)	42	106
<i>Setaria lutescens</i> (yellow foxtail)	70	45
<i>Amaranthus retroflexus</i> (1) (redroot pigweed)	36	49
<i>Amaranthus retroflexus</i> (2)	29	48
<i>Zea mays</i> (corn or maize)	21	10

With respect to Table 1.1, it can be said that C₃ plants grow considerably higher than C₄ plants under great CO₂ concentrations. For instance, the growth of *Glycine max* has increased more than double to 100%; whereas, the growth of *Zea mays* has declined significantly to 10 % at 1200 ppm CO₂ concentration [9].

The common biomass sources are divided into agricultural, forestry, municipal, energy crops and biological which are shown in Table 1.2 [10].

Table 1.2 : The biomass sources [10].

Biomass Source	Examples
Agricultural	Food grain, bagasse, corn stalks, straw, seed hulls, nutshells, manure from cattle, poultry and hogs
Forestry	Trees, wood waste, bark, sawdust (SW), timber slash and mill scrap
Municipal	Sewage sludge, refuse-derived fuel (RDF), food waste, waste paper and yard clippings
Energy Crops	Poplars, willows, switchgrass, alfalfa, prairie bluestem, corn, soybean, canola and other plant oil
Biological	Animal waste, aquatic species and biological waste

The properties of ideal energy crop are;

- High yield
- Low cost
- Low energy input to produce
- Composition with the least waste product
- Low nutrient necessities [5].

There are four main products obtained from biomass which are electrical and heat energy, transport fuel and chemical feedstock [5].

There are five approaches to generate energy from biomass which are;

- Yielding crops such as starch, sugar, cellulose and oil
- Burning solid waste
- Producing biogas using anaerobic digesters
- Producing methane from landfill

- Generating biofuel such as ethanol, methanol, biodiesel and their derivatives [11].

1.2.1 Biomass types

The types of biomass are classified as woody plants, herbaceous plants/grasses, aquatic plants and manures [5].

There are two main groups of biomass with respect to their sources that are shown in Table 1.3 [10].

Table 1.3 : The biomass groups [10].

Biomass Groups	Subclassification	Examples
Virgin Biomass	Terrestrial biomass	Forest biomass Grasses Energy crops Cultivated crops
	Aquatic Biomass	Algae Water plant
Waste Biomass	Municipal waste	MSW Biosolids, sewage Landfill gas
	Agricultural solid waste	Livestock and manures Agricultural crop waste
	Forestry residues	Bark, leaves, floor residues
	Industrial residues	Demolition wood, sawdust Waste oil/fat

1.2.2 Biomass advantages and disadvantages

There are diverse advantages of using biomass as energy source:

- Biomass has large potential as renewable energy source. It is the fourth largest energy source which contributes around 14% of the world's primary energy supply.

- In spite of the fact that its potential varies with respect to country, it is a widely abundant energy source through the world.
- It can be used directly to provide different energy necessities such as heat, electricity and transport fuel.
- Biomass is permanently renewable energy source. That is to say, it is capable of releasing its energy every time.
- The conventional or new conversion technologies of solid fuels can be carried out to biomass in order to generate heat and power [12].
- It has zero CO₂ effect; in other words, it takes part in a decline of global warming.
- It has low ash, sulfur and nitrogen contents and low amount of mineral matter, making it one of the most attractive energy sources through the world.
- Waste of biomass is also used as energy source. That is to say, it is a cheap energy source [13].

Besides, there are several drawbacks of using biomass:

- It has low density, low calorific value, high moisture content, and high oxygen to carbon ratio.
- It is difficult to mill and crush because of its fibrous structure.
- Excessive usage of biomass might cause deforestation. That is to say, it might contribute indirectly to global warming.
- It causes emission of particles.
- The transportation price of biomass is high since its density very low [13].
- High moisture content of biomass makes it likely to be decayed during storage.

1.2.3 Biomass properties

With regard to conversion process of biomass, the fundamental material properties of interest are;

- Moisture content
- Calorific value
- Proportions of fixed carbon and volatiles
- Ash content
- Alkaline metal content

- Ratio of cellulose to lignin

First five properties are significant parameter for dry biomass conversion process; while, the first and the last properties should be taken into consideration for wet biomass conversion processes [5].

The properties of biomass and fossil fuels can be compared with respect to their O:C and H:C ratios, which are shown in Van Krevelen diagram in Figure 1.2. The lower ratios show the higher energy content of material. That is to say; energy content depends on the carbon proportion in substance [14].

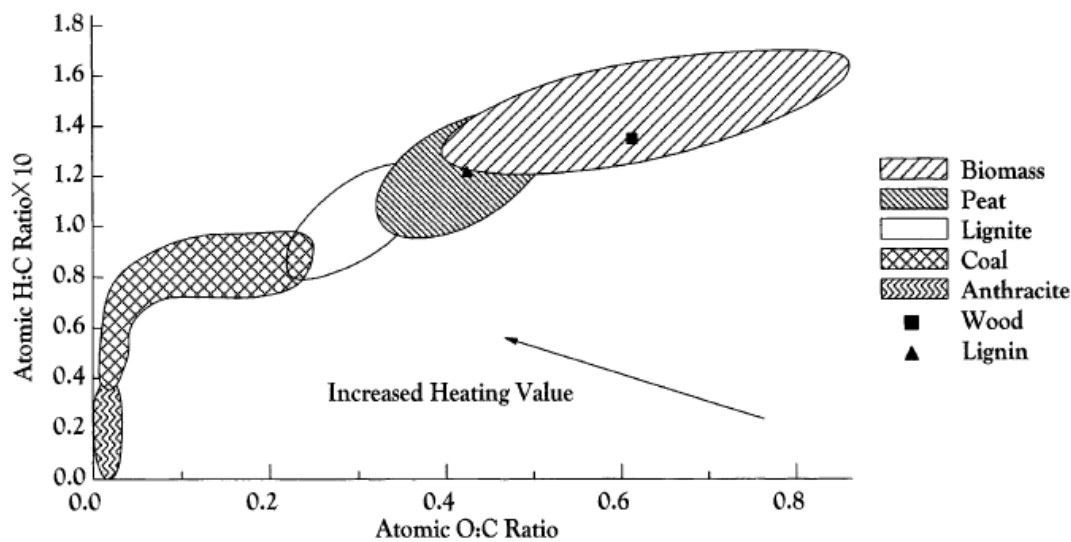


Figure 1.2 : Van Krevelen diagram for various solid fuels [14].

According to Van Krevelen diagram, the H:C and O:C ratios of raw biomass is in a ranges with 1.4-1.6 and 0.55-0.75, respectively. During thermal treatment technique such as torrefaction, the composition of biomass approaches to coal [15].

Biomass is composed of high amount of oxygen compared to fossil fuels; this is mainly due to the carbohydrate structure. Biomass generally contains 30-40 wt% of oxygen in dry matter basis. Moreover, the fundamental component of biomass is carbon which is between 30 wt% and 60 wt% of dry basis depending on ash content. The third principal constituent is hydrogen which is generally 5-6 wt% of biomass on dry basis. Furthermore, biomass is comprised of low amount of nitrogen, sulfur and chlorine which are around 1% of dry basis of matter [16].

The calorific value of dry ash free basis biomass is around 20 GJ/t, which has lower than those for the fossil fuels. This is mainly due to the high content of oxygen. The

fundamental substances of biomass, various sorts of biomass and fossil fuels are shown with their heat of combustion values in Table 1.4 [17].

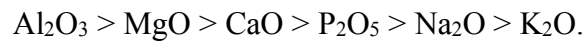
Table 1.4 : The heats of combustion of different substances [17].

Substance	Heat of Combustion (MJ/kg)
<i>Biomass components</i>	
Cellulose	18.8
Starch	18.8
Fats	38.9
Protein	23.4
Lignin	25.5
<i>Biomass types (on dry basis)</i>	
Grass	18.5
Wheat straw	17.6
Peanuts, rapeseed	29.5
Wood	17.6
Meat	24.3
<i>Fossil fuels</i>	
Oil	44.0
Bituminous coal	33.5
Anthracite	36.4

The proportion of inorganic elements affects the formation of pollutant emissions. Besides, ash reactions occur in case of Si, K, Na, S, Cl, P, Ca, Mg and Fe content which resulted in fouling and slagging. In addition, nitrogen and potassium are essential macronutrients for plants' growth [16].

In the presence of high amount of alkali metals in biomass leads to ash slagging, fouling and agglomeration. This is because; alkali silicates are formed by the reaction of alkali metals with silica which causes melting or softening at low temperatures such as lower than 700 °C with respect to the composition. Furthermore, the reaction of alkali metals with sulfur produces alkali sulfates on heat transfer surfaces of the combustor. The main source of alkali is potassium in biomass. As a consequence, the elemental composition of ash is taken into consideration in order to describe possible operational problems [18].

According to Du *et al.*, the melting temperature of ash gradually decreases with respect to following components in biomass;



That is to say; Al_2O_3 rich ashes do not lead the agglomeration of ash. On the other hand, the melting point of ash decreases in the presence of sodium, potassium and phosphorous [19].

1.2.4 Structure of biomass

Biomass contains organic substances such as carbohydrates, fats and proteins, small amounts of minerals such as sodium, phosphorous, calcium and iron [10]. Triglycerides, alkaloids, pigments, resins, sterols, terpenes, terpenoids and waxes are also minor constituents in biomass [20]. Furthermore, structure of biomass is comprised of extractives, fiber or cell wall component and ash [10].

Extractives: They contain protein, oil, starch and sugar which present in vegetable or animal tissue [10]. They can be dissolved in hot and cold water, ethers or methanol [20].

Cell wall: It generally contains carbohydrates and lignin. Carbohydrates are mostly cellulose or hemicellulose fibers that provide structural strength to the plant; whereas, lignin colligate the fibers together. Furthermore, some of cell walls contain starch and fat depending on plant type origin [10].

Ash: It is the inorganic constituents of the biomass [10].

Biomass is generally composed of hemicellulose, cellulose and lignin constituents.

Cellulose

Cellulose is the most abundant organic compound in nature [21]. The molecular weight of cellulose is around 32 MDa with respect to its glucose residue chain [22]. The elemental composition of cellulose is composed of 44-45% carbon (C), 6.0-6.5% hydrogen (H) and remaining oxygen (O) [23]. Consequently, the chemical formula of cellulose is $(\text{C}_6\text{H}_{10}\text{O}_5)_n$ [21]. The structure of cellulose is formed from β -1,4-glycosidic linkage that is shown in Figure 1.3 [24].

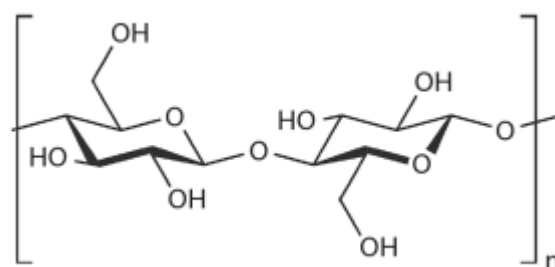


Figure 1.3: The structure of cellulose [24].

Hydrogen linkages between chains provide chemical stability and insolubility to plant structure. Furthermore, cellulose can be either amorphous or crystalline form [24]. In the presence of partial acid hydrolysis, cellulose is broken into cellobiose, cellotriose and cellotetrose which are glucose dimer, trimer and tetramer, respectively. On the other hand, it can be broken down into glucose under complete acid hydrolysis conditions [20].

Hemicellulose

Hemicellulose is other constituent of cell wall. It is formed from arabinose and xylose (pentoses), glucose, galactose, and mannose (hexoses), rhamnose and fucose (6-deoxyhexoses), and galacturonic, glucuronic, and 4-O-methylglucuronic acids (uronic acids) components [25]. The structure of hemicellulose is shown in Figure 1.4 [26].

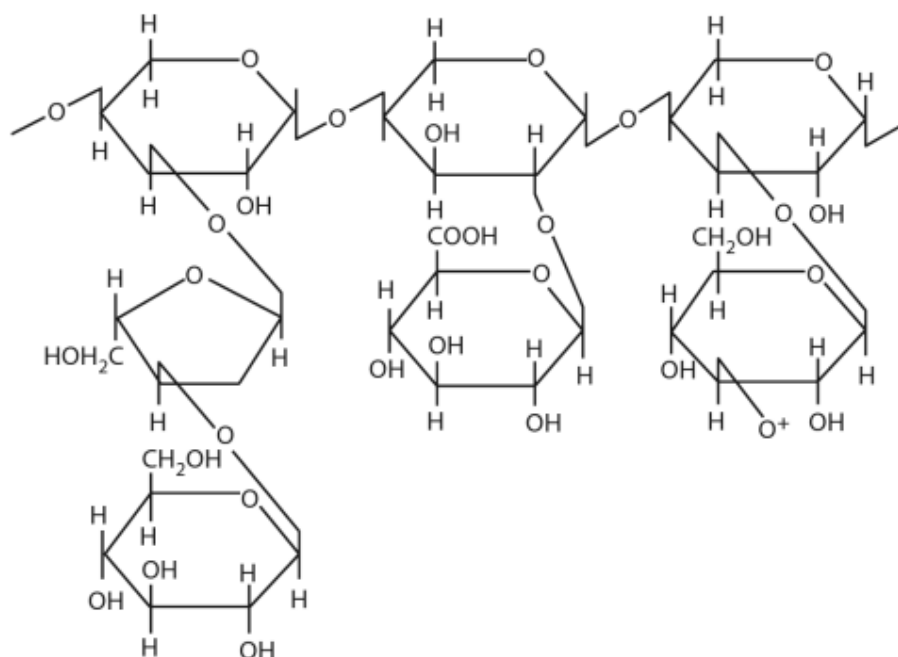


Figure 1.4 : Hemicellulose structure [26].

Hemicellulose has amorphous form in nature; therefore, it is more reactive than cellulose. Furthermore, extensive branching chain in hemicellulose structure leads it to more soluble in water [27]. The chemical formula of hemicellulose is $(C_5H_8O_4)_n$. Moreover, it produces more gases and less tar than cellulose. Hemicellulose can dissolve in the presence of weak alkaline solutions, and dilute acid or base can easily hydrolyze it [10].

Lignin

Lignin is a three dimensional phenolic polymer, and also the most abundant biopolymer in nature subsequent to cellulose. It is one of the important constituents in plant cell wall. Lignin is synthesized in case of dehydrogenation of the hydroxycinnamyl alcohols, the monolignols *p*-coumaryl, coniferyl, and sinapyl alcohols. Lignin structure is composed of each of these monolignols which generate one subunit type such as *p*-hydroxyphenyl (H), guaiacyl (G) and syringyl (S) [28]. Each of these monolignols and monomers are shown in Figure 1.5 [29].

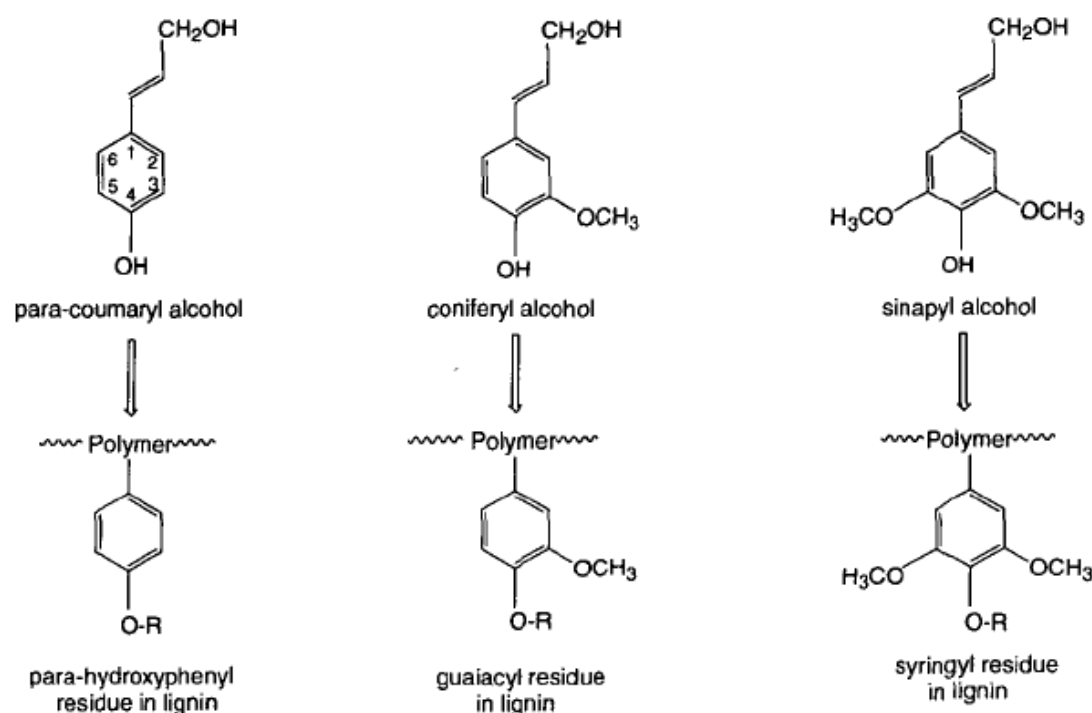


Figure 1.5 : The structure of monolignols and subunits of lignin [29].

The monomer composition of lignin depends on species, cell types of species and developmental stages of a cell [29]. For instance; hardwood lignin structure is mainly composed of G and S subunits with traces of H subunits; while, softwood lignin

generally contains G and low amounts of H subunits [30]. The structure of lignin is shown in Figure 1.6 [26].

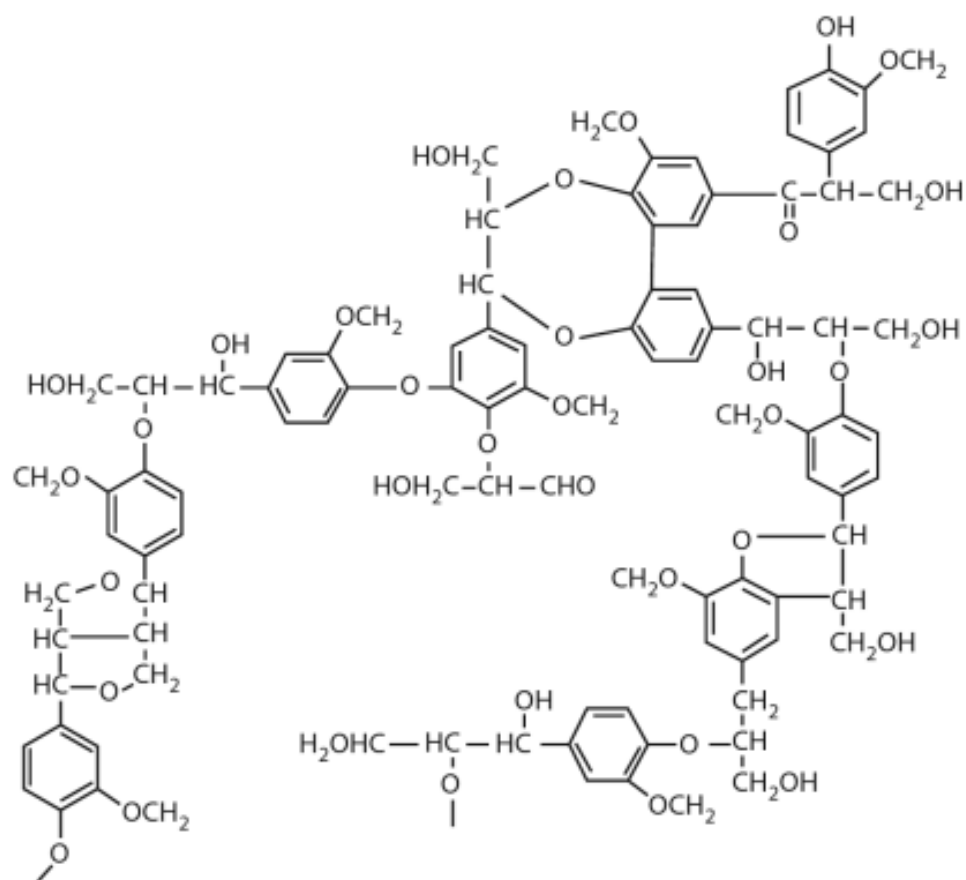


Figure 1.6 : The structure of lignin [26].

Lignin provides rigidity, compressive strength and hydrophobic properties to cell wall structure [29]. The lignin proportion is 20-25% of the biomass weight [13].

1.2.5 Biomass potential in Turkey

The total electricity generation is 239.497 GWh in Turkey in 2012, and its 3.1% was supplied from renewable energy and waste sources including geothermal, wind, solid biomass, biogas and waste. Furthermore, the hydropower shares 24.3% of total electricity generation in 2012 [31].

The total installed capacity reached to 64,268 MW in 2014 in Turkey [32]. It is estimated that at least 40,000 MW of new capacity will be required until 2020 [33]. Turkey tends to generate electricity from fossil fuels, and its primary energy is supplied from oil, lignite coal, natural gas, geothermal and hydroelectric resources [34].

Turkey's total primary energy production and consumption was 32.2 and 114.48 Mtoe, respectively [35].

Renewable energy is mainly hydropower, wind and biomass in Turkey. The biomass use has declined particularly in residential heating because of environmental and scarcity of supply concerns. The primary energy supply from renewable sources and estimations in Turkey are shown in Table 1.5 [34].

Table 1.5: The renewable energy supply in Turkey [34].

Renewable sources	2000	2005	2010	2015	2020
(ktoe)					
Hydropower	2656	4067	4903	7060	9219
Geothermal, solar and wind	978	1683	2896	4242	6397
Biomass and waste	6457	5325	4416	4001	3925
Renewable energy production	10,091	11,074	12,215	15,303	19,741

The essential source of biomass energy in Turkey is composed of agricultural residues such as grain dust, wheat straw and hazelnut shells, and municipal solid waste. Moreover, fuel wood has an important part among biomass energy resources in rural areas. The total forest potential is approximately 940 million m³ with around 25 million m³/year growth in Turkey [34]. The total biomass energy potential is approximately 32 Mtoe; whereas, the amount of usable biomass potential is around 17 Mtoe in Turkey [36].

In accordance with Renewable Energy Sources legislation No. 5346 in Turkey, the electricity generated from biomass energy sources fetches a price for 14 Euro cent/kWh. The agricultural residues of sunflower, cotton, hazelnut, banana and olive milling residue can be used as potential fuel sources in Turkey that are shown in Table 1.6 [37, 38].

Table 1.6 : The potential agricultural plantation and residues in Turkey [37, 38]

	Plantation (decare)	Agricultural waste (ton/year)
Sunflower	4,854,425	1,400,000
Cotton	6,300,000	1,102,500
Hazelnut	3,900,000	390,000
Banana	30,000	108,000
Olive milling residue	-	215,000

According to EPDK, the total installed capacity of biomass, biogas and landfill gas plants which have license in Turkey are 16.43 MWm, 22.34 MWm and 120.02 MWm, respectively [39]. By 2012, the total installed capacity of power plants based on biogas and biomass are 93 MW and 12.8 MW, respectively in Turkey [40].

1.3 Physical Processes

1.3.1 Pelletizing and briquetting

Biomass cannot be treated, transported and stored easily because of its high moisture content, low density, high dust level and unspecified form and size. In order to overcome this problem, biomass is densified in a pellet or briquette form [41, 42]. The main difference between pellet and briquette is in size. That is to say; the diameter of pellet is 5-12 mm; while, briquette's diameter is above 50 mm depending on its application area [42].

In case of pelletization, its density soars from 40-150 kg/m³ for grass type biomass, and 320–720 kg/m³ for most types of dried hard and softwoods to 1000-1400 kg/m³ with enhanced fuel quality and energy density. Furthermore, bulk densities are approximately 700 kg/m³ for typical biomass pellets, and 5.0 MWh energy can be generated from 1 ton of pellets which is same as 0.5 m³ oil. As a consequence, the price of transportation, handling and storage of biomass could be decreased [43, 44].

The compression force and temperature, particle size and chemical composition of biomass affect the mechanical durability of pellets. In case of pelletization, biomass has high tensile strength and low moisture content. On the other hand, biomass pellet could not tackle the ash related challenges of biomass feedstock. Therefore, pretreatment is required in order to improve its combustion characteristics. Take hydrothermal carbonization (HTC) technique as an example. In this technique, natural coalification is simulated; in other words, biomass feedstock is decomposed and

carbonized in the presence of water at desired temperature and autogenous pressure conditions [45].

Torrefaction is a thermal pretreatment technique to decrease moisture content along with the unstable constituents in biomass feedstock in a temperature range of 200-300 °C with heating rate <50 °C/min pellets in the absence of oxygen [46, 47]. The trace amount of moisture in pellet reduces the mechanical degradation, and prevents fungal and bacterial growth. As a consequence, torrefied pellets are stronger and more hydrophobic than untreated pellets [46]. According to Pirraglia et al., the energy bulk density of torrefied pellets could be twice as much as wood pellets. Furthermore, there are three potential application areas for torrefied pellets which are entrained flow gasification, small scale combustion using pellets and co-firing in pulverized coal fired power stations [48].

1.3.2 Dewatering and drying

The raw biomass often contains moisture in the range of 60-70 wt%, which obstructs direct combustion, pyrolysis and gasification. The high moisture content leads to the enhancement of energy consumption for dewatering and promoting endothermic water gas shift reaction in gasification or pyrolysis processes. Furthermore, the moisture content in biomass reduces the combustion efficiency and lowers the heating value (LHV) of fuel. As a consequence, dewatering or drying is preferred as the first step in a biomass combustion [49].

Dewatering processes are applied to decrease the moisture content in biomass. The moisture content could be reduced to around 80 wt% on wet basis, which is not sufficient to obtain low moisture content [50]. The equipment of dewatering process is filters, centrifuges, hydrocyclones, extrusion and expression presses, and water extractors etc. [8].

Drying process is employed to reduce high moisture content in biomass. It could decrease moisture content down to 15 wt% wet basis [51]. In case of gasification and pyrolysis processes, moisture content of biomass should be lower than 15 wt% and 10 wt%, respectively [52]. There are various types of dryers which are direct and indirect fired rotary dryers, conveyor dryers, cascade dryers, flash or pneumatic dryers, superheated steam dryers and microwave dryers. The suitable dryer is chosen with regard to size and characteristics of feedstock, capital cost, maintenance requirements,

environmental emissions, energy efficiency, and waste heat sources available and potential fire hazard [53].

According to Arlabosse et al., the thermally assisted mechanical dewatering (TAMD) process is a quite innovative dewatering process for mechanical fractionation of herbaceous biomass such as alfalfa. With regard to this study, the dry solid content of nature wet biomass such as spinach leaves and alfalfa stems and leaves was increased from 2 to 5% at 300 kPa. Moreover, the TAMD process is more effective process to remove water from alfalfa under mild conditions compared to conventional dewatering process with 69% and 55%, respectively [54].

1.4 Thermal Pretreatment Processes

1.4.1 Torrefaction

Torrefaction is a thermal pretreatment technique which produces a higher quality of biofuel from ligno-cellulosic biomass. The fundamental principle of torrefaction is that oxygen is removed in order to produce lower O/C ratio in a final product. That is to say; the calorific value of final product is higher than original biomass. Furthermore, torrefaction destroys the fibrous structure and tenacity, and increases hydrophobic properties of biomass [55].

The process is carried out in a temperature range of 200-300 °C in case of inert atmosphere and low heating rates. The high amount of CO (~20%) and CO₂ (~80%) and low amount of volatile organic matters are removed during torrefaction [56]. After torrefaction process, about 70% of the mass is remained as a solid product, which contains over 90% of its initial energy content [57]. Some biomass properties and improvements through torrefaction process are shown in Table 1.7 [58].

Table 1.7 : The biomass characteristics and improvements through torrefaction [58].

Biomass Properties	Improvements through torrefaction
Low calorific value because of low fixed carbon and high moisture content	Enhanced fixed carbon content
Lower energy density compared to fossil fuels (the energy density of wood chips and coal is around 2-4 GJ/m ³ , 25-40 GJ/m ³ , respectively)	Higher energy density (about 18-20 GJ/m ³)
Hydrophilic and hygroscopic	Higher hydrophobicity (the equilibrium moisture content of torrefied biomass is in a range of 1-3%)
Heterogeneous characteristics (broad spectrum of shapes, sizes and types) and quality	Produced a solid uniform product removing volatiles and moisture The particle size distributions, sphericity, and particle surface areas simulate to coal after grinding
Low combustion efficiency and high smoke during combustion	Reduced oxygen content and produced less smoke with higher combustion rate
Difficult to pulverize due to the tough and fibrous structure	Developed grinding ability
Biodegradable	Stable due to low moisture content

The partial decomposition of cellulose, hemicellulose and lignin is stimulated through torrefaction process which leads to decline of fibers length and mechanical stability. That is to say, the grindability characteristics of biomass are improved [59]. Consequently, it provides more efficient co-firing property to coal-fired power stations or entrained-flow gasification applications in order to produce chemicals and transportation fuels [60].

The thermal decomposition temperatures of hemicellulose, cellulose and lignin are in the ranges of 150-300 °C, 275-350 °C and 250-500 °C, respectively [61]. Furthermore, low calorific value gases such as CO₂, CO, CH₄ and H₂O and several types of organic acids such as formic, acetic and lactic acid are released during decomposition [62]. CO₂ is formed from up to 30% carbon depending on sort of biomass and torrefaction conditions such as temperature and treatment time during torrefaction [59].

The water absorbing capacity of fuel decreases considerably during torrefaction due to the replacement of OH-groups by unsaturated non-polar groups. As a consequence, degradation, self-heating and moisture uptake properties are reduced depending on torrefaction conditions [63].

In case of combination with densification such as pelletization or briquetting processes, the energy density of biomass is soared to 20-25 GJ/ton. In addition, homogeneous structure is produced preventing design problems, and providing better operational conditions [60]

The properties of various types of biomass fuel and their comparison with coal are given in Table 1.8. Torrefaction increases obviously calorific value of biomass due to the removal of moisture and organic compounds from original biomass [63].

Table 1.8 : The properties of various kinds of solid fuels [63].

	Wood	Wood pellets	Torrefaction pellets	Charcoal	Coal
Moisture content (% wt)	30-45	7-10	1-5	1-5	10-15
Lower heating value (MJ/kg)	9-12	15-18	20-24	30-32	23-28
Volatile matter (% db)	70-75	70-75	55-65	10-12	25-30
Fixed carbon (% db)	20-25	20-25	28-35	85-87	50-55
Density (kg/l)	0.2-0.25	0.55-0.75	0.75-0.85	~0.20	0.8-0.85
Bulk Energy density (GJ/m ³) (bulk)	2.0-3.0	7.5-10.4	15.0-18.7	6-6.4	18.4-23.8
Dust	Average	Limited	Limited	High	Limited
Hydroscopic properties	Hydrophilic	Hydrophilic	Hydrophobic	Hydrophobic	Hydrophobic
Biological degradation	Yes	Yes	No	No	No
Grindability	Poor	Poor	Good	Good	Good
Handling	Special	Special	Good	Good	Good
Quality variability	High	Limited	Limited	Limited	Limited

The torrefied fuel contains less ash compared to coal in a range of 0.7-5% db and 10-20% db, respectively. On the other hand, it has higher reactive characteristics than coal because of higher amounts of volatile matter [63].

There are three types of torrefaction processes which are dry torrefaction, ionic-liquid assisted torrefaction and wet torrefaction. The dry torrefaction is carried out in a temperature range of 200-300 °C with slow heating rate in an inert atmosphere condition. During dry torrefaction, hemicellulose, cellulose and lignin are decomposed

at different rates. That is to say, cellulose decomposition is the rate limiting step; while, hemicellulose undergoes the highest amount of degradation. After 300 °C, biomass energy density can be decreased because of heavy tars formation. Although, ionic-liquid assisted torrefaction provides increasing decomposition rate of cellulose below 300 °C, energy yield is lower compared to the dry torrefaction. Furthermore, wet torrefaction is carried out in case of pressurized liquid water up to 5 MPa and 260 °C conditions. Although, its energy yield is higher than dry torrefaction, the operational cost is also higher due to the high pressure conditions [64].

1.4.2 Pyrolysis

The pyrolysis is a thermal degradation process to produce carbon based materials from biomass in the absence of oxygen condition. Pyrolysis reactions and products are shown in Figure 1.7. First of all, gas and solid char are formed during primary decomposition reactions. Secondly, the condensable gases may collapsed to the non-condensable gases such as CO, CO₂, H₂ and CH₄, liquid and char [10].

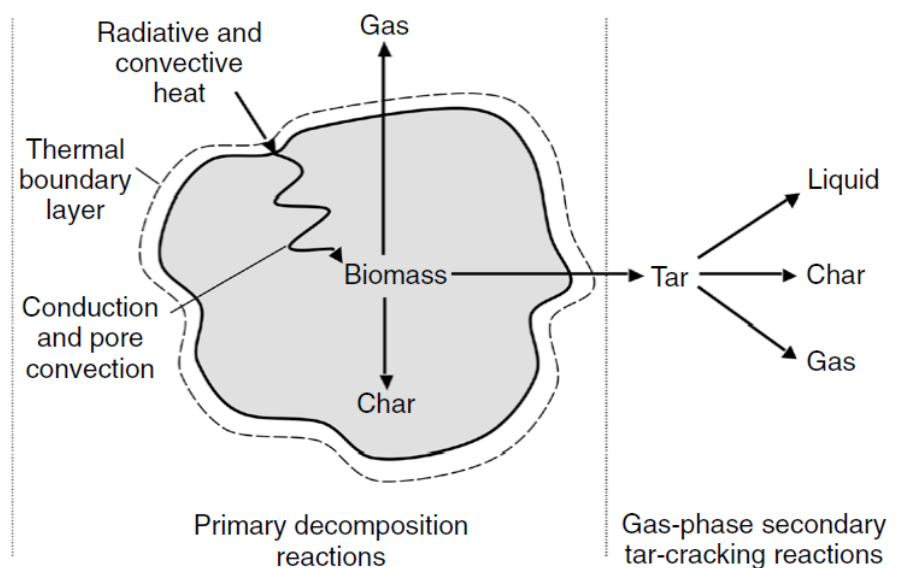
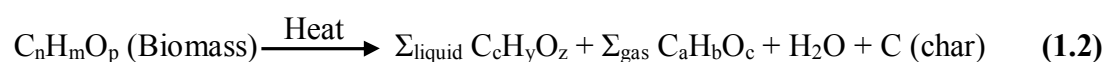


Figure 1.7 : Pyrolysis in a biomass particle [10].

The generic reaction of pyrolysis is indicated in Equation 1.2. It can be said that liquid, gas, char and H₂O are produced during reaction [10].



The pyrolysis products can be divided into solid form known as char (~18 MJ/kg), liquid form known as bio-oil (~22 GJ/m³ or 17 MJ/kg) and gas form known as syngas (~6 MJ/kg) depending on the pyrolysis conditions [65]. The syngas is composed of H₂,

CO, CH₄, CO₂, H₂O and various low molecular weight volatile organic compounds. The heat energy can be generated from burning of syngas in order to use in several application areas such as drying and electricity generation. Furthermore, the bio-oil is produced from cellulosic feedstock by fast pyrolysis, which contains ~20% w/w emulsion of water and numerous oxygenated organic compounds such as organic acids, aldehydes, alcohols, phenols, carbohydrates and lignin-derived oligomers. The bio-oil is not only used in industrial boilers, but also upgraded into synthetic transportation fuels. Moreover, high amount of heat is generated from burning of biochar. The activated carbon can be produced from biochar, and used as adsorbent to remove pollutants from air and waste water streams [65].

The pyrolysis is typically classified as slow, fast and flash pyrolysis. In slow pyrolysis (carbonization), high amount of charcoal is produced; while, liquid biofuels and other chemical materials are produced by fast pyrolysis. The slow pyrolysis is performed at low temperatures and long residence time [43]. The various types of pyrolysis and their process conditions are show in Table 1.9 [66].

Table 1.9 : Different types of pyrolysis and conditions [66].

	Residence time	Heating rate	Maximum temperature (°C)	Main product
Carbonization	Hours-days	Very low	400	Charcoal
Conventional	5-30 min	Low	600	Bio-oil, charcoal and gas
Fast	0.5-5s	Fairly high	650	Bio-oil
Flash				
Liquid	<1s	High	<650	Bio-oil
Gas	<1s	High	<650	Chemicals and fuel gas
Ultra	<0.5s	Very high	1000	Chemicals and fuel gas
Vacuum	2-30s	Medium	400	Bio-oil
Hydropyrolysis	<10s	High	<500	Bio-oil and chemicals
Methanopyrolysis	<10s	High	>700	Chemicals

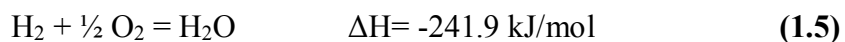
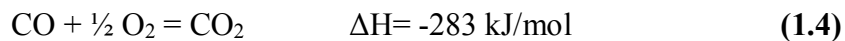
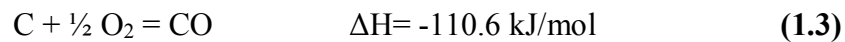
Fast pyrolysis is carried out in a temperature range of 500-700 °C with high heating rate such as 300 °C/min for a short residence time. Moreover, flash pyrolysis happens with high heating rate, and its reaction time is more or less a second leaded particle size of biomass to quite small between 105 µm and 250 µm [43].

1.4.3 Gasification

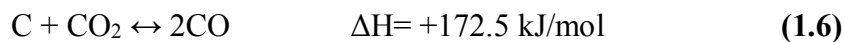
Gasification is a thermo-chemical process which produces combustible gas mixtures, called as syngas, from carbonaceous materials such as biomass. The syngas containing high amount of hydrogen is produced during gasification; therefore, it can be used for large scale hydrogen manufacture [67]

The main chemical reactions of gasification can be classified as combustion reactions, the Boudouard reaction, water gas reaction, methanation reaction, methane reforming, tar reforming and hydrocarbon reforming reactions which are shown in Eq. 1.3-1.13 [68, 69];

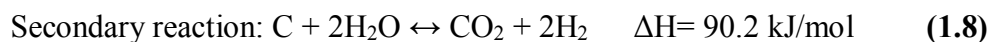
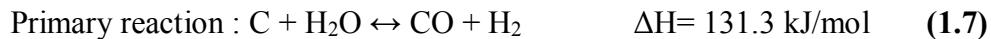
- Combustion reactions;



- The Boudouard reaction;



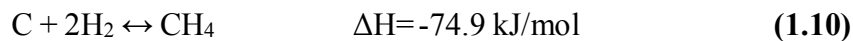
- The water gas reaction:



- Water gas shift reaction:



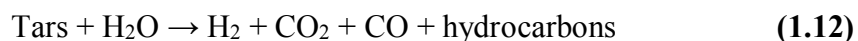
- The methanation reaction



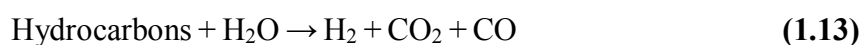
- Methane reforming:



- Tars reforming:



- Hydrocarbon reforming reaction:



With respect to the combustion reactions, it can be said that gasification not only provides easier handling compared to a solid fuel, but also produces heat which

contains generally in range of 75-88% heat of original fuel, making it the commercial process [68].

Air, pure oxygen, steam, CO₂ or their mixtures can be used as gasifying agent in gasification which is a significant factor for syngas composition as showed in Table 1.10 [70].

Table 1.10 : The syngas composition under different gasifying agents [70].

Oxidant	Composition (vol. %)					LHV (MJ/Nm ³)
	H ₂	CO	CO ₂	CH ₄	N ₂	
Air	9-10	12-15	14-17	2-4	56-59	3-6
Oxygen	30-34	30-37	25-29	4-6	-	10-15
Steam/CO ₂	24-50	30-45	10-19	5-12	-	12-20

It is obvious from Table 1.10 that air is the most common agent because of zero cost and the highest availability. On the other hand, it also involves high amount of N₂ which increases equipment sizes and reduces the calorific value of syngas. Furthermore, not only the calorific value but also H₂ composition in syngas is increased under pure oxygen and steam oxidant agents [70].

The sorts of gasifiers are divided into moving-bed, fluid-bed and entrained-flow gasifiers. The principle of moving-bed (or fixed-bed) gasifiers is that the counter current blast is carried out to the carbonaceous materials such as coal. The downward flowing coal is preheated and pyrolyzed by hot syngas produced from gasification zone. Furthermore, the oxygen consumption is very low during gasification, but syngas contains pyrolysis products. The fluid-bed gasifiers provide a good mixing between feed and oxidant that improves heat and mass transfers. On the other hand, components are distributed in the bed which led to removal of partially reacted fuel with ash. Moreover, the operation temperature should be below the softening point of the ash due to the prevention of distribution of ash slagging in fluidization of bed. In addition, too fine particles are generally in the syngas that can be addressed using a cyclone to return back to the bed. Furthermore, the feed and blast are carried out in a co-current flow in entrained-flow gasification. The process is operated at high temperatures with short residence times in order to provide a good conversion. The size of feed should be under 100 μm to enhance mass transfer in the gas. The main drawback of entrained-flow gasification is that a high amount of oxygen is required

due to the high operation temperature that causes high cost. Nevertheless, there are no specific technical limitations for feedstocks such as coal [68].

According to Nzihou et al., biomass gasification is generally performed at temperature between 800 and 900 °C with steam to carbon ratios of 0.8-1.5:1. The fluidized bed is the most suitable gasifier for large scale operations; whereas, moving-bed gasifiers are generally used in smaller units. Furthermore, the process is generally carried out under atmospheric pressures, and steam is added as gasifying agent in order to increase hydrogen composition in syngas. The composed carbon dioxide during reaction can also act as a gasifying agent [71].

1.4.4 Carbonization

Carbonization is a thermal degradation process to enrich carbon composition in solid fuels such as biomass by removing volatile matters in the form of carbon oxides (CO, CO₂), light hydrocarbons and hydrogen in the presence of inert gas, and the obtained product is referred as charcoal. Furthermore, slow heating rates, long residence time and low final temperature lead to increase in the yield of char [13]. The charcoal is generally used as activated carbon in adsorbent applications, as a material for electrodes and carbon nanotubes, and as renewable fertilizer in agriculture [72]. The char is also used as a fuel in the ferroalloy, aluminum, copper, tobacco and cement industries [73].

The carbonization process contains several physical and chemical steps. The first step is that raw material is dried at temperatures up to 170 °C. Secondly, the initial volatiles, which comprise CO, CO₂, methanol and acetic acid, are mainly formed from hemicellulose and lignin in a temperature range of 170-270 °C. The process is self-sustaining, and exothermic reactions outweigh beyond 270 °C. The final step is that charcoal is yielded containing about 84 mass% of carbon at 500 °C. This charcoal has lower ash content compared to coke [74].

The hydrothermal carbonization is a type of carbonization in which biomass is heated with water and a catalyst such as citric acid in a temperature range between 180 and 250 °C under saturated pressures between 2 and 10 MPa for several hours, and the product obtained in this way is called as hydrochars [75, 76]. According to Xiao et al., the carbonized products contain water soluble components and solid residues. The aqueous phase is composed of sugar and lignin derived constituents which can be

attractive material for biodiesel and chemical manufacture. The calorific value of hydrochar was reported to be higher compared to original material [75].

In a study of Katyal et al., the sugar cane bagasse was used as a feedstock in order to examine effects of different parameters such as temperature and heating rate on carbonization process. Experiments were carried out in a temperature range of 250-700 °C with heating rates between 5 °C/min and 30 °C/min under nitrogen sweep gas with flow rate of 350 mL/min conditions. The results are shown in Table 1.11 [73].

Table 1.11 : Proximate analysis of char produced from bagasse (moisture free basis) [73].

Heating rate (°C/min)	Temperature (°C)					
	250	300	400	500	600	700
<i>5 °C/min</i>						
Volatile Matter (%)	75.10	63.40	32.00	22.65	15.95	11.40
Ash (%)	5.05	6.30	10.75	14.50	18.10	20.60
Fixed Carbon (%)	19.85	30.30	57.25	62.85	65.95	68.00
<i>20 °C/min</i>						
Volatile Matter (%)	77.30	65.20	35.20	26.05	18.05	12.95
Ash (%)	4.95	6.10	10.25	13.75	18.10	19.95
Fixed Carbon (%)	17.75	28.70	54.55	60.20	63.85	67.10
<i>30 °C/min</i>						
Volatile Matter (%)	76.40	64.75	36.15	25.50	18.50	13.55
Ash (%)	4.80	5.95	9.95	14.10	18.50	20.50
Fixed Carbon (%)	18.80	29.30	53.90	60.40	63.00	65.95

With regard to this study, it can be said that there was a considerable amount of volatile matter below 400 °C for any heating rates due to limited decomposition of volatile extractive components and hemicellulose. The yield of fixed carbon increased significantly at higher temperatures because of removal of volatile matter from the biomass. Furthermore, the fixed carbon and ash forming inorganic components were remained in the biomass. The lower heating rates with longer residence times are also suitable conditions for high yield of carbon [73].

According to Liou [77], the valuable ceramic materials can also be produced using rice husk in an economic way. The rice husk is mainly composed of cellulose, hemicellulose, lignin and around one fifth of weight silica depending on its sort of paddy and geography. In case of mixing of carbonized rice husk with carbon/silica powder, the surface area was increased significantly. Furthermore, the high purity silica powder could be produced via combustion of the rice husk, and it could be used as a raw material for manufacture of fine ceramic powder. With regard to this study,

the higher specific surface area, pore volume and pore diameter could be obtained in case of the low heating rate such as 5 °C/min. As a consequence, the specific surface areas of carbon/silica and pure silica powders were obtained with 262 and 235 m²/g, and the mean pore diameters were with 2.2 and 5.4 nm, respectively, making them the high quality raw materials for production of ceramic materials [77].

Park et al. notified that the torrefied and low temperature carbonized (in a temperature range of 300-400 °C) woody biomass was blended with coal in order to investigate characteristics of co-combustion. Depending on the operational temperatures, the yield energy of torrefied and carbonized woody biomass varied with 80-98% and 45-63%, respectively. Nevertheless, the fuel characteristic of carbonized biomass was close to coal due to its high fixed carbon and low volatile matter content. Furthermore, the activation energy decreased with increase of blending ratio as a result of high reaction rate [78].

The biomass charcoal is mainly composed of lignin; therefore, lignin carbonization process should be taken into consideration to enhance the quality of charcoal. Cao et al. stated that there were four steps during lignin carbonization which were drying, pyrolysis, amorphous carbon formation and carbon structure reforming at temperature range from ambient to 1400 °C. In pyrolysis step in a temperature range between 200 °C and 500 °C, the activation energy was 54 kJ/mol, and volatile matters such as CO, CH₄, CO₂ and propanal were released from the lignin. In amorphous carbon formation step, from 500 °C to 900 °C, the activation energy was 70 kJ/mol, and aromatic structures were formed from benzene rings with emission of CO. The last step is carbon reforming which began at 900 °C with an activation energy of 178 kJ/mol. It was believed that a phenyl plane structure was formed between the amorphous carbon and graphite during cracking of C=C bonds at 1400 °C [79].

1.5 Biomass Pyrolysis Kinetics

1.5.1 Kinetic expressions for biomass thermal decomposition

Biomass pyrolysis is a complex process mainly due to the different chemical composition of ingredients [80]. The main components of biomass are hemicellulose, cellulose and lignin. The pyrolysis kinetics of these substances are generally stated as first order reaction kinetics mechanism. Nevertheless, the reaction order of lignin can

be considerably fitted higher than first order reaction [81]. With respect to data analysis, kinetic data approaches are divided into model-based (model-fitting) and isoconversional (model-free) methods. Model-based method is the most common methods to determine solid state reaction kinetics, particularly in non-isothermal studies. Nonlinear least square fitting is generally used to fit experimental data and determine Arrhenius parameters. On the other hand, isoconversional (model-free) evaluates kinetic parameters without model-based assumptions such as first order reaction [82].

The kinetics of biomass decomposition under isothermal conditions can be expressed by the following equation:

$$\frac{d\alpha}{dt} = k(T)f(\alpha) \quad (1.14)$$

where t refers time, α is the degree of conversion, or extent of reaction, $d\alpha/dt$ denotes the rate of the isothermal decomposition and $f(\alpha)$ is a conversion function which indicates the used reaction model.

$k(T)$ is the rate constant expressed by Arrhenius equation:

$$k(T) = A \exp\left(\frac{-E_a}{RT}\right) \quad (1.15)$$

where T is the absolute temperature in K, R is the universal gas constant, $k(T)$ is the temperature dependent reaction rate constant, A denotes the frequency factor and E_a refers the activation energy of the reaction.

$$\frac{d\alpha}{dt} = k(T)f(\alpha) = A \exp\left(\frac{-E_a}{RT}\right) f(\alpha) \quad (1.16)$$

The degree of conversion, α , can be expressed as:

$$\alpha = \frac{w_0 - w}{w_0 - w_f} = \frac{v}{v_f} \quad (1.17)$$

where w , w_0 and w_f denotes mass of substance present at any time t , initial and final mass of substance, respectively. Furthermore, v refers the mass of volatiles present at any time t and v_f is the total mass of volatiles.

Non-isothermal reaction rate is a function of temperature at a linear heating rate, β , which can be expressed as the following equation:

$$\frac{d\alpha}{dT} = \frac{d\alpha}{dt} \frac{dt}{dT} \quad (1.18)$$

Where dt/dT refers the inverse of the heating rate, $1/\beta$, $d\alpha/dt$ is the isothermal reaction rate and $d\alpha/dT$ denotes the non-isothermal reaction rate. As a consequence, the rate law for non-isothermal conditions can be expressed as:

$$\frac{d\alpha}{dT} = \frac{k(T)}{\beta} f(\alpha) = \frac{A}{\beta} \exp\left(\frac{-E_a}{RT}\right) f(\alpha) \quad (1.19)$$

The most common reaction mechanisms in solid state reactions are shown in Table 1.12. The differential or integral approach can be implemented to isoconversional models depending on the TGA (Thermogravimetric analysis) data. Furthermore, a fourth order Runge-Kutta method is usually performed to kinetic equations in order to take integral [82].

Table 1.12 : The most common reaction models in solid state reactions [82, 83].

Reaction Model	$f(\alpha)=(1/k)(d\alpha/dt)$	$g(\alpha)=kt$
Reaction order		
1 st order (n=1)	$(1-\alpha)$	$-\ln(1-\alpha)$
1/3 rd order	$(1-\alpha)^{1/3}$	$(3/2)[1-(1-\alpha)^{2/3}]$
1/2 nd order	$(1-\alpha)^{1/2}$	$2[1-(1-\alpha)^{1/2}]$
2/3 rd order	$(1-\alpha)^{2/3}$	$3[1-(1-\alpha)^{1/3}]$
2 nd order	$(1-\alpha)^2$	$-[1-(1-\alpha)^{-1}]$
Diffusional		
1-D	$1/2\alpha$	α^2
2-D (Valansi Barrer)	$[-\ln(1-\alpha)]^{-1}$	$\alpha+(1-\alpha)\ln(1-\alpha)$
3-D (Jander)	$(3/2)(1-\alpha)^{2/3}[1-(1-\alpha)^{1/3}]^{-1}$	$[1-(1-\alpha)^{1/3}]^2$
3-D (Ginstling-Brounshtein)	$(3/2)[(1-\alpha)^{-1/3}-1]^{-1}$	$1-(2/3)\alpha-(1-\alpha)^{2/3}$
Contracting Geometry		
Contracting area	$(1-\alpha)^{1/2}$	$1-(1-\alpha)^{1/2}$
Contracting volume	$(1-\alpha)^{1/3}$	$1-(1-\alpha)^{1/3}$
Nucleation		
Avrami-Erofeev; n=2	$2(1-\alpha)[- \ln(1-\alpha)]^{1/2}$	$[- \ln(1-\alpha)]^{1/2}$
Avrami-Erofeev; n=3	$3(1-\alpha)[- \ln(1-\alpha)]^{2/3}$	$[- \ln(1-\alpha)]^{1/3}$
Avrami-Erofeev; n=4	$4(1-\alpha)[- \ln(1-\alpha)]^{3/4}$	$[- \ln(1-\alpha)]^{1/4}$

1.5.2 Coats-Redfern method

The Coats-Redfern method is an integral model-fitting approach for non-isothermal reactions. It can be used to calculate frequency factor and activation energy. The rate of reaction is expressed as:

$$\frac{d\alpha}{dT} = k(t)(1 - \alpha)^n \quad (1.20)$$

Arrangement of Eq. (1.20) becomes:

$$\frac{d\alpha}{(1 - \alpha)^n} = \frac{A}{\beta} \exp\left(-\frac{E_a}{RT}\right) dT \quad (1.21)$$

Integration of Eq. (1.21) is:

$$\frac{1 - (1 - \alpha)^{1-n}}{1 - n} = \frac{A}{\beta} \int_0^T \exp\left(-\frac{E_a}{RT}\right) dT \quad (1.22)$$

Eq. (1.22) can be simplified by using asymptotic series and ignored higher order terms, and integrated it gives:

$$\frac{1 - (1 - \alpha)^{1-n}}{1 - n} = \frac{ART^2}{\beta E_a} \left[1 - \frac{2RT}{E_a} \exp\left(-\frac{E_a}{RT}\right)\right] \quad (1.23)$$

After taking logarithm of Eq. 1.23 gives:

$$\ln\left[\frac{1 - (1 - \alpha)^{1-n}}{(1 - n)T^2}\right] = \ln\left[\frac{AR}{\beta E_a} \left[1 - \frac{2RT}{E_a}\right]\right] - \frac{E_a}{RT} \quad \text{for } n \neq 1 \quad (1.24)$$

$$\ln\left[\frac{-\ln(1 - \alpha)}{T^2}\right] = \ln\left[\frac{AR}{\beta E_a} \left[1 - \frac{2RT}{E_a}\right]\right] - \frac{E_a}{RT} \quad \text{for } n = 1 \quad (1.25)$$

After simplification of Eq. (1.25) in case of $2RT \ll 1$ becomes:

$$\ln\left[\frac{g(\alpha)}{T^2}\right] = \ln\left(\frac{AR}{\beta E_a}\right) - \frac{E_a}{RT} \quad (1.26)$$

A straight line can be obtained by plotting $\ln[g(\alpha)/T^2]$ versus $1/T$. The slope gives $-E_a/R$, and the intercept is $\ln(AR/\beta E_a)$; therefore, E_a and A values can be derived from Eq. (1.26) [80, 83, 85, 86].

2. MATERIALS AND METHODS

2.1 Experimental Studies

The flow chart of experimental studies was shown in Figure 2.1.

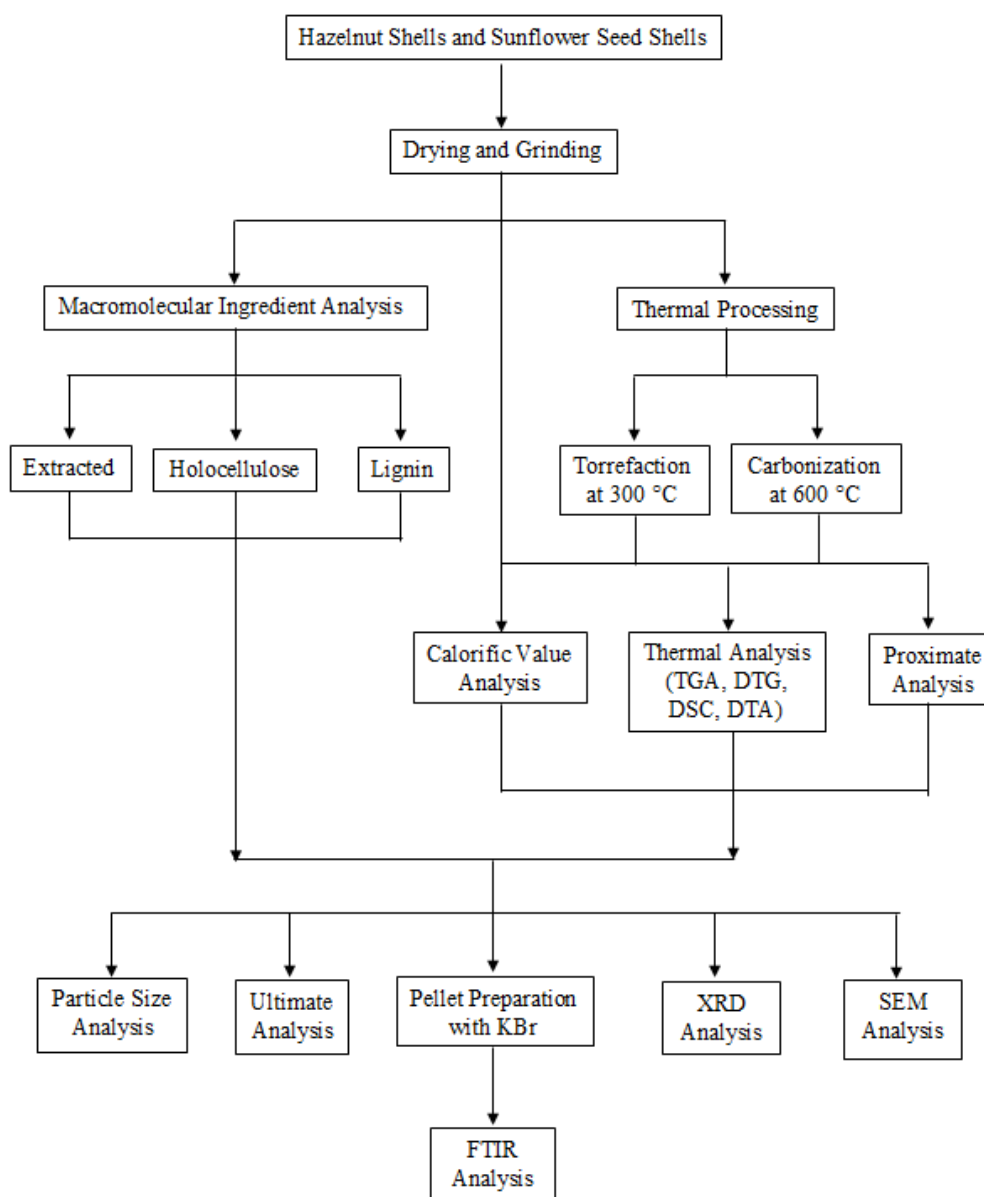


Figure 2.1 : The flowchart of experimental studies.

2.2 Sample Preparation

In this study, hazelnut shells (HS) and sunflower seed shells (SSS) were used as biomass samples. The samples were first dried in laboratory medium, and then in oven at 105 °C. After being drying step, they were milled, and sieved to a powder with a particle size of under 0.250 mm. The Retsch AS 200 was used as equipment to sieve samples. All analyses carried out to the samples were performed according to ASTM standards.

2.3 Macromolecular Ingredients Analysis

Extractive analysis was carried out according to ASTM D1105 [87] standard to determine macromolecular composition of each sample. Holocellulose content that is the sum of cellulose and hemicellulose contents was isolated according to reference [88]. Furthermore, van Soest method was performed to isolate lignin from each sample [89]. The obtained lignin is referred as ‘Klason Lignin’ which is insoluble in acids.

2.4 The Thermal Analyses (TGA, DTG, DTA, DSC)

The thermal analyses were carried out to determine the characterization of decomposition by using equipment SDT Q600 model of TA that is shown in Figure 2.2. The TGA (Thermogravimetric Analysis), DTG (Derivative Thermogravimetric), DTA (Differential Thermal Analysis) and DSC (Differential Scanning Calorimetry) curves can be obtained via that equipment. The stoichiometry of decomposition and the temperature range of reaction can be obtained from the TG curve. The onset of decomposition can be determined more sensitively from DTG curve compared to TG curve, and the maximum rate of decomposition can also be obtained. Furthermore, the temperature difference between the sample and thermally inert reference (alumina) can be determined from DTA curve to specify endothermic and exothermic transformations. The enthalpies of transition can be obtained from DSC curve. The thermal analysis equipment has Pt-Pt/Rh thermocouple, and its operating temperature can be set up to 1773 K.



Figure 2.2 : TA instruments, model SDT Q600.

In this study, each of main biomass and bio-char sample was weighted around 10 mg, and heated up to 600 °C with a heating rate 5 °C/min under dry air and pure oxygen (oxy-combustion) atmospheres with a flow rate of 100 mL/min. The samples were kept at that temperature for 30 min. The TG, DTG, DTA and DSC profiles were obtained. The ignition temperature of each sample was determined from DTA curve, and the maximum rate of combustion and the temperature at this rate, combustion time and combustion efficiency were obtained from DTG profile.

2.5 The Torrefaction and Carbonization Experiments in a Horizontal Tube Furnace

The horizontal tube furnace is made from stainless steel, and the size of combustion unit is 15cm x 72cm. The inner diameter of ceramic combustion unit (tube) is 5 cm. The equipment was shown in Figure 2.3. Each sample was weighted approximately 10 g. The horizontal tube furnace experiments were carried out at 300 °C and 600 °C with 10 °C/min heating rate under a nitrogen atmosphere with a flow rate 100 mL/min. Following this step, the samples were kept at these temperatures for 60 min in order to produce the torrefied and carbonized biochars by decreasing the content of the volatile matter.



Figure 2.3 : Horizontal tube furnace.

2.6 Characterization of Samples

2.6.1 Proximate analysis

The proximate analysis was used to determine the volatile matter, fixed carbon, moisture and ash contents of each sample. It was carried out by TGA equipment which is shown in Figure 2.2. Firstly, each biomass or bio-char sample was weighted approximately 10 mg, and then they were first heated to 105 °C with heating rate 10 °C/min under nitrogen atmosphere condition with flow rate 100 mL/min. Samples were kept at that temperature for 10 min in order to remove the moisture content. After that the sample was heated up to 900 °C with heating rate 40 °C/min under nitrogen atmosphere condition with flow rate 100 mL/min. Following this stage, the sample was kept at this temperature for 7 min in order to eliminate the volatile mater content. The temperature was decreased to 600 °C with cooling rate of 20 °C/min under nitrogen flow of 100 mL/min. Then, the sample was kept at this temperature under dry air with flow rate 100 mL/min until the weight of sample was constant. The remaining weight showed the ash content.

2.6.2 Calorific value analysis

The calorific value analysis was carried out to each biomass and produced bio-char sample by using IKA C2000 Basic Calorimeter, which has stainless steel calorimeter bomb and is shown in Figure 2.4. As a result of this analysis, the higher calorific value for each sample was obtained.



Figure 2.4 : IKA C2000 Basic Calorimeter Bomb.

2.6.3 Particle size analysis

The particle size analysis was carried out to all samples by using Malvern InstrumentsTM Mastersizer 2000 particle sizing instrument with Hydro 2000G wet sample dispersion unit which is shown in Figure 2.5. This method is based on a laser diffraction to measure the size of particles. It measures the intensity of light which is scattered a laser beam passing through a dispersed particulate sample.



Figure 2.5 : Malvern InstrumentsTM Mastersizer 2000 particle sizing instrument.

2.6.4 Scanning electron microscopy (SEM) analyses

The Scanning Electron Microscope (SEM) is a type of electron microscope which produces images of sample with high resolution by focused beam of electrons. In this study, the structural differences of all biomass samples, their macromolecular components and produced bio-chars were investigated by using Jeol, JSM-6000 instrument.

2.6.5 Ultimate analysis

The ultimate analysis was performed to all samples by using Leco TruSpec® CHN ultimate equipment with Leco TruSpec® S module which is shown in Figure 2.6. Firstly, around 0.5 g sample was weighted. There are three phases which are purge, combust and analysis during an analysis cycle. In the purge phase, the encapsulated sample was placed in the loading head, sealed and purged of helium gas which entered during sample loading. In the combust phase, the sample was dropped into a hot furnace kept at 950 °C and flushed with oxygen to complete the combustion rapidly. The products of combustion were passed through a secondary furnace called as afterburner at 850 °C to perform secondary oxidation and remove the unburned particulates. The combustion gases were then collected in a collection vessel known as the ballast. In the analyze phase, oxygen flows into the furnace to combust the sample. After that, the produced gases were collected in the ballast. The homogeneous combustion gases in the ballast were purged through the CO₂ and H₂O infrared detectors and the 3cc aliquot loop. Carbon was measured as CO₂ by CO₂ detector; while, hydrogen was measured as vapor by H₂O detector. The gases in the aliquot loop were transferred to the helium carrier flow, swept through hot copper to remove oxygen and reduce NO_x to N₂. After that, they flow through Lecosorb and Anhydron to remove CO₂ and H₂O, respectively. The nitrogen content was determined by a thermal conductivity cell. The sum of carbon, hydrogen, nitrogen, sulfur and ash contents on dry basis was subtracted from 100 to calculate elemental oxygen content.



Figure 2.6 : Leco TruSpec® CHN model elemental analysis instrument.

2.6.6 X-ray diffraction (XRD) analysis

X-Ray Diffraction (XRD) analysis examines crystalline material structure which contains atomic arrangement, crystallite size and imperfections. In this experiment, all biomass samples, their macromolecular components and produced biochar samples were characterized by using Panalytical X'Pert Pro PW 3040/60 model X-Ray diffractometer with a Cu X-ray target radiation of wavelength 1.54060 \AA under 40 kV and 40 mA conditions.

2.6.7 Fourier transform infrared (FTIR) spectroscopy analysis

Fourier Transform Infrared Spectroscopy (FTIR) is an analytical technique to determine mainly organic substances. The main principle is the absorption of infrared radiation by chemical bonds; therefore, molecular structure of sample can be determined.

In this experiment, all biomass samples, their macromolecular components and produced bio-char samples were ground with KBr (potassium bromide) with a proportion of 1:100 w/w in a dry agate mortar. The spectrum of KBr was used for background correction in order to remove interfering peaks arising from atmospheric water and carbon dioxide. Each sample was pressed between two 13 mm disks under 8 MPa pressure to produce pellet. FTIR analysis of each sample was carried out by using Bruker Alpha FTIR instrument with measurement of frequency interval between 650 and 4000 cm^{-1} . All functional groups were determined according to literature values.

3. RESULTS AND DISCUSSION

3.1 Characterization of Main Samples

3.1.1 Proximate analysis results

Proximate analysis results were determined from the TGA profiles obtained through the sequential heating process described in section 2.6.1. TGA profiles used for proximate analyses result are illustrated in Figures 3.1 and 3.2 for sunflower seed shells and hazelnut shells, respectively.

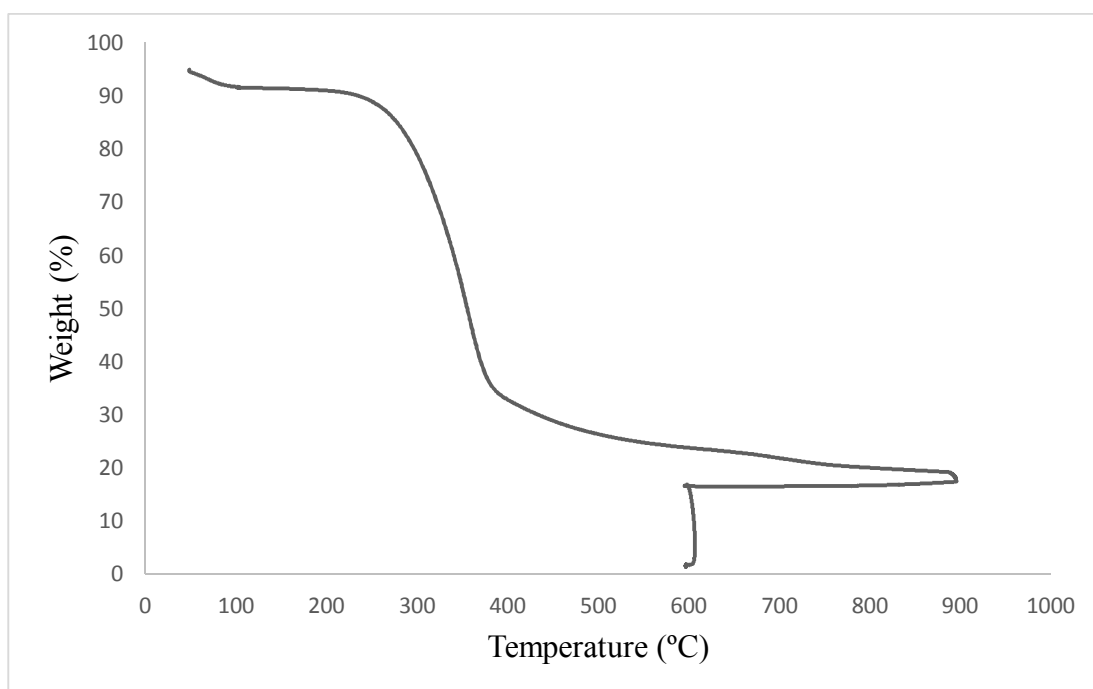


Figure 3.1 : The proximate analysis TGA profile of SSS.

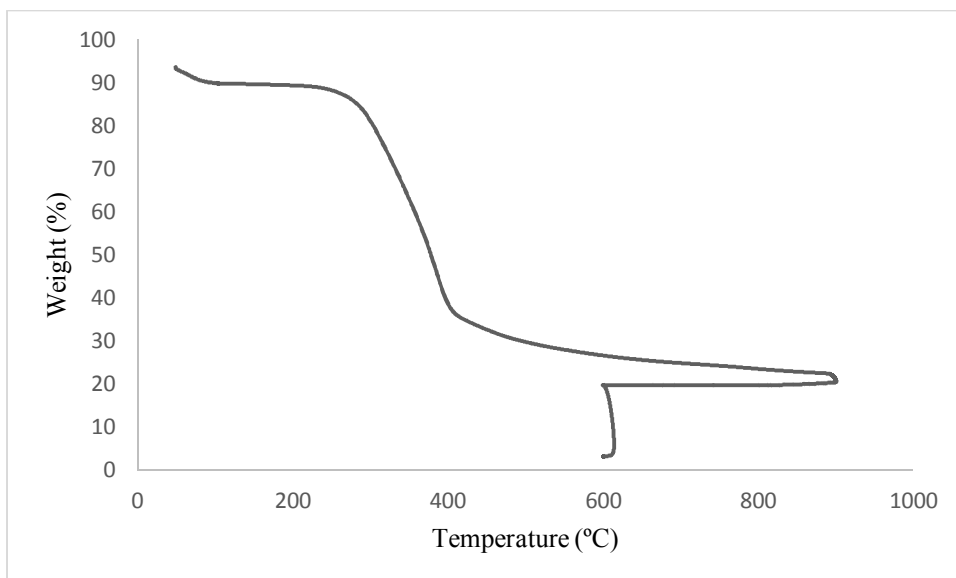


Figure 3.2 : The proximate analysis TGA profile of HS.

Proximate analysis results derived from these curves along with the higher heating values (HHV) determined from the bomb calorimeter experiments are given in Table 3.1.

Table 3.1: The proximate analysis and HHV results.

Sample	Proximate Analysis				HHV (cal/g)
	Moisture (%)	Volatile Matters (%)	Ash (%)	Fixed Carbon (%)	
Sunflower seed shells	8.44	74.12	1.61	15.83	4357
Hazelnut shells	10.21	69.39	3.13	17.27	4359

Results in Table 3.1 indicate that the moisture, volatile matters, and fixed carbon contents of the main samples are comparable with each other, while ash contents differ to some extent. Nevertheless, HHV values of the samples are almost the same. Basing on data in Table 3.1, it is likely to mention that the ratios of fixed carbon to volatiles are rather low in comparison to those in coal samples, and these ratios are 0.21 and 0.25 for sunflower seed shells and hazelnut shells, respectively.

3.1.2 Macromolecular analysis results

The results of the analytical experiments applied to specify the macromolecular components of the main biomass samples are shown in Table 3.2.

Table 3.2 : Macromolecular analysis results of the main samples (on dry basis).

Sample	Extractive substance (%)	Holocellulose (%)	Lignin (%)
Sunflower seed shells	5.27	67.12	27.06
Hazelnut shells	4.50	56.63	40.03

Holocellulose that is the sum of cellulose and hemicellulosics accounts for most of the organic structure of the biomass samples. Of these, sunflower seed shell is highly rich in holocellulose, while lignin is considerably less than holocellulose in this biomass. This predicts that sunflower seed shell will be very reactive during any thermal conversion process due to its high holocellulose content and relatively low lignin content [8]. On the other hand, although the holocellulose content in hazelnut shell is also higher than the lignin content, holocellulose to lignin ratio is not comparable with that in case of sunflower seed shell. Accordingly, it can be expected that hazelnut shells will not as reactive as sunflower seed shells during the thermal conversion processes. Besides both biomass species have extractive substances in the range of 4.50-5.27 wt % that are resulted from elimination of not only organics but also soluble inorganics from biomass over extraction in which ethyl alcohol, benzene, and warm water were used. Meszaros et. al. [90] reported that treatment even hot water is capable of removing some inorganics as well as some unsteady organic compounds from biomass species.

3.2 Effects of Torrefaction and Carbonization Processes

3.2.1 Effects on sample characteristics and fuel quality

Thermally treated biomass samples (chars) in the horizontal furnace at 300 °C and/or 600 °C as described in section 2.5 were removed from the furnace and kept in tightly closed small bottles in a desiccator to avoid moisture uptake. The thermally treated samples, namely torrefied at 300 °C or carbonized at 600 °C, were first compared according to proximate and ultimate analyses. TGA curves that used for determination of the proximate analysis results of the biochar samples are given in Figures 3.3-3.6.

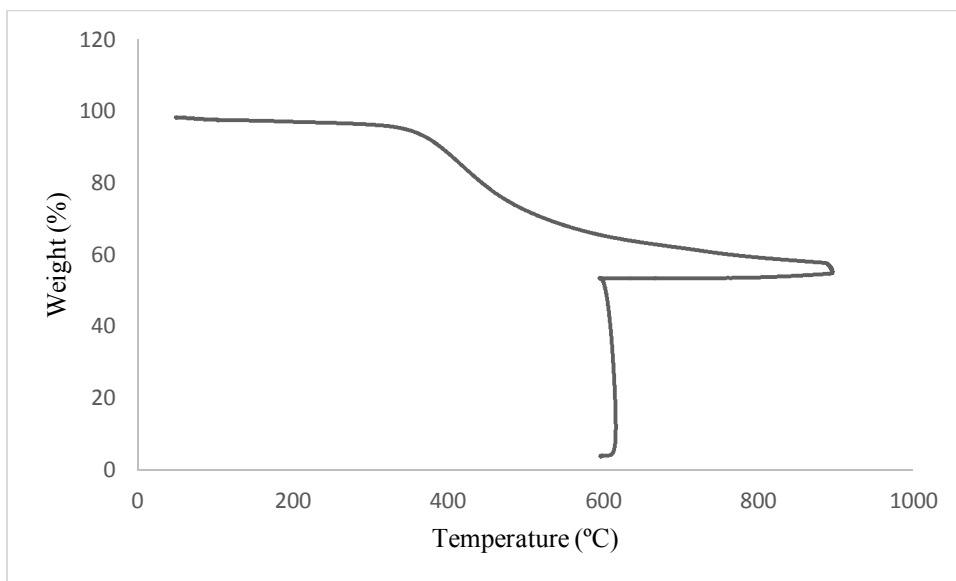


Figure 3.3 : The proximate analysis TGA profile of SSS biochar at 300 °C.

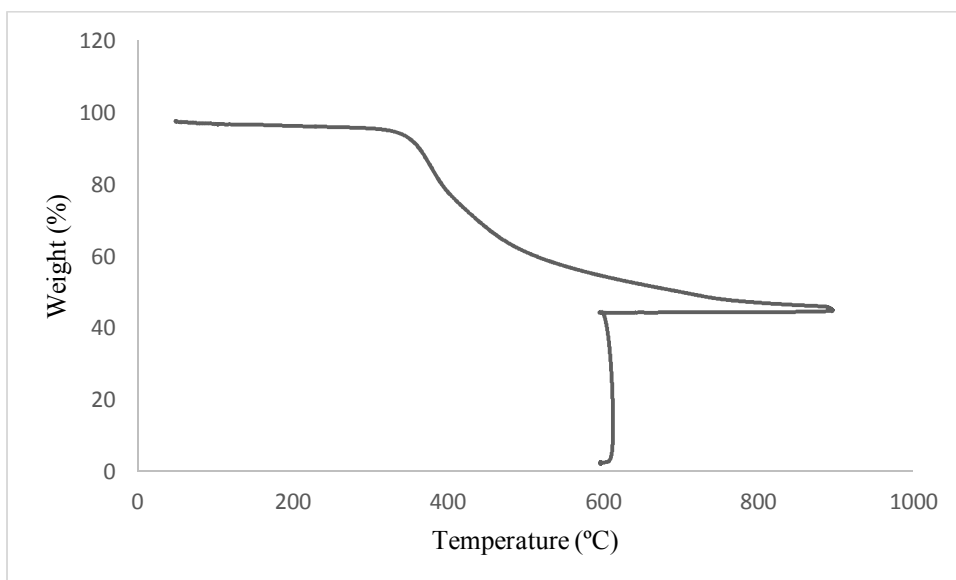


Figure 3.4 : The proximate analysis TGA profile of HS biochar at 300 °C.

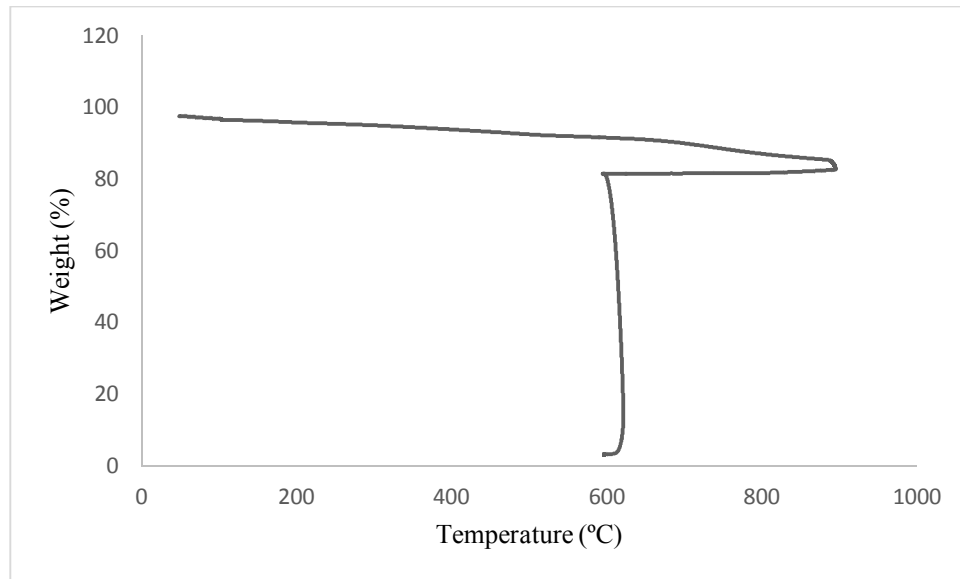


Figure 3.5 : The proximate analysis TGA profile of SSS biochar at 600 °C.

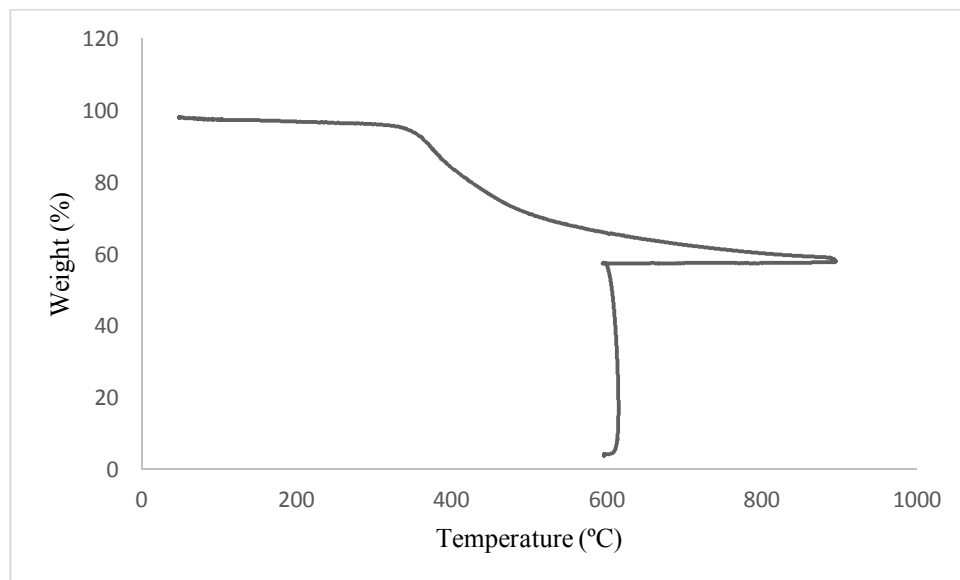


Figure 3.6 : The proximate analysis TGA profile of HS biochar at 600 °C.

Since, the thermal treatments yield fairly dried samples, for a reasonable comparison of the changes in the structures of the biomass samples due to thermal treatment, the proximate analysis results are tabulated in Table 3.3 on dry basis for the treated samples as well as their parent samples.

Table 3.3: Proximate analysis and HHV results on dry basis.

Sample	Volatile Matter (%)	Ash (%)	Fixed Carbon (%)	HHV (cal/g)
Sunflower seed shells	80.95	1.76	17.29	4357
Sunflower seed shells biochar at 300 °C	43.78	3.89	52.34	6579
Sunflower seed shells biochar at 600 °C	14.29	3.17	82.54	7556
Hazelnut shells	77.28	3.49	19.23	4359
Hazelnut shells biochar at 300 °C	53.79	2.47	43.74	6356
Hazelnut shells biochar at 600 °C	40.62	4.01	55.37	6754

Table 3.3 confirms the fact that the thermal treatments applied in this study led to significant variations in biomass samples. Consequently, the ratios of fixed carbon to volatiles increased seriously, and this increase was very apparent in case of carbonization implemented at 600 °C. Namely, volatile matter content decreased from 80.95 % to 14.29 % for sunflower seed shells, while its fixed carbon content enhanced from 17.29 % to 82.54 % which is nearly five-fold. That's why the thermal processes conducted at medium to ambient temperature intervals under non-oxidizing conditions are called as "carbonization". Meanwhile, holocellulose-rich nature of this biomass facilitated decompositions at 600°C to give off volatiles, leaving the fixed carbon as the left over the applied process. Besides, the ash content became relatively concentrated as a result of such a significant decrease in volatiles.

The increase in fixed carbon content and the decrease in volatiles content were relatively limited in case of hazelnut shell. It is possible to mention that the performances of the applied thermal treatments were affected from the distributions of the macromolecular compounds found in biomass species. That is, hazelnut shell contains a great deal of amount of lignin in its complex structure, and lignin is not as thermally reactive as the holocellulose content. Hence, the treatments at either 300 °C or 600 °C could not provide high levels of devolatilization. For this reason, in proximate analysis, solid fuels are heated up to 900 °C for completely removal of the volatiles. Basing on these findings, it can be reported that 600 °C is not so effective to provide efficient removal of the volatile matter from hazelnut shell, and exposure to higher carbonization temperatures may be suggested for this biomass species.

Depending on the improving fuel quality of the biomass species, calorific values also increased thanks to the thermal treatments including torrefaction and carbonization. The increase in the calorific value was very obvious in case of sunflower seed shell due to efficient removal of the volatiles. However, the high content of volatiles even in case of carbonized biochar from hazelnut shell led to relatively less improvement in the calorific value. Nevertheless, the calorific values of the biochars were in so fairly good level that they can be comparable with the calorific values of high quality bituminous coals.

3.2.2 Ultimate analysis results

Ultimate analysis results can be seen in Table 3.4. These results show that the applied processes improved the fuel qualities of the biomass samples by increasing carbon contents and lowering oxygen contents. These variations are more evident in case of sunflower seed shell. On the other hand, hydrogen contents also decreased due to thermal treatments and it is known that the level of the decrease in the hydrogen content is a reliable parameter to predict the severity of the applied thermal process [91]. Similarly, increase in carbon and decrease oxygen may also be used for this purpose since there is reasonable relation between the temperatures of the applied processes and the measured contents of these parameters.

Table 3.4 : Ultimate analysis results (on dry basis)

Sample	C (%)	H (%)	N (%)	S (%)	O* (%)
Sunflower seed shells	45.7	6.4	0.4	0.2	45.5
Sunflower seed shells char at 300 °C	66.8	5.1	0.5	0.1	23.6
Sunflower seed shells char at 600 °C	82.6	2.3	0.7	0.1	11.1
Hazelnut shell	46.2	6.4	0.1	0.3	43.6
Hazelnut shell char at 300 °C	62.8	5.2	0.1	0.1	29.5
Hazelnut shell char at 600 °C	70.0	4.5	0.1	0.1	21.3

* calculated by difference

These explanations show that the thermal treatments applied in this study gave rise obvious improvements in the quality of biomass as fuel with respect to lowering

moisture, oxygen and volatile matter contents, and increasing carbon, fixed carbon content and calorific value.

3.2.3 Effects on burning characteristics

3.2.3.1 Burning of the main samples with dry air

Figure 3.7 shows the DTG burning profile of sunflower seed shells which presents the rates of the mass losses from the sample versus temperature.

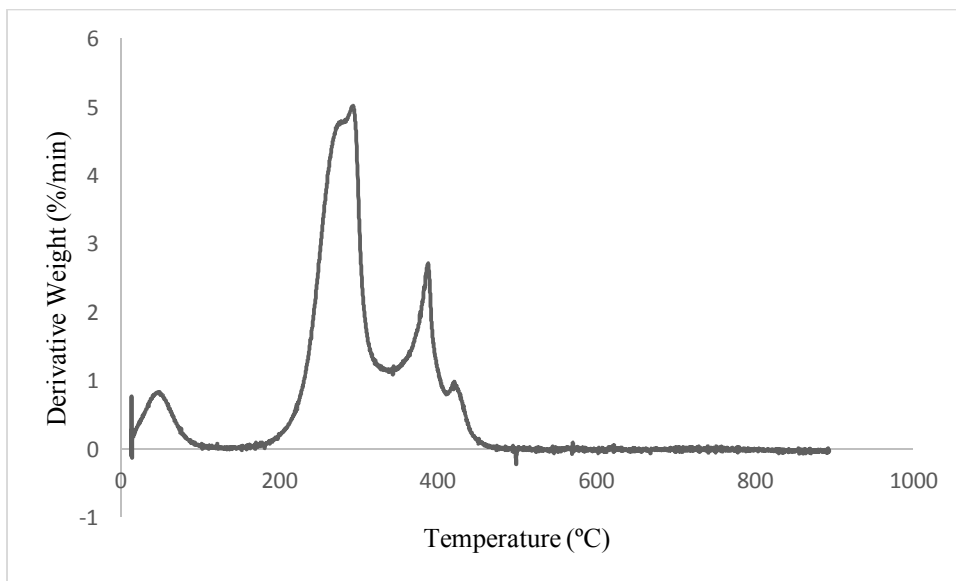


Figure 3.7 : The burning DTG profile of SSS main sample under dry air.

As temperature increases from the room temperature up to 900 °C, a couple of different mechanisms governed the mass losses from the sample depending on temperature. Namely, moisture content left the structure first at around 100°C, and then a region was observed in temperature interval of 100-200 °C in which no important decomposition occurred. Then, the main decomposition stage started just before 200 °C, and the rate of the mass losses reached the maximum level (R_{max}) of 5.02 %/min at 293 °C (T_{Rmax}) and then slowed down until a second acceleration between 350 °C and 400 °C. Finally, mass losses completed at 472 °C and no further reduction took place in the mass up to 900°C. Although TGA and DTG curves provide valuable information on the mass loss characteristics from the sample at given temperatures, it is impossible to decide that whether the mass losses resulted from burning or devolatilization. In this context, DTA and DSC curves help us to evaluate the endothermic and exothermic phenomena taken place throughout the burning

process. DTA and DSC curves of sunflower seed shell are given in Figures 3.8 and 3.9, respectively.

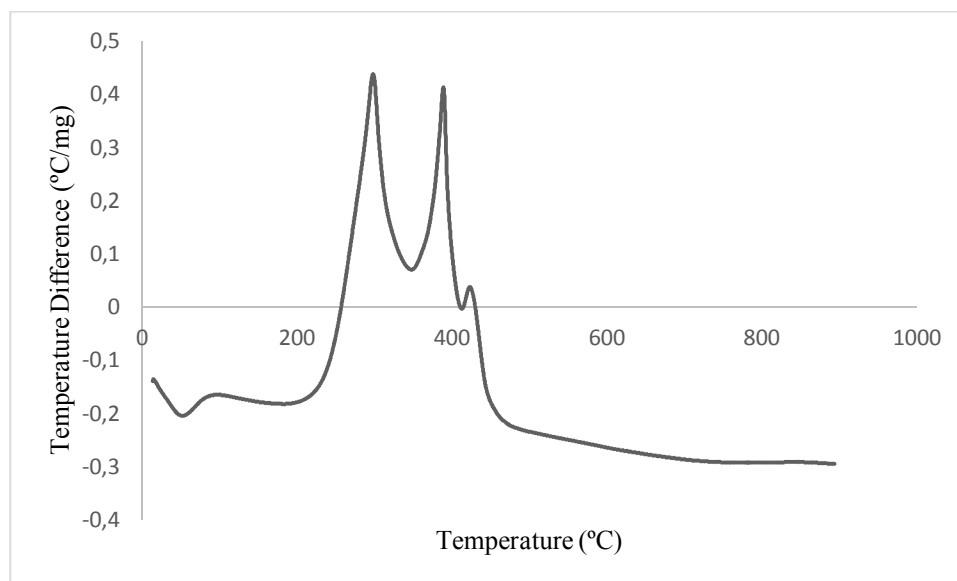


Figure 3.8 : The burning DTA profile of SSS main sample under dry air.

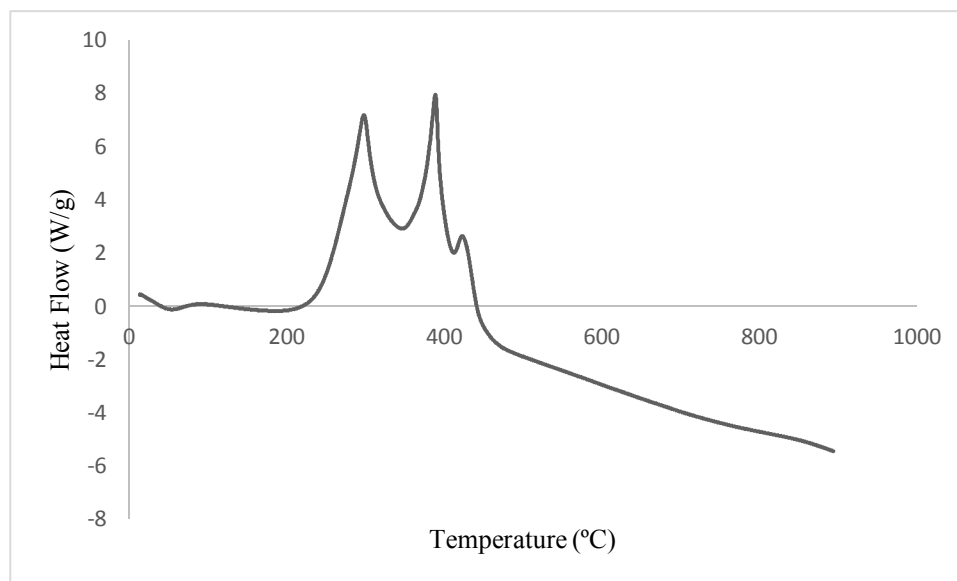


Figure 3.9 : The burning DSC profile of SSS main sample under dry air.

DTA curve indicates that the previously mentioned mass losses seen in DTG curve just before 200 °C did not result from burning of the sample because during which the process was not exothermic. This predicts the fact that hemicellulose and some unsteady ingredients in biomass began to decompose at these relatively low temperatures and their removal was the source of the mass losses. Actually, the onset of burning was detected as 261 °C at which ignition of combustible volatiles took place and it was homogeneous burning in gaseous phase. Therefore, mass losses suddenly

increased and reached the maximum point. During the devolatilization and subsequent burning of the volatiles, the biomass turned into sponge-like porous structure through which oxygen diffused to burn the remaining solid matrix by heterogeneous burning. Therefore, another individual exothermic peak formed at higher temperature region in comparison to the previous homogeneous burning region. The end point of burning was determined as 408 °C. On the other hand, the endothermic character of the process beyond the end point can be interpreted by the heat capacity of the ash forming minerals and their phase transitions.

DSC profile indicates the extent of the heat flows during the endothermic and exothermic transitions comparatively. The heat flowing from surrounding to the sample is known as endothermic; whereas, from the sample to surrounding is called as exothermic. According to Figure 3.9, it can be regarded that the burning of sunflower seed shells main sample started after 200 °C since the heat flow values turned from negative to positive ones.

Burning characteristics of hazelnut shell main sample under dry air atmosphere are given in Figures 3.10-3.12.

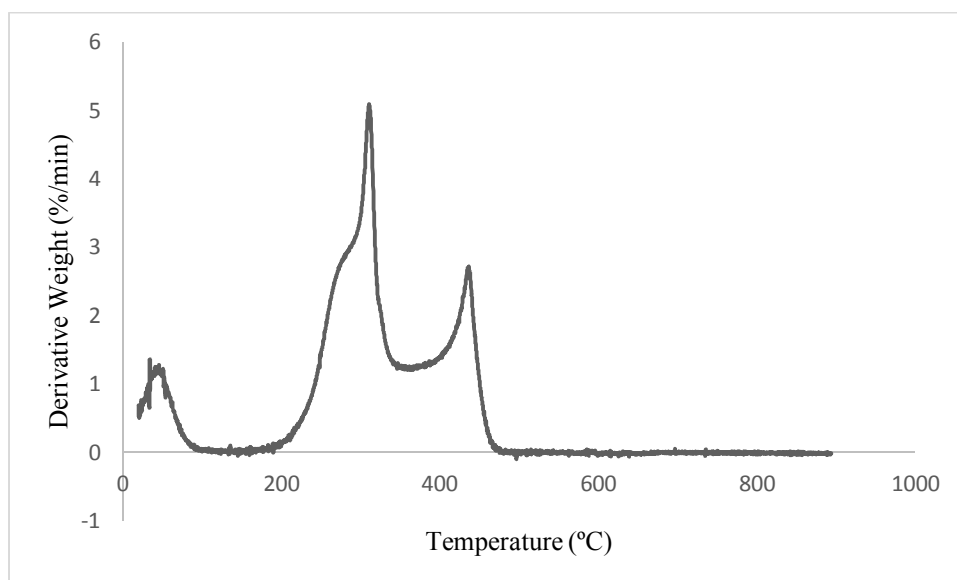


Figure 3.10 : The burning DTG profile of HS main sample under dry air.

DTG burning profile of hazelnut shell main sample is basically similar to that for sunflower seed shell in terms of the sequence of the stages of moisture evolution, volatile matter evolution and its burning, followed by surface oxidation of the remaining mass. R_{\max} and $T_{R\max}$ were detected as 5.1 %/min and 311 °C, respectively.

Comparison of these R_{\max} and $T_{R_{\max}}$ values with those for sunflower seed shell revealed the fact that although R_{\max} values are very close to each other, $T_{R_{\max}}$ value for sunflower seed shell was 293 °C that is a bit lower than that for hazelnut shell. This indicates that the thermal reactivity of hazelnut shell is lower than sunflower seed shell which in good agreement with the high lignin content of hazelnut shell. Likewise, DTA and DSC curves of hazelnut shell also indicate that exothermic region shifted to higher temperatures. That is, both the onset temperature and the end point of burning were found as 290 °C and 449 °C, respectively, which are considerably higher than those measured for sunflower seed shell. In addition, the heat flow changed between 8 W/g and -6 W/g for burning of hazelnut shells main sample. The negative values can be attributed to the energy need of the mineral matter to be decomposed thermally while temperature increases.

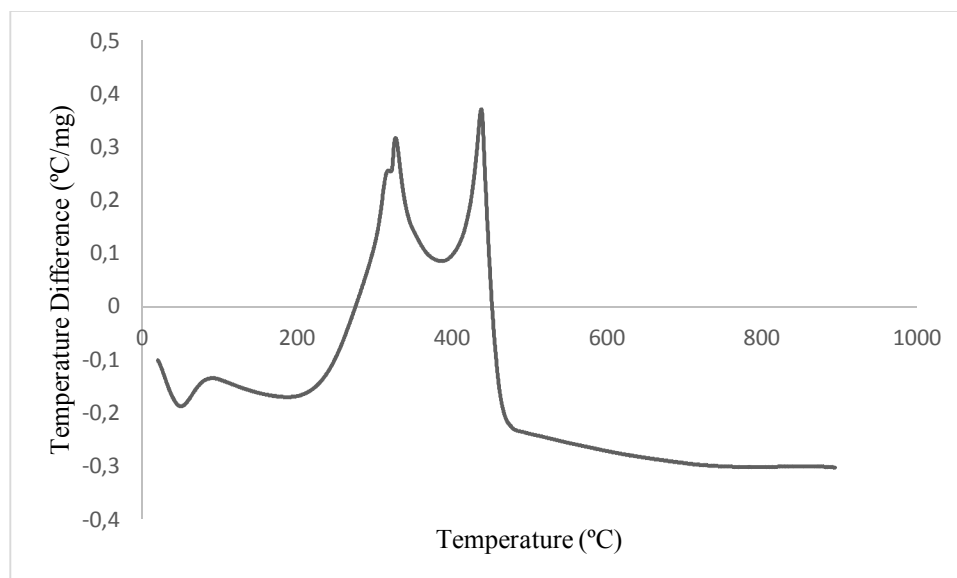


Figure 3.11 : The burning DTA profile of HS main sample under dry air.

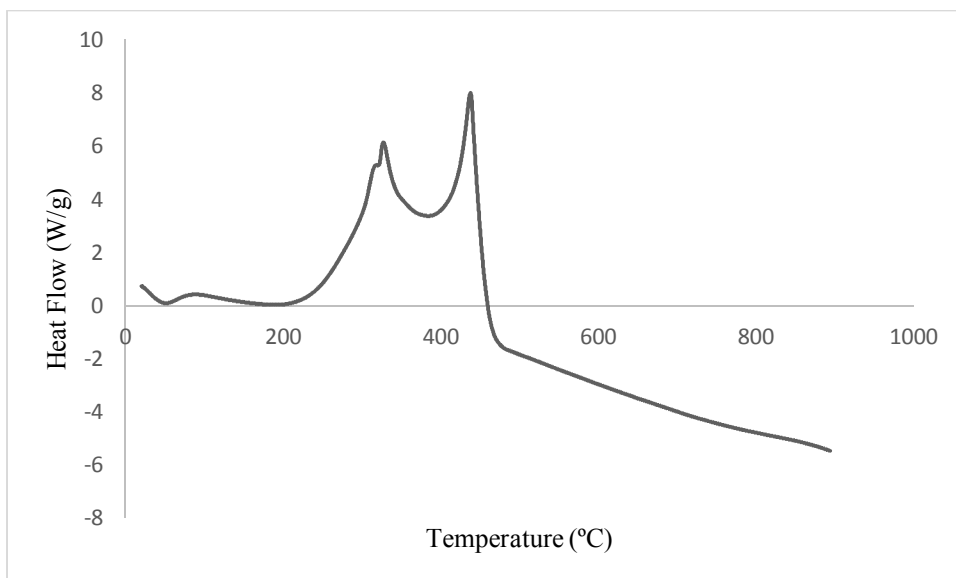


Figure 3.12 : The burning DSC profile of HS main sample under dry air.

Table 3.5 summarizes the results derived from DTG and DTA curves of the main samples under dry air.

Table 3.5 : The results from DTG and DTA of the main samples under dry air.

Sample	from DTG curves		from DTA curves		
	R_{\max} (%/min)	$T_{R_{\max}}$ (°C)	Onset Temp. of Burning (°C)	ΔT_{\max} (°C/mg)	End Point of Burning (°C)
Sunflower seed shell	5.02	293	261	0.44	408
Hazelnut shell	5.10	311	290	0.37	449

3.2.3.2 Burning of the main samples with pure oxygen

Burning of the main biomass samples in the thermal analyzer using pure oxygen was carried out under the conditions that are the same with those of burning with dry air except the change in the oxidizing medium from dry air to pure oxygen. DTG burning profile of sunflower seed shell main sample under pure oxygen is shown in Figure 3.13. At the first sight, the most apparent effect of the usage of pure oxygen over dry air is that the rates of the mass losses in the volatile matter evolution and homogeneous combustion regions increased when pure oxygen was used. Namely, the value of R_{\max} enhanced to 5.97, while it was 5.02 under dry air atmosphere. In addition, this rate was measured at 264 °C which is lower than the corresponding temperature of 293 °C in case of dry air usage. The parameters of R_{\max} and $T_{R_{\max}}$ reveal that when pure oxygen

was used, decomposition of sunflower seed shell became faster even at low temperatures.

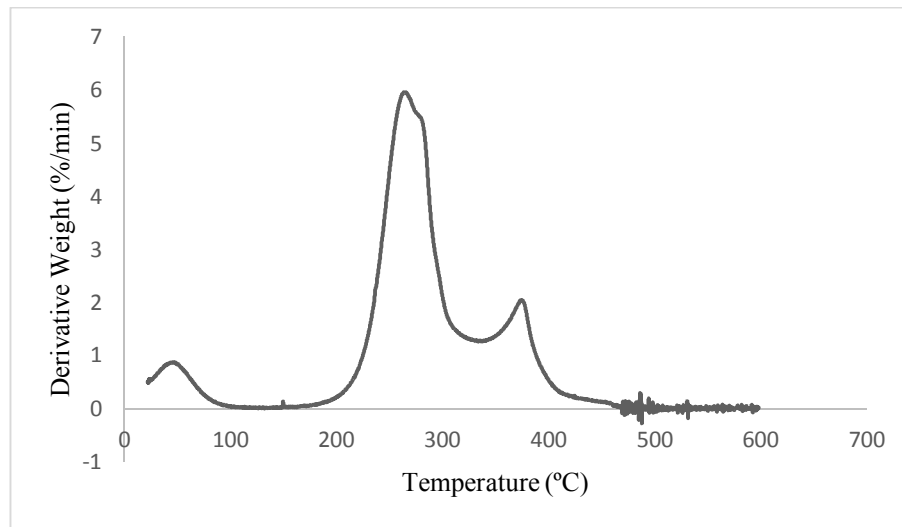


Figure 3.13 : The burning DTG curve of SSS under pure oxygen.

DTA and DSC profiles of sunflower seed shell main sample are illustrated in Figures 3.14 and 3.15, respectively.

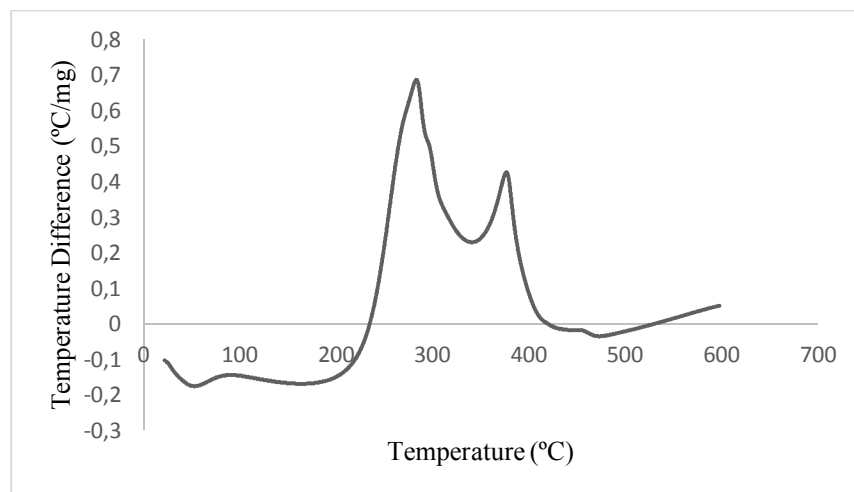


Figure 3.14 : The burning DTA curve of SSS under pure oxygen condition.

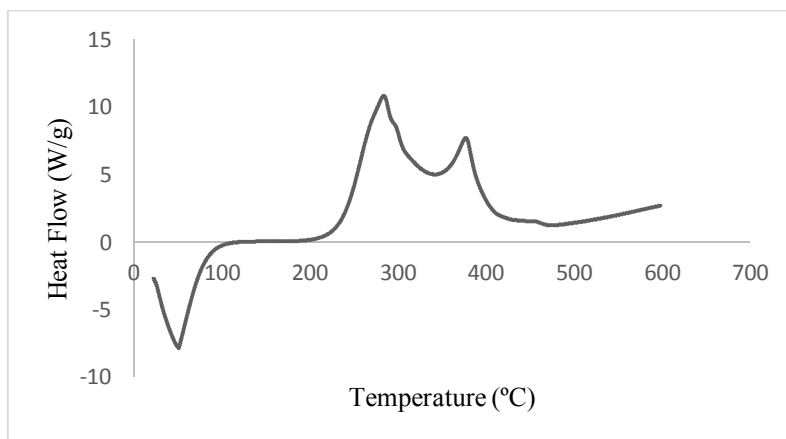


Figure 3.15 : The burning DSC curve of SSS under pure oxygen condition.

DTA and DSC burning profiles of sunflower seed shell supported the outcomes obtained from DTG profile that the onset temperature of burning was 247 °C which is a bit lower than 261 °C that countered in case of burning of this sample with dry air. Besides, the end point of burning also followed this trend that it decreased from 408 °C to 390 °C as a result of the presence of pure oxygen as the oxidant medium. On the other hand, ΔT_{\max} increased from 0.44 °C/mg to 0.69 °C/mg which indicates that more intensive heat production is in question when pure oxygen is utilized in comparison to the dry air usage. In addition, heat flow values increased to over 10 W/g which are higher than those measured in case of burning with dry air. The burning DSC profile of sunflower seed shells is also consistent with the burning of DTA profile.

DTG burning profile of hazelnut shell main sample under pure oxygen is shown in Figure 3.16.

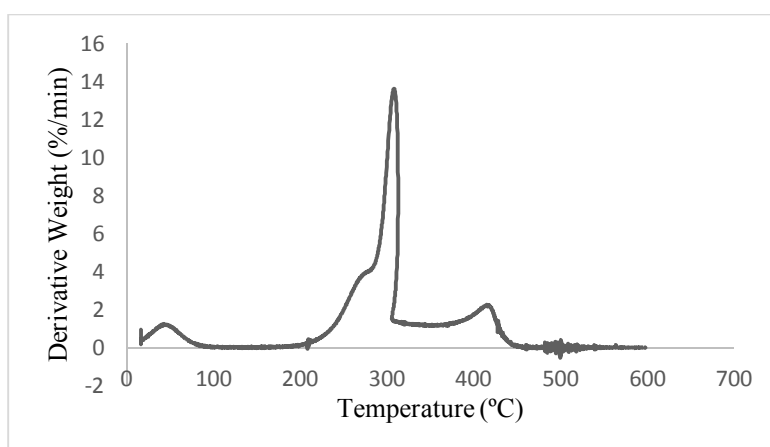


Figure 3.16 : The burning DTG profile of HS under pure oxygen condition.

It is likely to say that the major losses in mass took place in the form of a sharp peak at temperatures around 300 °C. R_{\max} value was observed as 13.65 (%/min) at 308 °C which was nearly three-fold of the R_{\max} value of dry air condition. This result confirms the increasing thermal reactivity not only sunflower seed shell but also hazelnut shell during burning with pure oxygen.

DTA and DSC burning profiles of hazelnut shell main sample under pure oxygen condition are given in Figures 3.17 and 3.18.

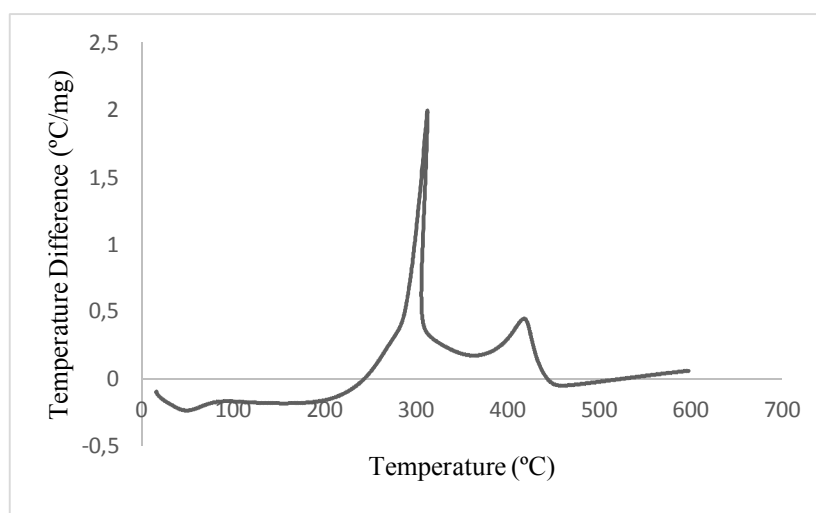


Figure 3.17 : The burning DTA profile of HS under pure oxygen condition.

The appearance of both DTA and DSC curves changed seriously if we compare them with corresponding curves obtained under dry air. The first decomposition region turned into very sharp peak that shows rapid burning of the volatiles. In this context, DTA profile revealed that an enormous increase in ΔT_{\max} value formed for pure oxygen condition. That is, this value was only 0.37 °C/mg for dry air condition and pure oxygen increased it 1.99 °C/mg, which is the proof of the increasing intensity of the heat of combustion. Similarly, maximum point of heat flow from DSC curve intensified several times. The maximum heat flow was approximately 28 W/g at 310 °C in DSC profile of hazelnut shells which was consistent with the DTA profile.

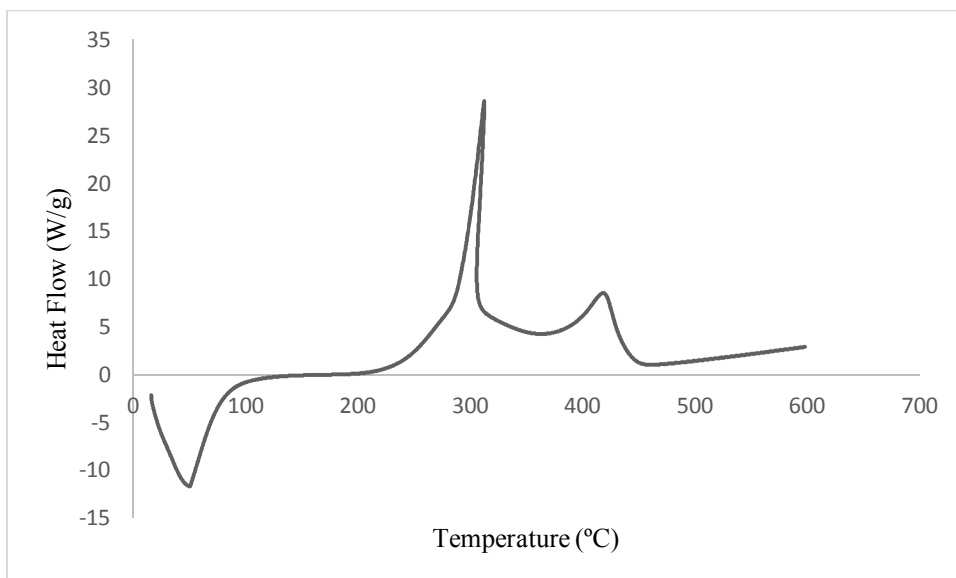


Figure 3.18 : The burning DSC profile of HS under pure oxygen condition.

The results determined from DTG and DTA profiles of the main samples under pure oxygen condition are tabulated in Table 3.6.

Table 3.6 : The results from DTG and DTA of the main samples with pure oxygen.

Sample	from DTG curves		from DTA curves		
	R_{\max} (%/min)	$T_{R\max}$ (°C)	Onset Temp. of Burning (°C)	ΔT_{\max} (°C/mg)	End Point of Burning (°C)
Sunflower seed shells	5.97	264	247	0.69	390
Hazelnut shells	13.65	308	280	1.99	438

3.2.3.3 Burning of the torrefied biochars with dry air

DTG burning profile of the torrefied sunflower seed shells at 300 °C in Figure 3.19 gave so different a shape that we have not seen such a behavior from the previous experiments. Since, some of the volatiles had already been eliminated during the torrefaction process, the volatiles remaining in biomass started to leave the biomass at temperatures which are a bit higher than the temperatures encountered in case of the thermally untreated original biomass samples. Notice that the volatile matter contents on dry basis were 80.95 % in parent sample, and 43.75 % in torrefied biochar. This predicts that a great deal of amount of volatiles still exists in the biochar and it affects the burning character of the biochar.

Moreover, combustion process lasted relatively in a narrow temperature range. Maybe, the most important point is that the extent of R_{\max} reached 26.38 %/min at 394 °C, whereas it was 5.02 %/min at 293 °C for its parent sample (the untreated sunflower seed shell) under dry air condition. In addition to significant increase in the rate, there exists shift of the relevant temperature to the higher temperature.

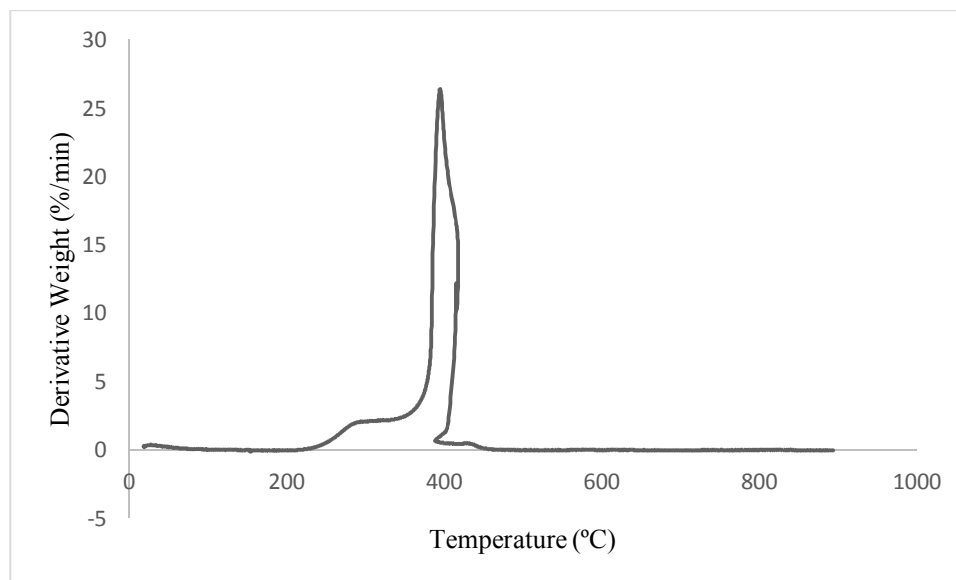


Figure 3.19 : The burning DTG curve of the torrefied SSS under dry air.

DTA and DSC burning profiles of the torrefied sunflower seed shells at 300 °C are presented in Figures 3.20 and 3.21, respectively. It is clear from these figures that the heterogeneous burning of the remaining solid remnant after partially devolatilization is responsible for the exothermic phenomenon. In other words, the contribution of the homogeneous combustion of the volatiles is relatively quiet limited. Therefore, the burning of this biochar is represented by a sharp peak. Furthermore, endothermic region at low temperatures could not be seen in these figures. Additionally, both the onset temperature of burning and the end point temperature are lower than the corresponding temperatures of the parent biomass samples.

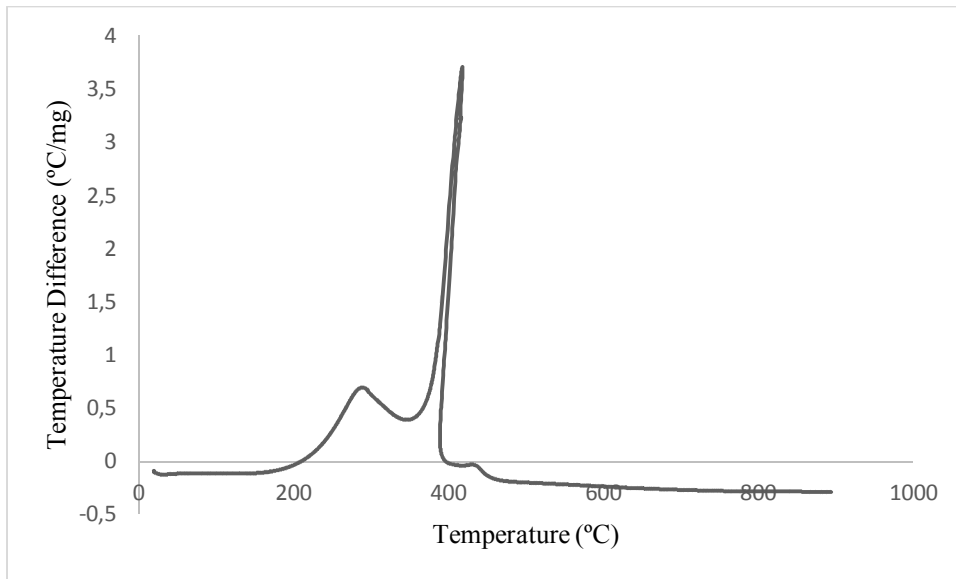


Figure 3.20 : The burning DTA curve of the torrefied SSS under dry air.

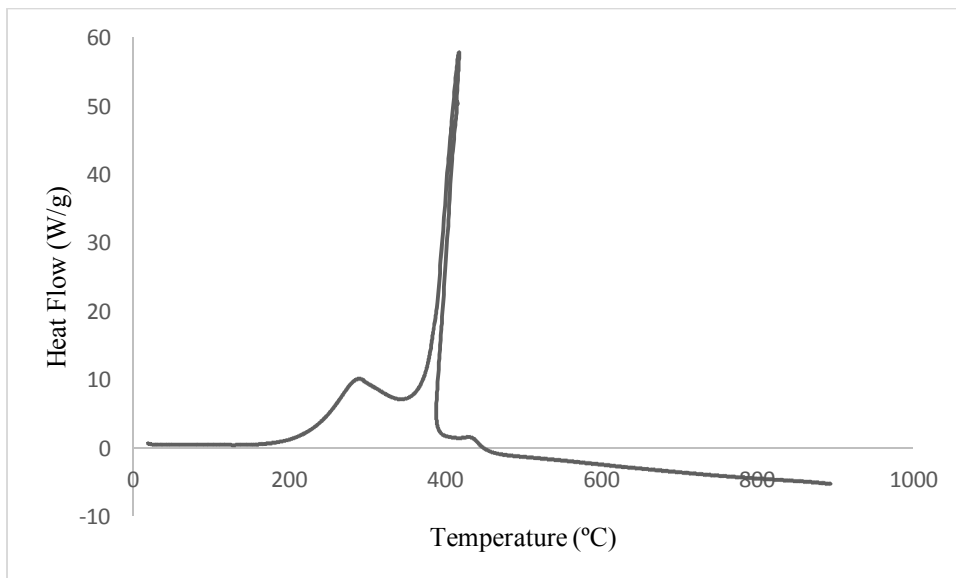


Figure 3.21 : The burning DSC curve of the torrefied SSS under dry air

DTG, DTA, and DSC burning profiles of the torrefied hazelnut shell at 300 °C are given in Figures 3.22, 3.23, and 3.24, respectively, and the explanations made for biochar produced from sunflower seed shell are also valid for the biochar obtained from hazelnut shell. The volatile matter content of torrefied biochar was 53.79 % on dry basis (Table 3.3). However, this initial decomposition is not exothermic and it cannot be regarded as the ignition of the biochar. In fact, the onset temperature of burning was determined as 269 °C from DTA profile, and burning lasted up to 435 °C. Moreover, the heat flow changed between around 58 W/g and -5 W/g, which means higher heat flow in comparison with the untreated samples.

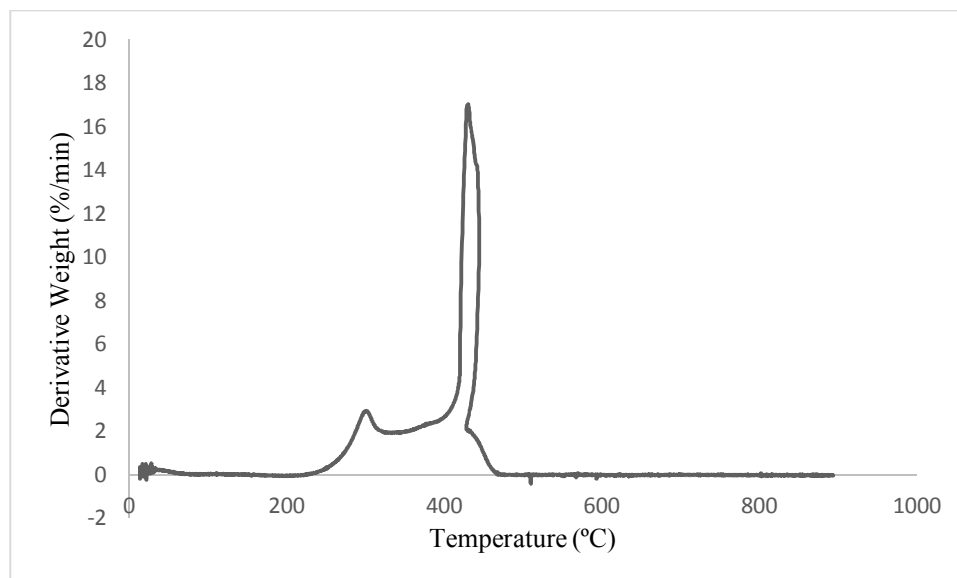


Figure 3.22 : The burning DTG curve of the torrefied HS under dry air condition.

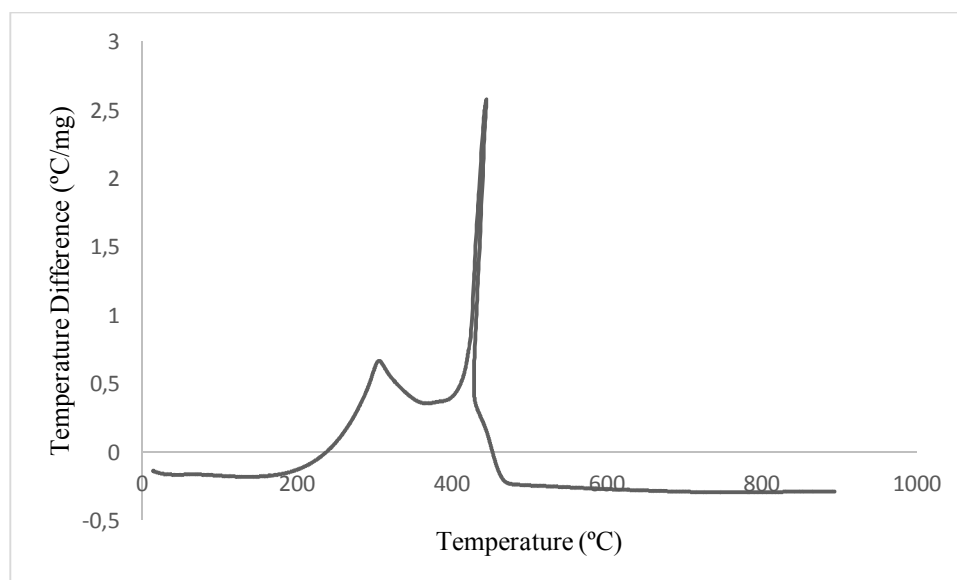


Figure 3.23 : The burning DTA curve of the torrefied HS under dry air.

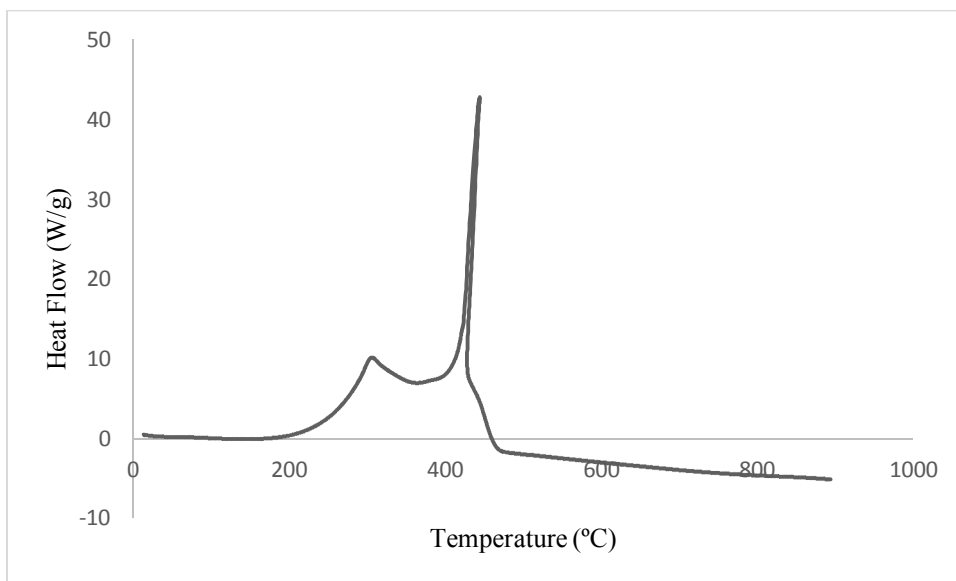


Figure 3.24 : The burning DSC profile of the torrefied HS under dry air.

The summary of these results derived from DTG and DTA burning profiles of the torrefied biochars under dry air condition can be seen in Table 3.7.

Table 3.7 : The results from DTG and DTA of the torrefied biochars with dry air.

Sample	from DTG curves		from DTA curves		
	R_{\max} (%/min)	$T_{R_{\max}}$ (°C)	Onset Temp. of Burning (°C)	ΔT_{\max} (°C/mg)	End Point of Burning (°C)
Biochar at 300 °C from Sunflower seed shells	26.38	394	237	3.70	388
Biochar at 300 °C from Hazelnut shells	17.02	431	269	2.58	435

3.2.3.4 Burning of the torrefied biochars with pure oxygen

DTG, DTA, and DSC burning profiles of the 300 °C biochars from sunflower seed shells using oxygen are shown in Figures 3.25-3.27, respectively. DTG profile indicates that the rates of the mass losses from the biochar is relatively negligible at temperatures lower than approximately 350 °C, and then very large area formed in which very high rates of decomposition were available. Accordingly, exothermic regions in DTA and DSC profiles were right-handed in shape because of the cooling trend of the sample. The real temperature of the sample is considerably higher than the

furnace temperature due to the extremely high burning rates, and the sudden increase in the sample temperature is generally followed by subsequent heat transfer from sample to the medium. Such factors are responsible for the reduction in sample temperature.

Although the most part of the biochar burned at temperatures above 350 °C, the onset temperature of burning was under the effect of the volatiles remained after torrefaction process. Therefore, the onset temperature of burning was determined as 226 °C.

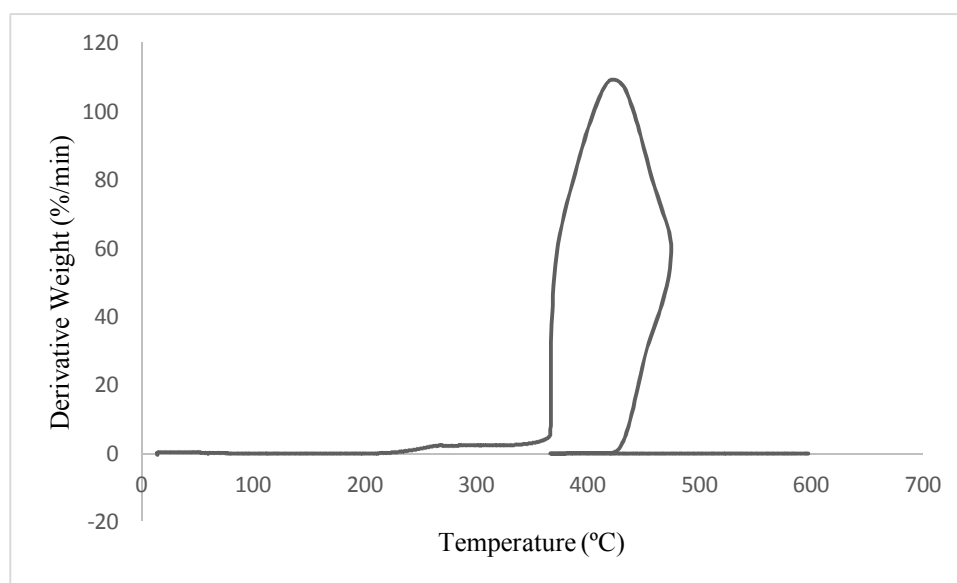


Figure 3.25 : The burning DTG profile of torrefied SSS under pure oxygen.

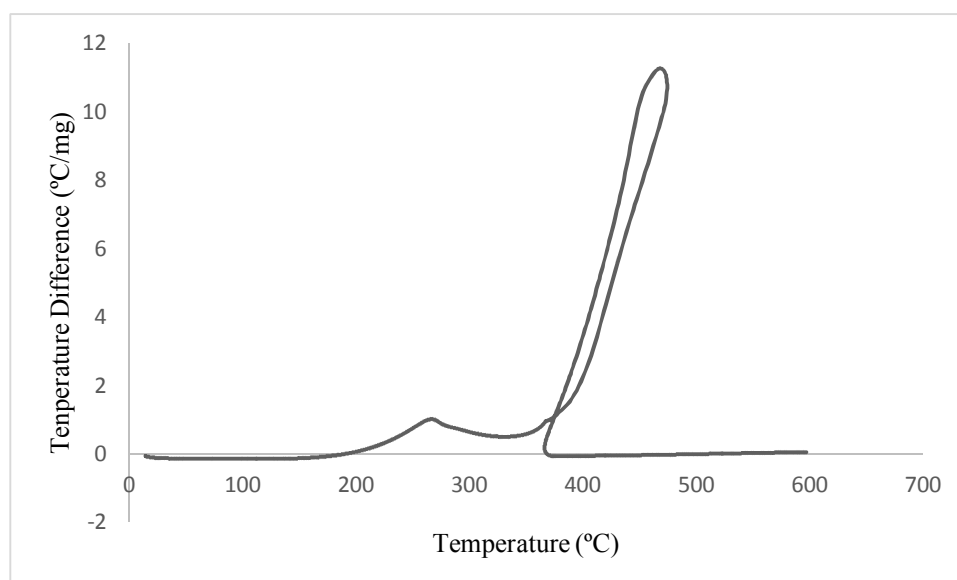


Figure 3.26 : The burning DTA profile of torrefied SSS under pure oxygen.

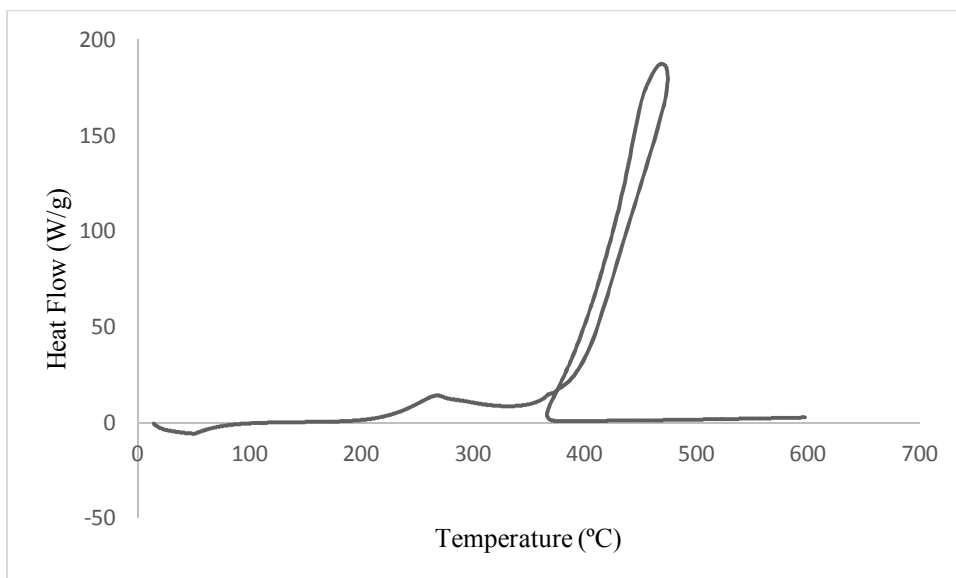


Figure 3.27 : The burning DSC profile of torrefied SSS under pure oxygen.

DTG, DTA, and DSC burning profiles of the 300 °C biochars from hazelnut shells using oxygen are shown in Figures 3.28-3.30, respectively.

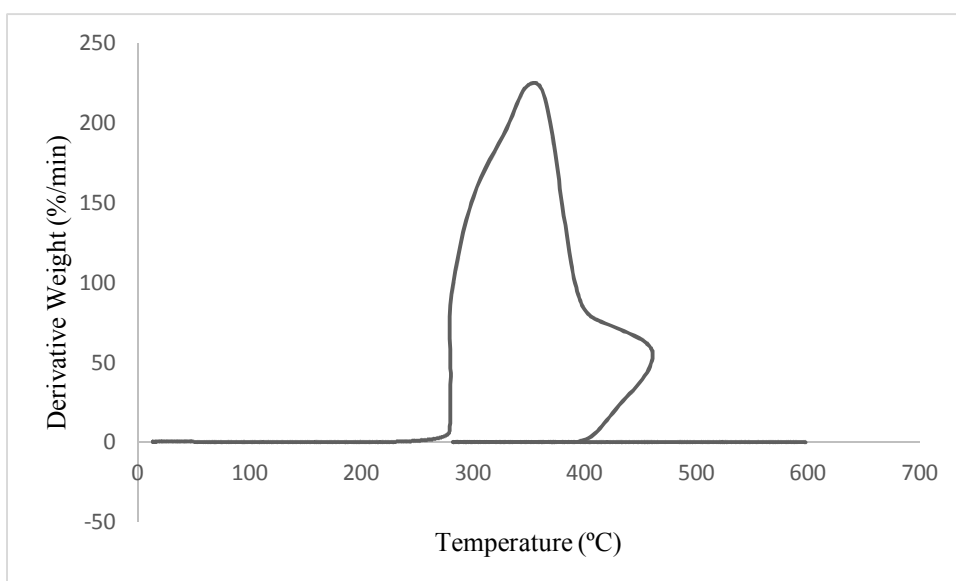


Figure 3.28 : The burning DTG profile of torrefied HS under pure oxygen.

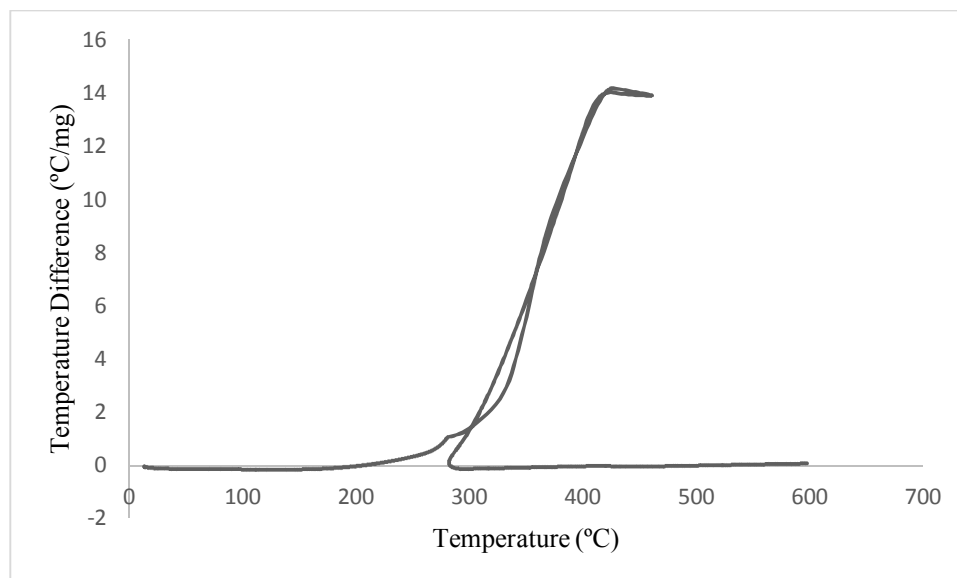


Figure 3.29 : The burning DTA profile of torrefied HS under pure oxygen.

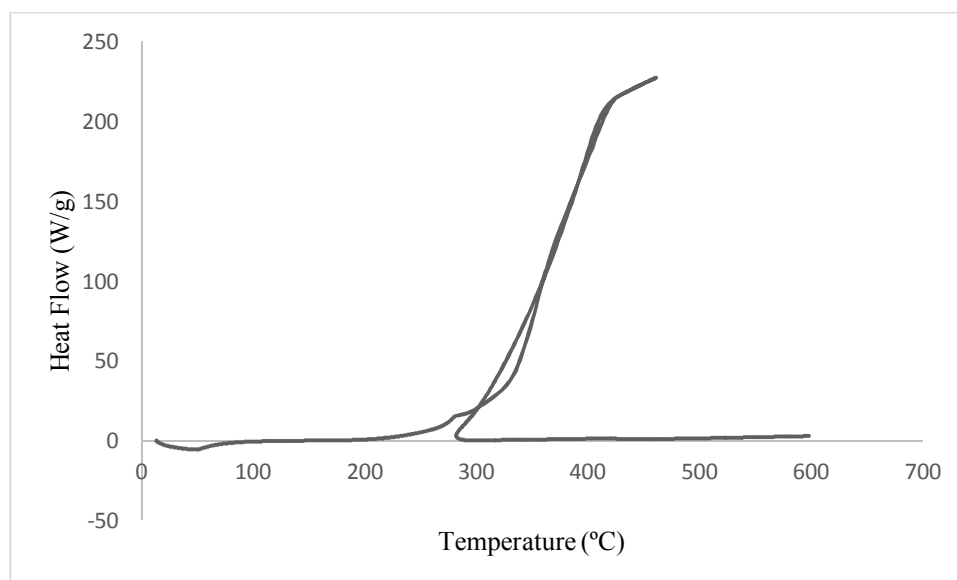


Figure 3.30 : The burning DSC profile of biochar from HS under pure oxygen.

The burning behavior of the biochar produced from hazelnut shells at 300 °C is consistent with the explanation made for the burning characteristics of the biochar produced from sunflower seed shell at the same temperature. First of all, the DTG profile indicates that there is only one large region in which the weight losses took place. As to the temperature range of this region, it happened relatively at high temperatures in comparison to the thermally untreated parent biomass material. On the other hand, DTA and DSC profiles revealed the fact that the exothermic reaction of the biochar realized so rapidly that variations in temperature difference or heat flow formed only lines that are right-handed rather than forming large area on these figures.

Table 3.8. presents some results derived from DTG and DTA burning profiles of torrefied biochars under pure oxygen condition.

Table 3.8 : The results from DTG and DTA of torrefied biochars under pure oxygen.

Sample	from DTG curves		from DTA curves		
	R _{max} (%/min)	T _{Rmax} (°C)	Onset Temp. of Burning (°C)	ΔT _{max} (°C/mg)	End Point of Burning (°C)
Torrefied biochar from sunflower seed shells	109	419	226	11.2	473
Torrefied biochar from hazelnut shells	223	360	271	14.2	460

3.2.3.5 Burning of the carbonized biochars with dry air

Burning behavior of the carbonized biochar from sunflower seed shells under dry air condition can be seen from DTG, DTA, and DSC profiles shown in Figures 3.31-3.33. R_{max} value was determined as 123.61 %/min at 382 °C, and this shows that the rates of the mass losses reached very high levels. Moreover, the decomposition took place in quite a narrow temperature interval which lies between 275-360 °C, despite some negligible mass losses accompanied it until 440 °C. Interestingly, DTA and DSC profiles also gave very similar situations with DTG profile.

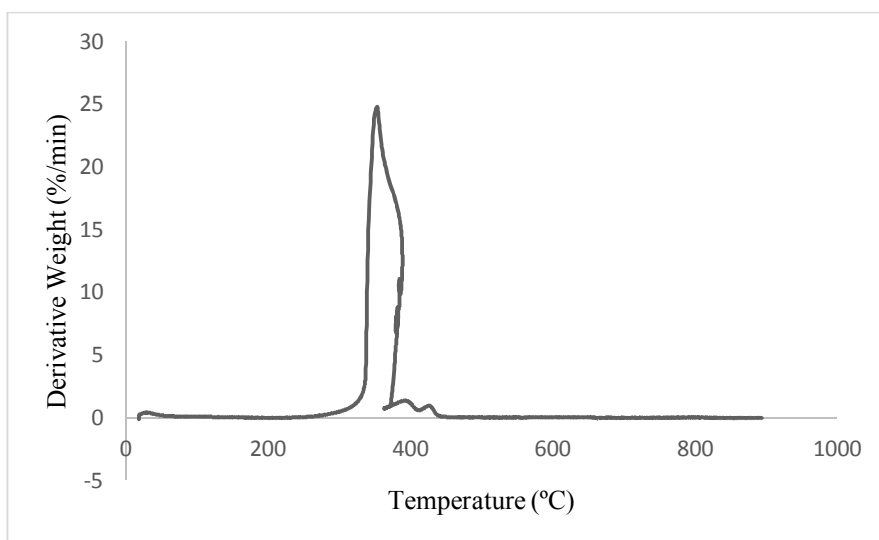


Figure 3.31 : The burning DTG profile of carbonized SSS under dry air.

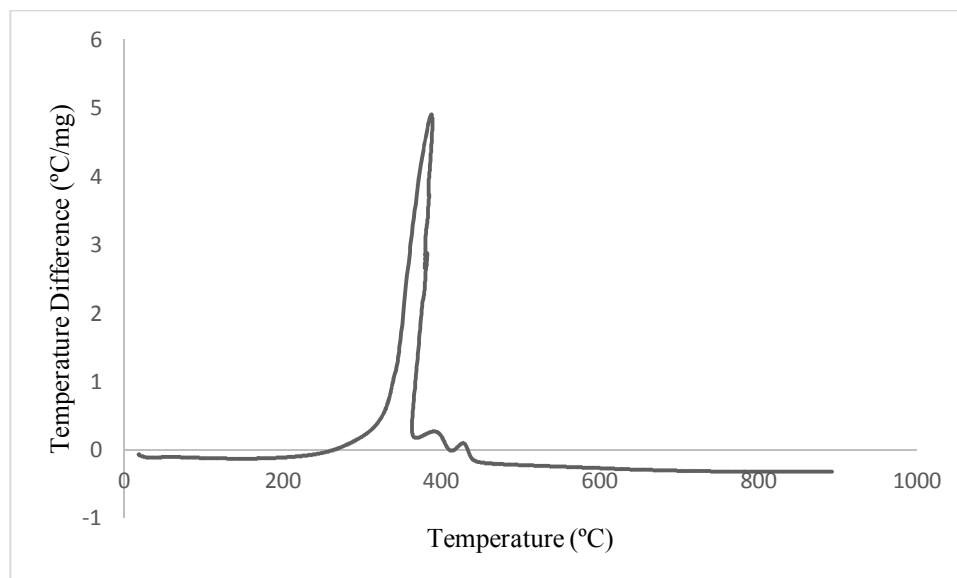


Figure 3.32 : The burning DTA profile of carbonized SSS under dry air.

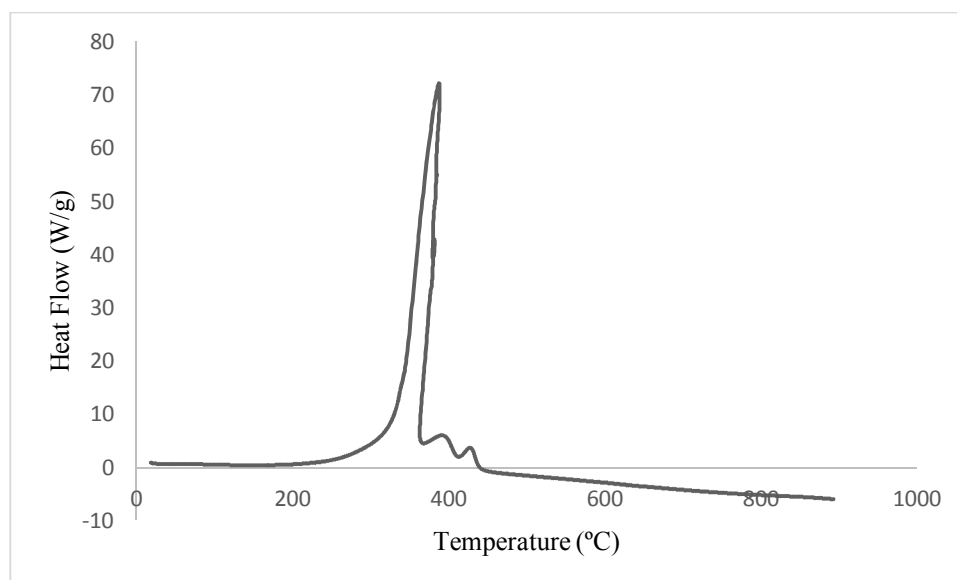


Figure 3.33 : The burning DSC profile of carbonized SSS under dry air.

The burning characteristics of the carbonized biochar from hazelnut shell can be seen from DTG, DTA, and DSC profiles given in Figures 3.34-3.36, respectively.

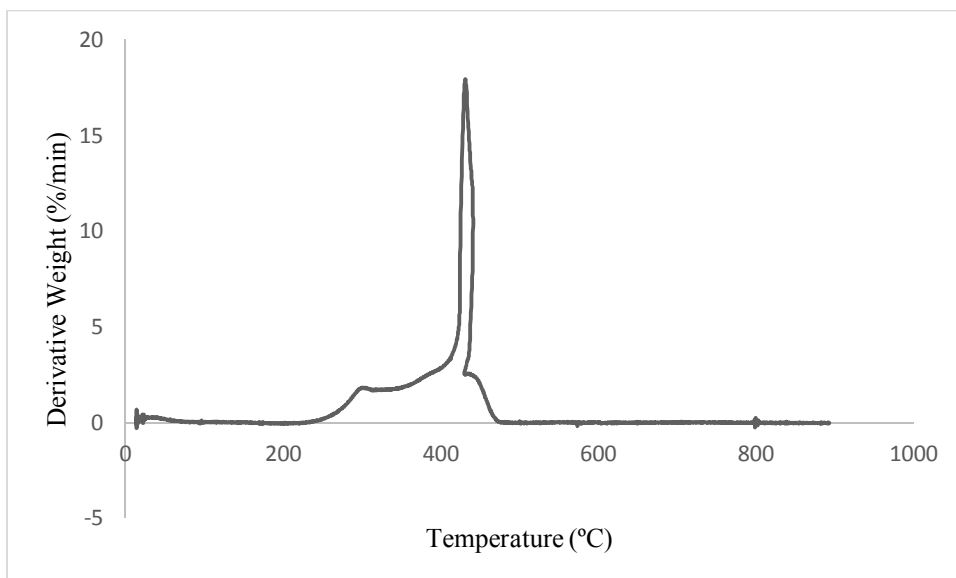


Figure 3.34 : The burning DTG profile of carbonized HS under dry air.

The shape of the derivative weight versus temperature in DTG curve exhibits that the volatile matter that remained after the carbonization process started the initial weight losses just after 250 °C. However, the contribution of such initial decomposition to either temperature difference on DTA or heat flow on DSC was quite limited. On the other hand, after a broad exothermic region between 225-400 °C, very sharp exothermic peak appeared that shows the high intensity of burning of the carbonized biochar. Furthermore, the maximum heat flow was 33 W/g according to DSC profile under dry air which was lower than torrefied hazelnut shell.

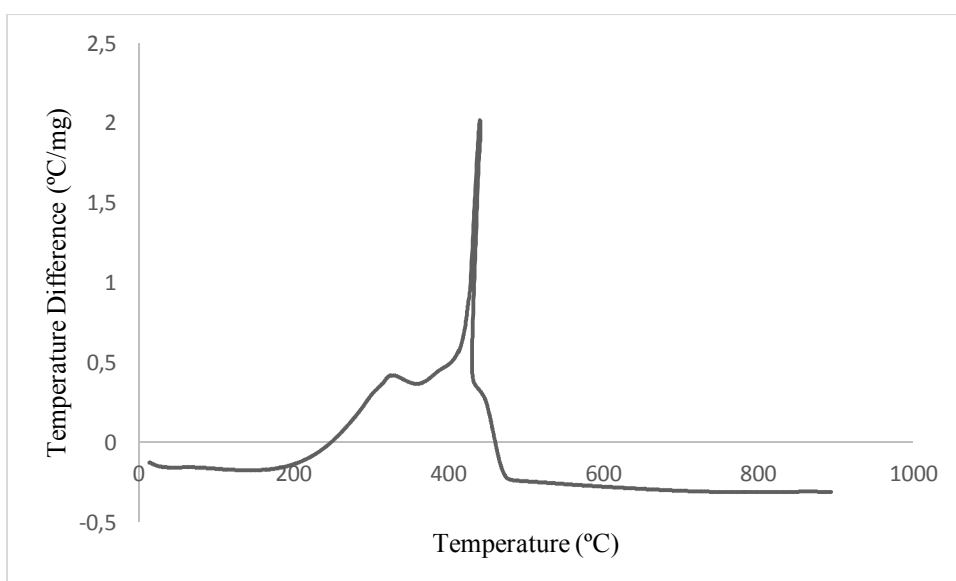


Figure 3.35 : The burning DTA profile of carbonized HS under dry air.

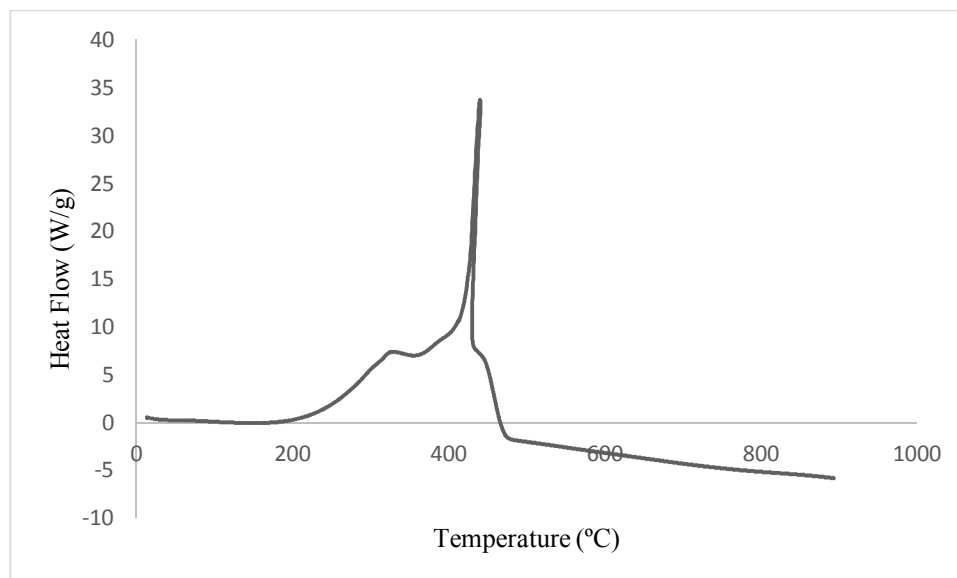


Figure 3.36 : The burning DSC profile of carbonized HS under dry air.

Summary of the results derived from DTG and DTA burning profiles of carbonized biochars under dry air condition are given in Table 3.9.

Table 3.9 : The results from DTG and DTA of carbonized biochars under dry air.

Sample	from DTG curves		from DTA curves		
	R_{\max} (%/min)	$T_{R\max}$ (°C)	Onset Temp. of Burning (°C)	ΔT_{\max} (°C/mg)	End Point of Burning (°C)
Biochar at 600°C from sunflower seed shells	123.61	382	317	4.90	433
Biochar at 600 °C from hazelnut shell	24.14	350	296	2.02	434

3.2.3.6 Burning of the carbonized biochars with pure oxygen

DTG, DTA, and DSC burning profiles of the carbonized biochars with pure oxygen are shown in Figures 3.37-3.39, respectively.

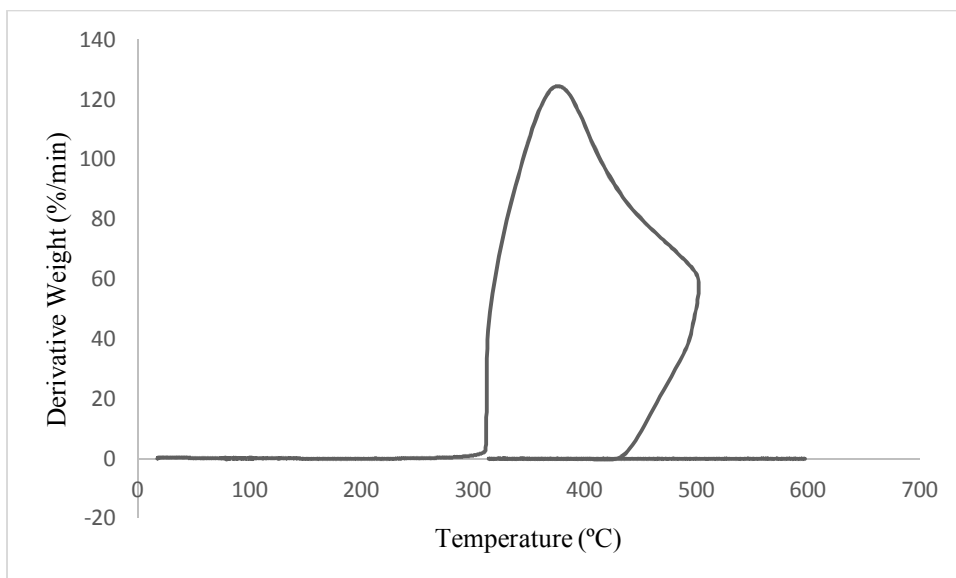


Figure 3.37 : The burning DTG curve of carbonized SSS with pure oxygen.

Carbonized biochar from sunflower seed shell started to burn around 300 °C with a R_{max} value of 123.61 %/min at 382 °C. A broad burning area formed and at around 500 °C temperature reduction took place.

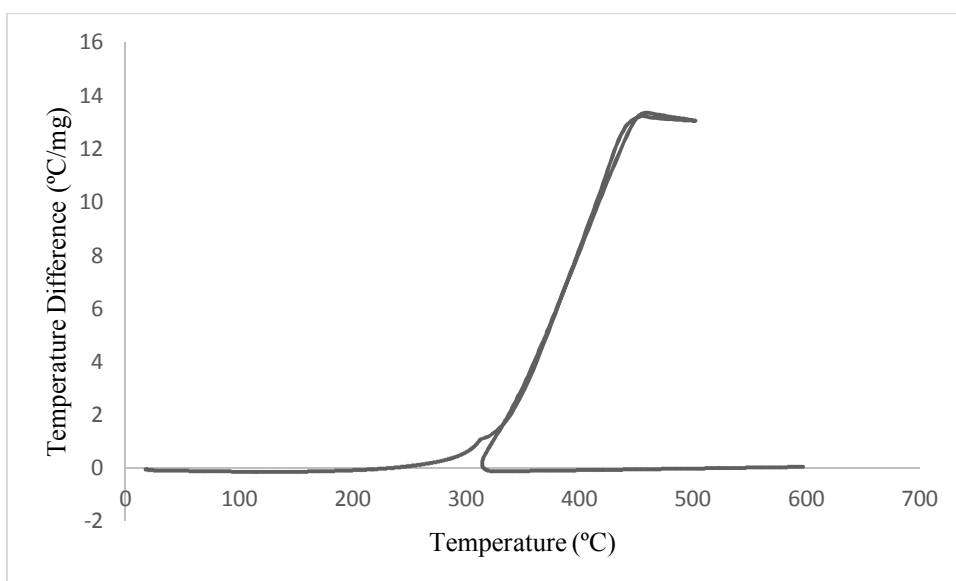


Figure 3.38 : The burning DTA curve of carbonized SSS with pure oxygen.

DTA burning profile of the carbonized biochar from sunflower seed shells gave the highest ΔT_{max} value among all samples investigated in this study, and this is consistent with the fact that carbonized sunflower seed shell was the sample that had the highest calorific value. In addition, the highest heat flow was obtained from carbonized sunflower seed shells biochar under pure oxygen condition among all DSC profiles of sunflower seed shells samples.

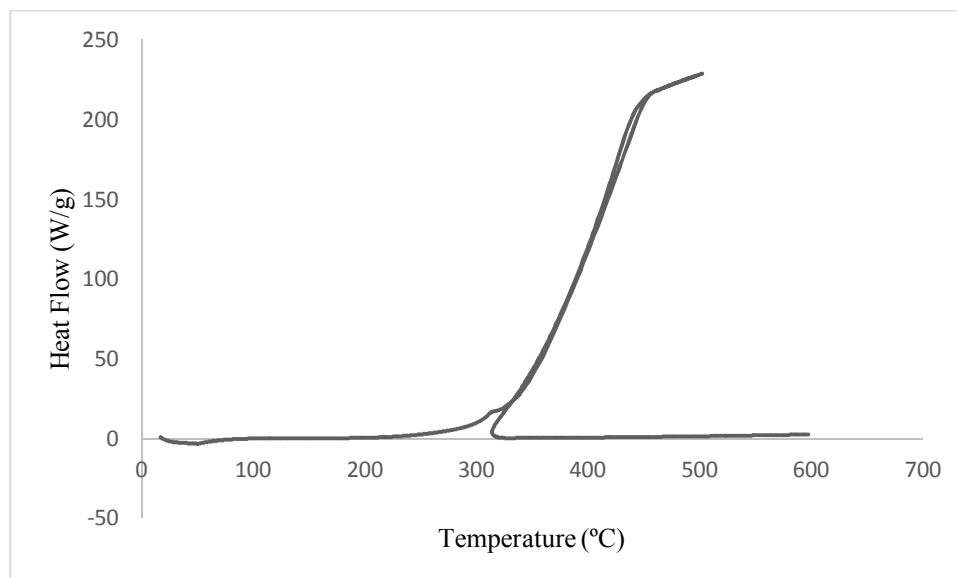


Figure 3.39 : The burning DSC curve of carbonized SSS with pure oxygen.

Burning profiles of carbonized hazelnut shell are given in Figures 3.40-3.42. The DTG burning profile seen in Figure 3.40 reveals that although mass losses started just beyond 250 °C due to irremovable volatile contents, the main burning region that have remarkable rates of weight losses were approximately in the temperature range of 400-500 °C. Meanwhile, R_{max} was determined as 84.95 %/min at 473°C which is the highest value of T_{Rmax} measured in this study.

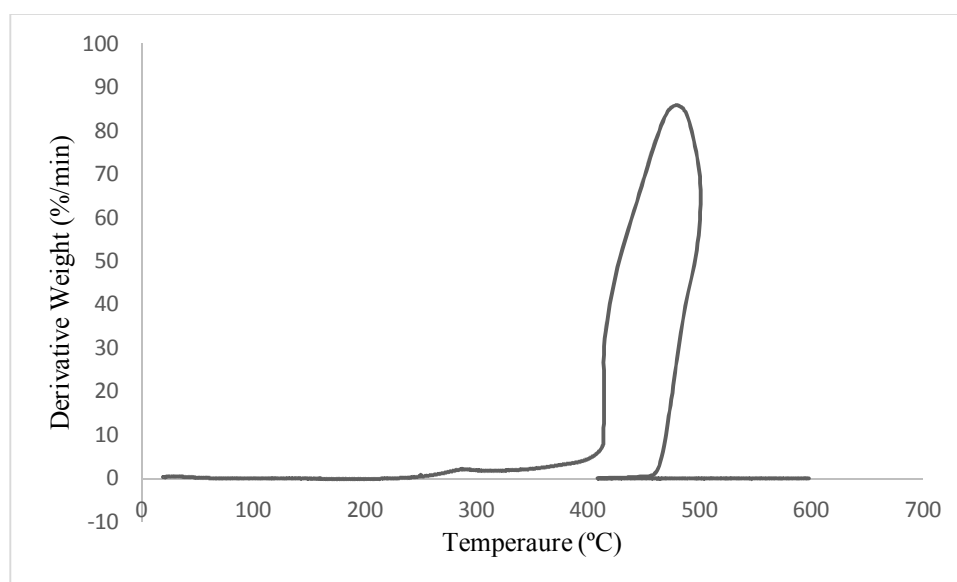


Figure 3.40 : The burning DTG profile of carbonized HS under pure oxygen.

DTA and DSC burning profiles of the carbonized biochar from hazelnut shells showed that both temperature difference and heat flow characteristics in the temperature range of 400-500 °C were highly dominant in comparison to the situations observed at lower

temperatures. This predicts that the burning of the biochar samples take place at higher temperatures and accordingly the main burning regions shift to the right on the temperature axis.

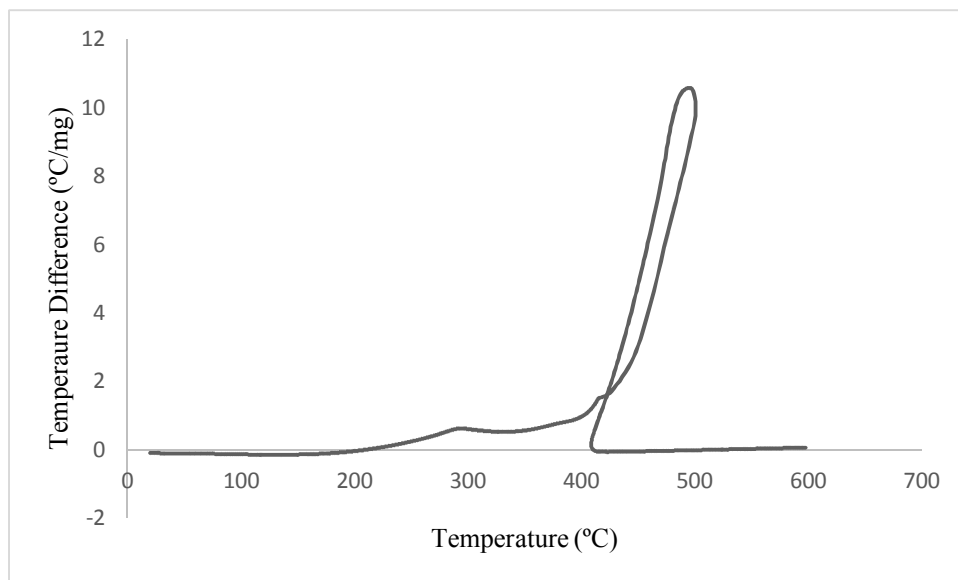


Figure 3.41 : The burning DTA profile of carbonized HS under pure oxygen.

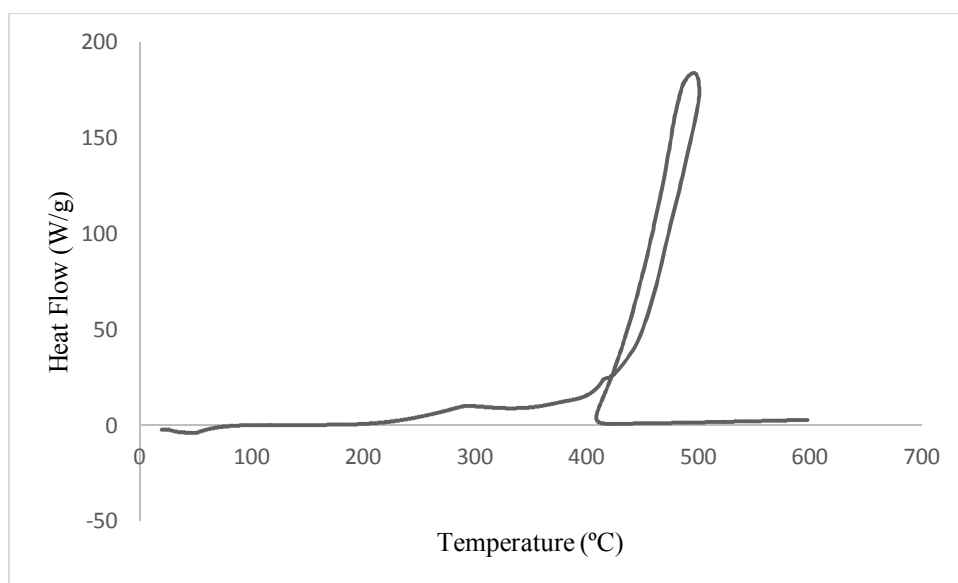


Figure 3.42 : The burning DSC profile of carbonized HS under pure oxygen.

Summary of the results derived from DTG and DTA burning profiles of carbonized biochars under pure oxygen condition are given in Table 3.9.

Table 3.10 : The DTG and DTA results of carbonized biochars under pure oxygen.

Sample	from DTG curves		from DTA curves		
	R _{max} (%/min)	T _{Rmax} (°C)	Onset Temp. of Burning (°C)	ΔT _{max} (°C/mg)	End Point of Burning (°C)
Biochar at 600°C from sunflower seed shells	123.61	382	314	13.36	502
Biochar at 600 °C from hazelnut shells	84.95	473	407	10.55	501

3.3 Particle Size Analysis Results

Specific surface area and mean diameter results of the samples are tabulated in Table 3.11.

Table 3.11 : The results of specific surface area and mean diameter.

Sample	Specific Surface Area (m ² /g)	Mean Diameter (μm)
Sunflower Seed Shell		
Main Sample	0.0654	189.3
Extractives-free	0.0320	289.0
Holocellulose	0.1280	122.5
Lignin	0.0227	498.8
Torrefied	0.0439	174.8
Carbonized	0.0547	308.4
Hazelnut Shell		
Main Sample	0.0913	176.1
Extractives-free	0.0440	193.2
Holocellulose	0.2010	105.4
Lignin	0.0447	259.6
Torrefied	0.0860	140.6
Carbonized	0.0950	121.7

The results given in Table 3.11 show that the isolated holocelluloses from both biomass species have the largest surface areas with 0.128 and 0.201 m²/g, while lignins have the narrowest surface areas with 0.0227 and 0.0447 m²/g. This is consistent with the high thermal reactivity of holocellulose and the low thermal reactivity of lignin.

On the other hand, the mean diameter results were in good agreement with the surface area results. That is, the lowest mean diameters belonged to holocelluloses, while lignins had the biggest mean diameters.

A general trend in specific surface area or mean diameter could not be found out for torrefaction or carbonization process.

3.4 SEM Results

Figures 3.43 and 3.44 indicate that holocellulose and lignin that account for the macromolecular structure of biomass have quite different appearances in the SEM images. That is holocellulose has just a cylindrical shape in the micro level size, while lignin rather has an amorphous shape which looks like a stronger structure. It is also clear that holocellulose structure can be decomposed easily since there are not strong connections between the parts in this ingredient.

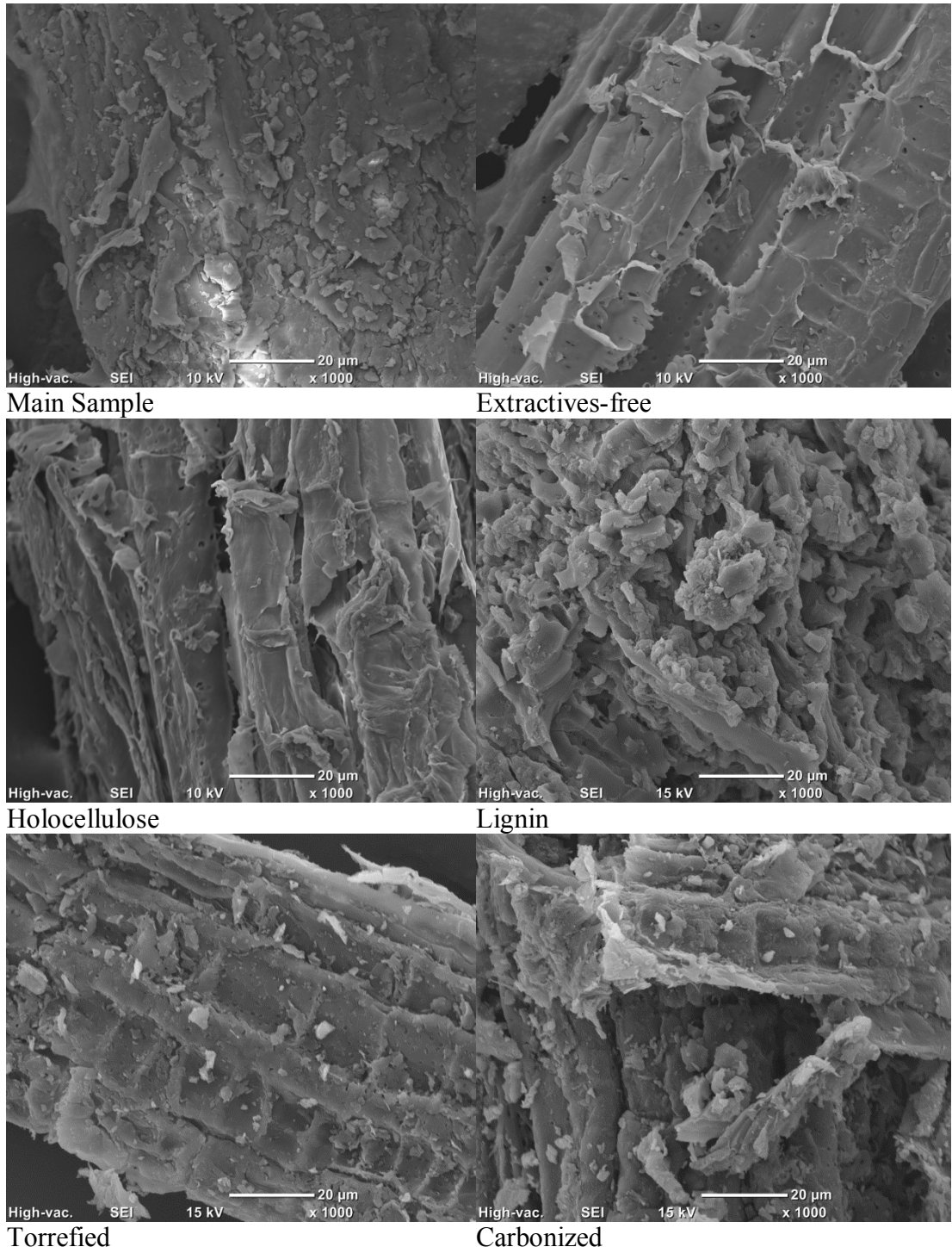


Figure 3.43 : SEM micrographs of the samples derived from sunflower seed shells.

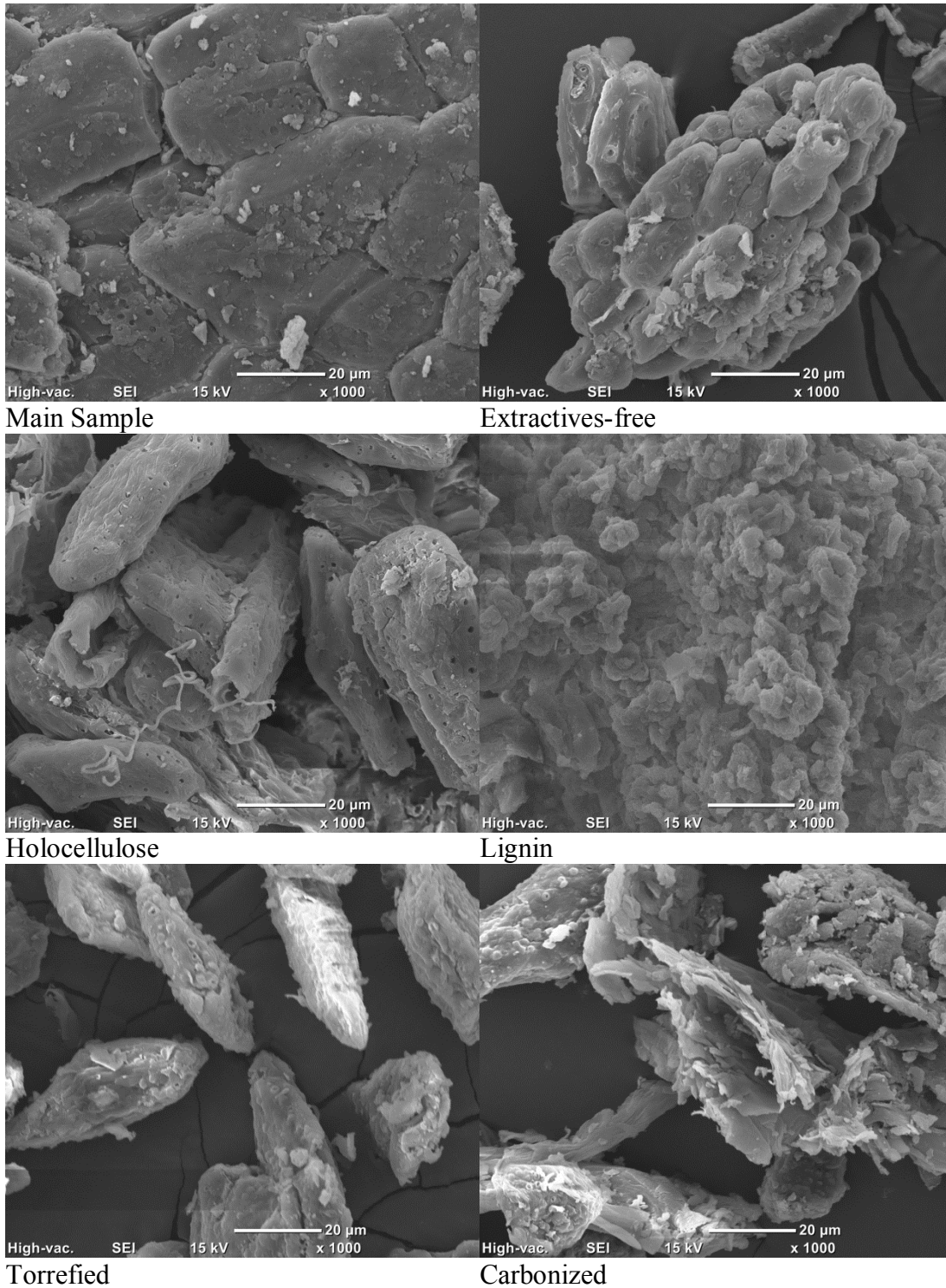


Figure 3.44 : SEM micrographs of the samples derived from hazelnut shells.

Torrefaction and carbonization processes led to some changes in the biomass structures in several ways. For instance, the bright points resulting from the presence of inorganics became more evident due to increasing ash contents in the thermally treated samples. This is quite obvious in case of either torrefied or carbonized hazelnut shell. On the other hand, formation of some very small new particles can also be

noticed from these images. Besides, the removal of volatile matter during the thermal treatments changed the structure in such a way that the carbonized residues became more fragile and fractal which can be easily seen from the carbonized hazelnut shell.

3.5 XRD Results

Mineral phases found by XRD technique are given in Table 3.12.

Table 3.12 : The mineral phases.

Sample	Minerals
Sunflower Seed Shell Main Sample	Silicon Dioxide (SiO ₂), Zeolite SSZ-24 (SiO _{2.267}), Chabazite (SiO ₂), Sodium Carbonate (Na ₂ CO ₃)
Extractives-free	Cristobalite (SiO ₂), Silicon Dioxide (SiO ₂), Disodium Calcium Silicate (SiCaNa ₂ O ₄), Zeolite-X (Al ₉₂ Ca _{23.2} Mg _{22.4} O ₃₈₄ Si ₁₀₀), Potassium Sulfide (K ₂ S), Zeolite ZSM-48 (SiO ₂)
Holocellulose	Niningerite (MgS), Eitelite (C ₂ MgNa ₂ O ₆), Aluminum Oxide (Al _{10.7} O ₁₆), Calcite (CaCO ₃), Dolomite (CaMgCO ₃), Zeolite (SiO ₂), Anorthite (Al _{1.55} Ca _{0.55} Na _{0.45} O ₈ Si _{2.45})
Lignin Torrefied Sample	Haueyne (Al ₆ Ca _{2.28} K _{0.95} Na _{4.35} O ₃₂ S ₂ Si ₆) n/a
Carbonized Sample	n/a
Hazelnut Shell Main Sample	Silicon Dioxide (SiO ₂), Potassium Sulfide (K ₂ S), Magnesium Silicate Spinel (Mg ₂ SiO ₄), Zeolite (SiO ₂)
Extractives- free	Magnesium Silicate (MgSiO ₃), Potassium Sulfide (K ₂ S), Analcime (Al _{15.26} Na _{14.88} O ₉₆ Si _{32.74})
Holocellulose	Cristobalite (SiO ₂), Niningerite (MgS), Calcite (CaCO ₃), Sodium Aluminum Silicon Oxide (Al _{1.65} Na _{1.65} O ₄ Si _{0.35}), Tridymite (SiO ₂), Chabazite (Al _{3.7} Ca _{1.78} O ₂₄ Si _{8.3})
Torrefied Sample	Cristobalite (SiO ₂), Potassium Oxide (K ₂ O)
Carbonized Sample	Calcite (CaCO ₃), Nyerereite (C ₂ CaK _{0.36} Na _{1.64} O ₆)

n/a : not available

These results given in Table 3.12 indicate that both the main biomass samples and their derivatives contain considerable amounts of silicon oxides either in the forms of silicon dioxide, cristobalite, chbazite or zeolites. Likewise, it is also reported in literature that many types of biomass species are very rich in silicon oxides and it is the major form of the mineral matter [16, 92]. Furthermore, as in the case of the main hazelnut shell sample, silicon may form some other combinations with other elements like magnesium to form magnesium silicate spinel.

In addition, potassium sulfide was determined in the main sample of hazelnut shells. In fact, the high potassium content in hazelnut shell is an important concern in the utilization of this waste material in energetic purposes since it causes undesirable deposits such as slagging and fouling [16].

In fact, the main challenge in determination of the mineral forms in a carbon containing material by XRD is that carbon masks the inorganics and it makes difficult to predict the inorganics. Some chemical treatments make it easier to detect the presence of inorganics. That why we were able to determine different types of inorganic phases in the cases of holocellulose and lignin fractions.

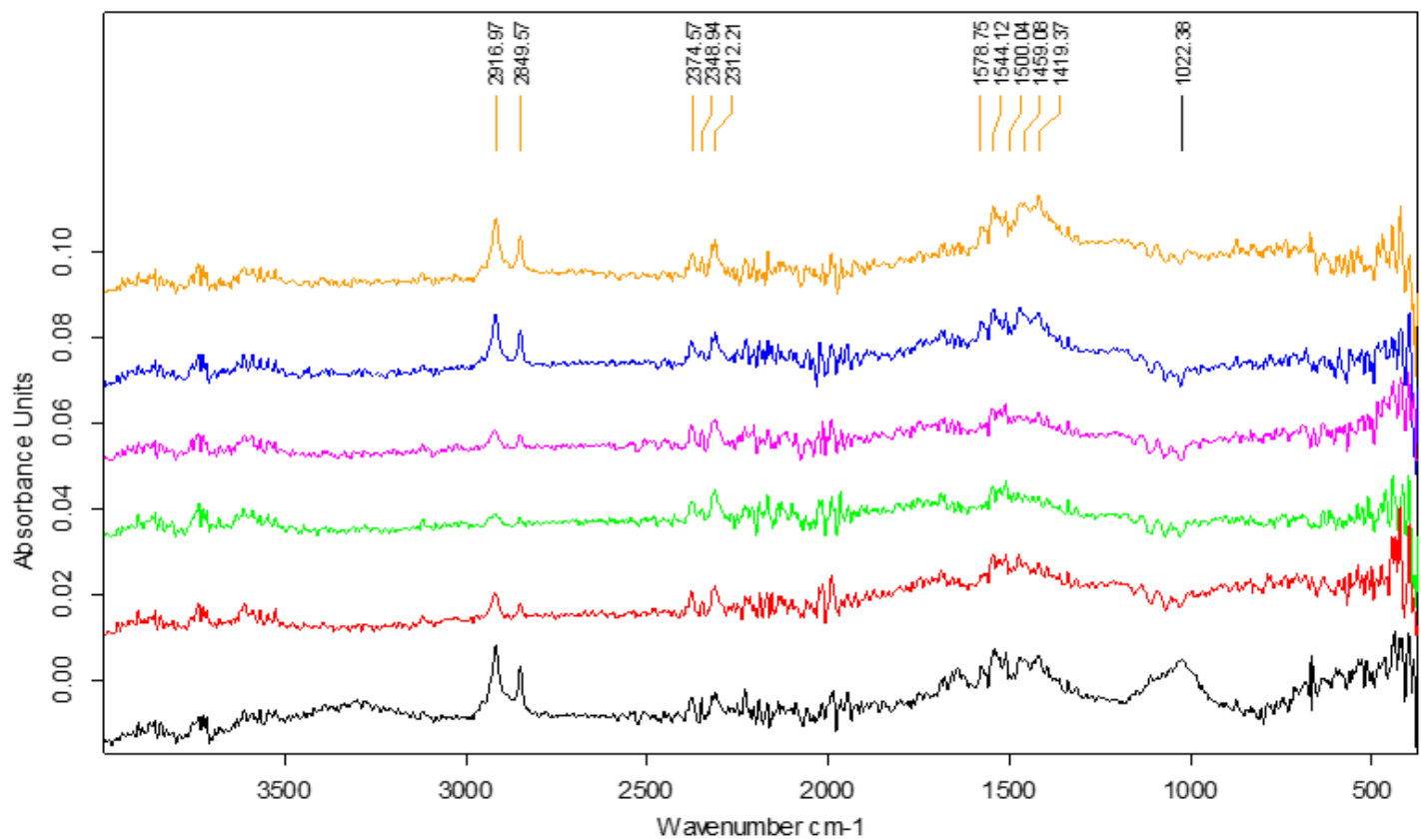
In contrast to this, the increasing carbon contents in torrefied or carbonized samples make it more difficult or even impossible to detect the mineral phases. Consequently, nothing could be specified for torrefied or carbonized sunflower seed shells. Similarly, only calcite and nyerereite which is the combination of inorganics with the carbon matrix could be determined for the carbonized hazelnut shell.

3.6 FTIR Analysis Results

The FTIR spectra that show the absorbance levels of the functional groups in the main samples and their derivatives are seen in Figures 3.45 and 3.46 for sunflower seed shell and hazelnut shell, respectively. It is clear from these figures that the absorbance values at certain wavenumbers are highly characteristic and they confirm the presence of special functional groups in such complex structures. That is, the evident wavenumbers of this study which can be attributed to the bands of the functional groups are given in Table 3.13.

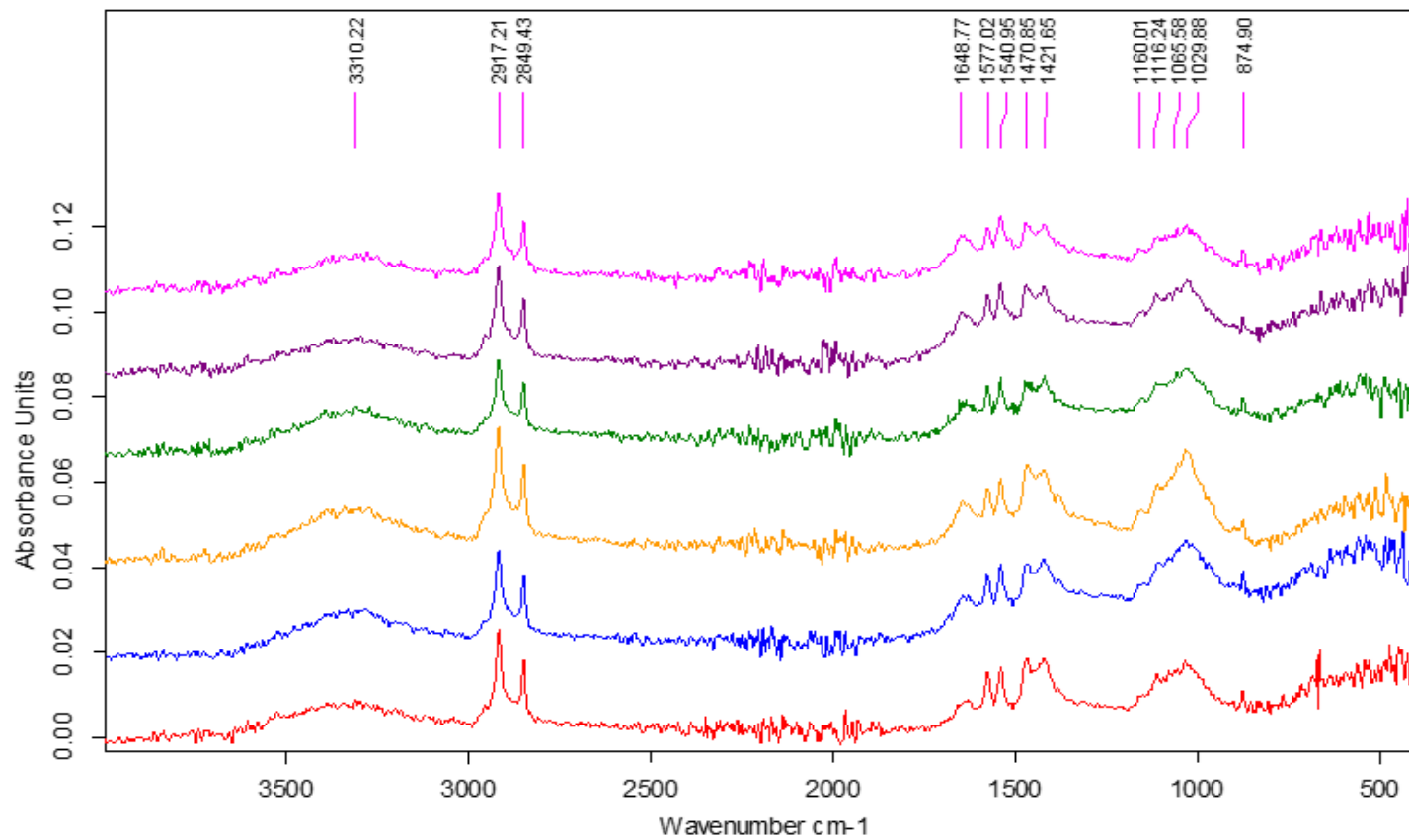
Table 3.13 : Wavenumbers and corresponding functional groups [93-95].

Wavenumber (cm⁻¹)	Possible Functional Groups
3310	O-H stretching
2917	CH ₃ in aromatic ring
2849	C-H stretching
2374	C=O stretching
2348	C=O stretching
2312	C=O stretching
1648	Olefinic C=C vibrations or N-H in-plane bending
1577	Aromatic skeletal C=C vibration or C=C stretching in olefin double bonds
1540	Aromatic skeletal C=C vibration
1500	Aromatic skeletal C=C vibration
1470	Aromatic skeletal C=C vibration
1459	Aromatic skeletal C=C vibration
1420	C=C absorptions
1160	Ether type structures
1116	C-O-C vibrations or P-OC stretching in polyphosphate esters
1066	C-O-C vibrations
1025	C-O-C vibrations
874	C-H aromatic out-of-plane



C:\Program Files\OPUS_65\MFAS\A-24.04.2015	A-24.04.2014	ATR platinum Diamond 1 Ref	24/04/2014
C:\Program Files\OPUS_65\MFAS\F-24.04.2014	A-F-24.04.2014	ATR platinum Diamond 1 Ref	24/04/2014
C:\Program Files\OPUS_65\MFAS\H-24.04.2014	A-H-24.04.2014	ATR platinum Diamond 1 Ref	24/04/2014
C:\Program Files\OPUS_65\MFAS\I-24.04.2014	A-I-24.04.2014	ATR platinum Diamond 1 Ref	24/04/2014
C:\Program Files\OPUS_65\MFAS\A300-24.04.2014	A300-24.04.2014	ATR platinum Diamond 1 Ref	24/04/2014
C:\Program Files\OPUS_65\MFAS\A600-24.04.2014	A600-24.04.2014	ATR platinum Diamond 1 Ref	24/04/2014

Figure 3.45 : The FTIR spectra for sunflower seed shell main sample and its derivatives.



C:\Program Files\OPUS 65M\FAS\F-24.04.2015	F-24.04.2014	ATR platinum Diamond 1 Ref	24/04/2014
C:\Program Files\OPUS 65M\FAS\F-24.04.2014	F-F-24.04.2014	ATR platinum Diamond 1 Ref	24/04/2014
C:\Program Files\OPUS 65M\FAS\F-L-24.04.2014	F-L-24.04.2014	ATR platinum Diamond 1 Ref	24/04/2014
C:\Program Files\OPUS 65M\FAS\F-H-24.04.2014	F-H-24.04.2014	ATR platinum Diamond 1 Ref	24/04/2014
C:\Program Files\OPUS 65M\FAS\F300-24.04.2014	F300-24.04.2014	ATR platinum Diamond 1 Ref	24/04/2014
C:\Program Files\OPUS 65M\FAS\F600-24.04.2014	F600-24.04.2014	ATR platinum Diamond 1 Ref	24/04/2014

Figure 3.46 : The FTIR spectra for hazelnut seed shell main sample and its derivatives.

The results that can be obtained from the FTIR spectrum of sunflower seed shell derivatives were summarized as follows:

1. C-O-C vibrations at around 1022 cm^{-1} seriously decreased due to thermal treatment. This shows the influence of torrefaction and carbonization processes to reduce the oxygen content of the sample.
2. Similarly, some reductions took place in the intensities of C-H stretching bands at 2917 and 2849 cm^{-1} due to the decreasing hydrogen content.
3. Meanwhile, C=C stretching and C=C vibration bands between 1578 - 1459 cm^{-1} became more apparent after the thermal treatments, and it can explained by increasing the carbon content at the expense of oxygen and hydrogen contents.

Evaluation of the bands in FTIR spectra for hazelnut shell derivatives revealed the following outcomes:

1. The most evident C-O-C bands in the range of 1160 - 1029 cm^{-1} were seen in case of holocellulose fraction that is quite convenient with the fact that holocellulose ingredients such as cellulose and hemicellulose are very rich in weak ether bonds and therefore holocellulose forms the reactive part of biomass.
2. Similarly, C-H stretching band at 2849 cm^{-1} is also distinctive in case of holocellulose.
3. The bands below 500 cm^{-1} are generally regarded as “finger print region” and inorganics have significant contribution to the absorbance in this region. Actually, this biomass contains relatively high content of ash forming minerals and thermal treatments further concentrated them, leading increasing the intensities below 500 cm^{-1} seriously.

Applied thermal treatments did not cause to increase in the absorbances of C=C vibrations at the wavenumbers between 1648 - 1421 cm^{-1} because the effectiveness of the treatments methods were not so good at increasing the carbon content, and the improvements in the biomass structure was quite limited in case of hazelnut sample.

3.7 Kinetic Analysis of Burning Profiles

In this study, Coats-Redfern method was performed to each sample with regard to different reaction models, such as reaction order, diffusion, contracting geometry and nucleation. The DTG and DTA profiles were used to determine E_a and A values for each sample. The pyrolytic decomposition of biomass that is followed by homogeneous combustion of combustible volatiles in gaseous phase occurred in Region I under both burning conditions started by removal of volatile matters. After homogeneous combustion, the biochar that is the remnant from the volatile removal stage was burned through the surface oxidation that forms the Region II of the burning process. Therefore, each region was taken into account for kinetic approaches, individually. The activation energies and frequency factors of sunflower seed shells under dry air and pure oxygen burning conditions were shown in Table 3.14.

With respect to Region I under dry air burning condition, the E_a value was gone up slightly from 38.74 to 58.60 kJ/mol in case of increasing reaction order. It can be said that the most suitable reaction order mechanism is first order. The highest frequency factor was determined in second order reaction model at 441.71 s⁻¹. In addition, calculated activation energies from diffusional models were highest among the reaction models. The calculated activation energies from each model in Region I were lower compared to pure oxygen burning condition.

As regards Region II under dry air burning condition, the activation energies were lower than Region I. For instance, the calculated activation energy from first order reaction decreased considerably from 45.93 kJ/mol to 29.52 kJ/mol. Moreover, the frequency factors were also lower than Region I. Take 3-D Ginstling-Brounshtein model as an example. The A value was plummeted from 1.2x10⁴ s⁻¹ to 0.0230 s⁻¹. In addition, it can be said that Avrami-Erofeev, particularly in n=4 reaction model was not fitted well for all regions and reaction conditions.

Concerning pure oxygen burning condition, the most suitable models were first order and 3-D Ginstling-Brounshtein for both regions. The calculated activation energy from first order in Region I was considerably lower than 3-D Ginstling-Brounshtein model with 51.32 kJ/mol and 96.78 kJ/mol, respectively. Furthermore, the frequency factor at first order was also far lower than 3-D Ginstling-Brounshtein model at 71.39 s⁻¹ as opposed to 1.2 x10⁵ s⁻¹.

Table 3.14 : The activation energies and frequency factors of sunflower seed shells.

Reaction Model	f(α)	Dry Air						Pure Oxygen					
		Region I			Region II			Region I			Region II		
		R ²	E _A (kJ/mol)	A (s ⁻¹)	R ²	E _A (kJ/mol)	A (s ⁻¹)	R ²	E _A (kJ/mol)	A (s ⁻¹)	R ²	E _A (kJ/mol)	A (s ⁻¹)
Reaction order													
1 st order	(1-α) ⁿ	0.9680	45.93	15.54	0.9799	29.52	0.2925	0.9688	51.32	71.36	0.9700	29.94	0.4251
1/3 rd order	(1-α) ⁿ	0.9635	38.74	2.24	0.8936	7.02	0.0006	0.9606	42.67	7.03	0.9479	7.18	0.0008
1/2 nd order	(1-α) ⁿ	0.9651	40.45	3.55	0.9514	11.31	0.0025	0.9632	44.70	12.17	0.9663	11.55	0.0032
2/3 rd order	(1-α) ⁿ	0.9664	42.21	5.72	0.9716	16.44	0.0108	0.9655	46.82	21.50	0.9711	16.75	0.0142
2 nd order	(1-α) ⁿ	0.9671	58.60	441.71	0.9660	90.82	2.2 x10 ⁵	0.9709	66.88	4237.17	0.9574	91.34	4.8x10 ⁵
Diffusional													
1-D	1/2α	0.9679	79.99	1.1x10 ⁴	0.8947	12.23	0.0019	0.9632	86.58	7.5 x10 ⁴	0.9606	11.93	0.0020
2-D	[-ln(1-α)] ⁻¹	0.9704	86.23	2.9x10 ⁴	0.9583	23.18	0.0204	0.9674	93.93	2.5 x10 ⁵	0.9808	23.07	0.0258
3-D (Jander)	3/2(1-α) ^{2/3} [1-(1-α) ^{1/3}] ⁻¹	0.9723	93.38	4.1 x10 ⁴	0.9840	43.97	0.6931	0.9711	102.52	5.1 x10 ⁵	0.9827	44.18	1.0769
3-D (Ginstling-Brounshtein)	3/2[(1-α) ^{-1/3} -1] ⁻¹	0.9712	88.61	1.2 x10 ⁴	0.9729	29.66	0.0230	0.9688	96.78	1.2 x10 ⁵	0.9834	29.67	0.0312
Contracting geometry													
Contracting area	(1-α) ^(1-1/n) ; n=2	0.9651	40.45	1.78	0.9514	11.31	0.0013	0.9632	44.70	6.09	0.9663	11.55	0.0015
Contracting volume	(1-α) ^(1-1/n) ; n=3	0.9664	42.21	1.91	0.9716	16.44	0.0036	0.9655	46.82	7.17	0.9711	16.75	0.0047
Nucleation													
Avrami-Erofeev	n(1-α)[-ln(1-α)] ^(1-1/n) ; n=2	0.9520	18.49	0.023	0.9523	9.22	0.002	0.9549	21.22	0.05	0.9333	9.63	0.002
Avrami-Erofeev	n(1-α)[-ln(1-α)] ^(1-1/n) ; n=3	0.9200	9.34	0.002	0.7689	2.45	0.0001	0.9297	11.18	0.003	0.7440	2.86	0.0002
Avrami-Erofeev	n(1-α)[-ln(1-α)] ^(1-1/n) ; n=4	0.8427	4.77	0.0004	0.4698	n/a	n/a	0.8768	6.16	0.0007	0.1552	n/a	n/a

n/a : not available

The activation energies and frequency factors of torrefied sunflower seed shells biochar at 300 °C under dry air and pure oxygen burning conditions were shown in Table 3.15. Regarding dry air and pure oxygen burning conditions, the calculated activation energies from reaction order models were lower than diffusional models. For instance; the calculated activation energy from first order for Region I under dry air burning was considerably lower than 3-D Ginstling-Brounshtein model at 59.28 kJ/mol compared to 120.60 kJ/mol. Furthermore, the frequency factors under dry air burning condition were significantly higher than under pure oxygen. Take first order reaction model for Region I as an example. The A value plunged from 90.84 s⁻¹ to 0.0103 s⁻¹. First order and 3-D Ginstling-Brounshtein models were best fitting models for torrefied sunflower seed shells at 300 °C under both burning conditions. Moreover, it can be said that calculated activation energies under dry air burning condition were considerably higher than pure oxygen burning condition. It clarifies that reaction rates under pure oxygen burning circumstance were faster than dry air.

The activation energies and frequency factors of carbonized sunflower seed shells biochar at 600 °C under dry air and pure oxygen burning conditions were shown in Table 3.16. It can be stated that the most suitable model was 3-D Ginstling-Brounshtein model for both burning conditions. The highest activation energies and frequency factors were calculated from diffusional models. The calculated activation energies from first order and 3-D Ginstling-Brounshtein for Region I under dry air burning were at 78.16 kJ/mol and 153.55 kJ/mol, respectively. The activation energies decreased significantly under pure oxygen burning condition compared to dry air. For instance; it decreased from 153.55 kJ/mol to 81.19 kJ/mol using 3-D Ginstling-Brounshtein reaction model approach. In addition, the frequency factor plummeted from 9.8x10⁷ s⁻¹ to 43.86 s⁻¹.

All in all, it can be obviously stated that carbonization and torrefaction treatments increased the activation energy compared to main sample. This is mainly due to the high amount of carbon composition of sample; in other words, torrefaction removed the volatile matters, and carbonization increased the carbon content of samples. Pure oxygen burning condition was more reactive than dry air resulted in a lower activation energy for each model [96]. That is to say, reactions are much faster under pure oxygen burning condition.

Table 3.15 : The activation energies and frequency factors of torrefied sunflower seed shells biochar at 300 °C.

Reaction Model	f(α)	Dry Air						Pure Oxygen		
		Region I			Region II			Region I		
		R ²	E _A (kJ/mol)	A (s ⁻¹)	R ²	E _A (kJ/mol)	A (s ⁻¹)	R ²	E _A (kJ/mol)	A (s ⁻¹)
Reaction order										
1 st order	(1-α) ⁿ	0.9928	59.28	90.84	0.9809	40.50	1.45	0.9513	16.90	0.0103
1/3 rd order	(1-α) ⁿ	0.9890	54.86	30.73	0.9827	25.53	0.04	0.9232	5.07	0.0002
1/2 nd order	(1-α) ⁿ	0.9900	55.94	40.09	0.9834	29.23	0.11	0.9410	7.58	0.0006
2/3 rd order	(1-α) ⁿ	0.9910	57.04	52.48	0.9834	33.20	0.27	0.9479	10.38	0.0015
2 nd order	(1-α) ⁿ	0.9964	66.37	511.34	0.9753	75.16	2611.57	0.9460	43.77	7.2740
Diffusional										
1-D	1/2α	0.9890	114.97	3.3x10 ⁶	0.9870	48.93	3.19	0.9802	13.11	0.0016
2-D	[-ln(1-α)] ⁻¹	0.9909	119.14	4.4x10 ⁶	0.9883	60.40	24.47	0.9807	20.68	0.0070
3-D (Jander)	3/2(1-α) ^{2/3} [1-(1-α) ^{1/3}] ⁻¹	0.9926	123.54	2.8x10 ⁶	0.9877	77.44	183.43	0.9759	32.11	0.0286
3-D (Ginstling-Brounshtein)	3/2[(1-α) ^{-1/3} -1] ⁻¹	0.9915	120.60	1.4x10 ⁶	0.9792	68.89	28.09	0.9792	24.38	0.0041
Contracting geometry										
Contracting area	(1-α) ^(1-1/n) ; n=2	0.9900	55.94	20.04	0.9834	29.23	0.05	0.9410	7.58	0.0003
Contracting volume	(1-α) ^(1-1/n) ; n=3	0.9910	57.04	17.49	0.9834	33.20	0.09	0.9479	10.38	0.0005
Nucleation										
Avrami-Erofeev	n(1-α)[-ln(1-α)] ^(1-1/n) ; n=2	0.9892	24.90	0.063	0.9682	15.48	0.006	0.6992	2.77	0.0001
Avrami-Erofeev	n(1-α)[-ln(1-α)] ^(1-1/n) ; n=3	0.9825	13.44	0.004	0.9270	6.64	0.0005	0.7400	n/a	n/a
Avrami-Erofeev	n(1-α)[-ln(1-α)] ^(1-1/n) ; n=4	0.9687	7.72	0.0008	0.7179	2.22	7.6x10 ⁻⁵	0.9652	n/a	n/a

n/a : not available

Table 3.16 : The activation energies and frequency factors of carbonized sunflower seed shells biochar at 600 °C.

Reaction Model	f(α)	Dry Air			Pure Oxygen		
		R ²	E _A (kJ/mol)	A (s ⁻¹)	R ²	E _A (kJ/mol)	A (s ⁻¹)
Reaction order							
1 st order	(1- α) ⁿ	0.9299	78.16	1317.99	0.9721	43.27	0.83
1/3 rd order	(1- α) ⁿ	0.9404	70.27	240.87	0.9892	33.44	0.10
1/2 nd order	(1- α) ⁿ	0.9378	72.19	364.43	0.9866	35.72	0.16
2/3 rd order	(1- α) ⁿ	0.9352	74.14	555.36	0.9827	38.12	0.27
2 nd order	(1- α) ⁿ	0.9140	91.11	2.1x10 ⁴	0.9277	61.57	40.28
Diffusional							
1-D	1/2 α	0.9527	143.63	1.1x10 ⁸	0.9934	69.90	37.07
2-D	[-ln(1- α)] ⁻¹	0.9480	150.93	2.5x10 ⁸	0.9923	77.96	101.11
3-D (Jander)	3/2(1- α) ^{2/3} [1-(1- α) ^{1/3}] ⁻¹	0.9428	158.80	2.9x10 ⁸	0.9864	87.71	168.93
3-D (Ginstling-Brounshtein)	3/2[(1- α) ^{-1/3} -1] ⁻¹	0.9462	153.55	9.8x10 ⁷	0.9907	81.19	43.86
Contracting geometry							
Contracting area	(1- α) ^(1-1/n) ; n=2	0.9378	72.19	182.21	0.9866	35.72	0.08
Contracting volume	(1- α) ^(1-1/n) ; n=3	0.9352	74.14	185.12	0.9827	38.12	0.09
Nucleation							
Avrami-Erofeev	n(1- α)[-ln(1- α)] ^(1-1/n) ; n=2	0.9091	33.82	0.26	0.9526	15.91	0.004
Avrami-Erofeev	n(1- α)[-ln(1- α)] ^(1-1/n) ; n=3	0.8779	19.04	0.01	0.8978	6.78	0.0004
Avrami-Erofeev	n(1- α)[-ln(1- α)] ^(1-1/n) ; n=4	0.8281	11.65	0.002	0.6407	2.22	5.7x10 ⁻⁵

The activation energies and frequency factors of hazelnut shells under dry air and pure oxygen burning conditions were shown in Table 3.17. The first order and 3-D Ginstling-Brounshtein were the best fitting models for under both burning conditions. It can be said that contracting geometry models were also suitable to model-fitting kinetic approach for hazelnut shells, particularly in Region II. The highest activation energy was obtained from diffusional models; in contrast, the lowest one was calculated from Avrami-Erofeev model.

With respect to Region I under dry air burning, the calculated activation energy from first order was significantly lower than 3-D Ginstling-Brounshtein model at 44.23 kJ/mol and 84.52 kJ/mol, respectively. Furthermore, the frequency factors were at 7.85 s⁻¹ and 3040 s⁻¹, respectively.

The calculated activation energies under dry air burning condition were not quite as high as under pure oxygen for Region I. In contrast, the activation energies under dry air were slightly higher than pure oxygen burning conditions for Region II. For instance; the calculated activation energy from first order reaction kinetic model under dry air and pure oxygen for Region II were 81.87 kJ/mol and 79.86 kJ/mol, respectively.

Table 3.17 : The activation energies and frequency factors of hazelnut shells.

Reaction Model	f(α)	Dry Air						Pure Oxygen					
		R ²	Region I		Region II		R ²	Region I		Region II			
Reaction order			E _A (kJ/mol)	A (s ⁻¹)	R ²	E _A (kJ/mol)	A (s ⁻¹)	R ²	E _A (kJ/mol)	A (s ⁻¹)	R ²	E _A (kJ/mol)	A (s ⁻¹)
1 st order	(1- α) ⁿ	0.9947	44.23	7.85	0.8602	81.87	5272.21	0.9900	47.59	20.62	0.9379	79.86	5552.83
1/3 rd order	(1- α) ⁿ	0.9909	36.41	1.03	0.9564	18.96	0.01	0.9904	41.51	4.13	0.9773	16.79	0.008
1/2 nd order	(1- α) ⁿ	0.9924	38.27	1.67	0.9428	29.19	0.12	0.9905	42.98	6.10	0.9745	27.09	0.097
2/3 rd order	(1- α) ⁿ	0.9935	40.19	2.76	0.9219	42.62	2.16	0.9904	44.48	9.08	0.9650	40.65	1.89
2 nd order	(1- α) ⁿ	0.9932	57.89	251.14	0.7489	296.48	1x10 ²¹	0.9861	57.77	290.81	0.8834	291.74	1.6x10 ²¹
Diffusional													
1-D	1/2 α	0.9903	75.09	2628	0.9818	22.64	0.02	0.9918	86.31	4.6x10 ⁴	0.9706	18.37	0.0082
2-D	[-ln(1- α)] ⁻¹	0.9930	81.93	7214.84	0.9790	44.05	1.15	0.9921	91.85	9.5x10 ⁴	0.9867	39.22	0.58
3-D (Jander)	3/2(1- α) ^{2/3} [1-(1- α) ^{1/3}] ⁻¹	0.9949	89.72	1.1x10 ⁴	0.9380	96.93	1x10 ⁴	0.992	97.93	9.7x10 ⁴	0.9725	92.74	7764.73
3-D (Ginstling-Brounshtein)	3/2[(1- α) ^{-1/3} -1] ⁻¹	0.9938	84.52	3040	0.9687	59.44	6.08	0.9921	93.87	3.5x10 ⁴	0.9857	54.81	3.55
Contracting geometry													
Contracting area	(1- α) ^(1-1/n) ; n=2	0.9924	38.27	0.84	0.9428	29.19	0.06	0.9905	42.98	3.05	0.9745	27.09	0.048
Contracting volume	(1- α) ^(1-1/n) ; n=3	0.9935	40.19	0.92	0.9219	42.62	0.72	0.9904	44.48	3.03	0.9650	40.65	0.63
Nucleation													
Avrami-Erofeev	n(1- α)[-ln(1- α)] ^(1-1/n) ; n=2	0.9913	17.44	0.0152	0.8249	35.10	0.47	0.9854	19.31	0.03	0.9180	34.21	0.48
Avrami-Erofeev	n(1- α)[-ln(1- α)] ^(1-1/n) ; n=3	0.9834	8.52	0.0012	0.7673	19.50	0.02	0.9762	9.89	0.002	0.8869	18.99	0.02
Avrami-Erofeev	n(1- α)[-ln(1- α)] ^(1-1/n) ; n=4	0.9582	4.05	0.0002	0.6802	11.70	0.002	0.9538	5.17	0.0004	0.8350	11.38	0.002

The activation energies and frequency factors of torrefied hazelnut shells biochar at 300 °C under dry air and pure oxygen burning conditions were shown in Table 3.18. It can be said that all reaction models were suitable for Region I under dry air burning condition. In contrast, first order and 3-D Ginstling-Brounshtein models were the best reaction model approaches to Region II under dry air and Region I under pure oxygen conditions.

As regards dry air burning conditions, the activation energies were decreased dramatically from Region I to Region II. Take first order reaction model as an example. It decreased from 87.23 kJ/mol to 40.05 kJ/mol. Furthermore, the frequency factor declined from $3.6 \times 10^4 \text{ s}^{-1}$ to 1.04 s^{-1} . With respect to Region I under dry air and pure oxygen burning conditions, there was a considerable fall in activation energies, which meant reaction rates were slower under dry air than pure oxygen burning condition. For instances, the calculated activation energy from 3-D Ginstling-Brounshtein model under dry air and pure oxygen were at 176.75 kJ/mol and 67.71 kJ/mol, respectively.

The activation energies and frequency factors of carbonized hazelnut shells biochar at 600 °C under dry air and pure oxygen burning conditions were shown in Table 3.19. The first order and 3-D Ginstling-Brounshtein models were suitable kinetic approach for carbonized hazelnut shells biochar. The activation energies in Region I were significantly higher than Region II under dry air burning condition. For instance; the calculated activation energy from first order reaction model for Region I and Region II were 66.96 kJ/mol and 51.54, respectively. Furthermore, the frequency factor decreased from 283.12 s^{-1} in Region I to 8.03 s^{-1} in Region II. The lowest activation energies were calculated under pure oxygen burning condition. With respect to Region I under both conditions, the calculated activation energy from first order decreased from 66.96 kJ/mol to 14.89 kJ/mol.

Table 3.18 : The activation energies and frequency factors of torrefied hazelnut shells biochar at 300 °C.

Reaction Model	f(α)	Dry Air						Pure Oxygen		
		Region I			Region II			Region I		
		R ²	E _A (kJ/mol)	A (s ⁻¹)	R ²	E _A (kJ/mol)	A (s ⁻¹)	R ²	E _A (kJ/mol)	A (s ⁻¹)
Reaction order										
1 st order	(1- α) ⁿ	0.9972	87.23	3.6x10 ⁴	0.9637	40.05	1.04	0.9754	37.30	0.60
1/3 rd order	(1- α) ⁿ	0.9963	82.95	1.3x10 ⁴	0.9585	20.64	0.01	0.9626	27.12	0.05
1/2 nd order	(1- α) ⁿ	0.9966	84.01	1.7x10 ⁴	0.9611	24.88	0.03	0.9691	29.43	0.09
2/3 rd order	(1- α) ⁿ	0.9968	85.07	2.1x10 ⁴	0.9626	29.52	0.10	0.9733	31.90	0.16
2 nd order	(1- α) ⁿ	0.9981	93.92	1.7x10 ⁵	0.9620	81.55	5492.66	0.9503	57.21	61.15
Diffusional										
1-D	1/2 α	0.9963	171.20	4x10 ¹¹	0.9735	38.28	0.30	0.9624	56.49	9.48
2-D	[-ln(1- α)] ⁻¹	0.9968	175.33	5.2x10 ¹¹	0.9745	51.72	2.83	0.9736	64.41	29.89
3-D (Jander)	3/2(1- α) ^{2/3} [1-(1- α) ^{1/3}] ⁻¹	0.9972	179.59	3x10 ¹¹	0.9735	70.69	33.53	0.9805	74.44	65.29
3-D (Ginstling-Brounshtein)	3/2[(1- α) ^{-1/3} -1] ⁻¹	0.9969	176.75	1.6x10 ¹¹	0.9743	57.92	2.34	0.9768	67.71	14.13
Contracting geometry										
Contracting area	(1- α) ^(1-1/n) ; n=2	0.9966	84.01	8374.78	0.9611	24.88	0.02	0.9691	29.43	0.04
Contracting volume	(1- α) ^(1-1/n) ; n=3	0.9968	85.07	7166.47	0.9626	29.52	0.03	0.9733	31.90	0.05
Nucleation										
Avrami-Erofeev	n(1- α)[-ln(1- α)] ^(1-1/n) ; n=2	0.9964	38.89	1.61	0.9308	14.21	0.004	0.9541	13.33	0.003
Avrami-Erofeev	n(1- α)[-ln(1- α)] ^(1-1/n) ; n=3	0.9952	22.77	0.04	0.8250	5.59	0.0003	0.8838	5.34	0.0003
Avrami-Erofeev	n(1- α)[-ln(1- α)] ^(1-1/n) ; n=4	0.9934	14.72	0.01	0.3072	1.28	3.5x10 ⁻⁵	0.4612	1.34	3.7x10 ⁻⁵

Table 3.19 : The activation energies and frequency factors of carbonized hazelnut shells biochar at 600 °C.

Reaction Model	f(α)	Dry Air						Pure Oxygen		
		Region I			Region II			Region I		
Reaction order		R ²	E _A (kJ/mol)	A (s ⁻¹)	R ²	E _A (kJ/mol)	A (s ⁻¹)	R ²	E _A (kJ/mol)	A (s ⁻¹)
1 st order	(1- α) ⁿ	0.9878	66.96	283.12	0.9812	51.54	8.03	0.8678	14.89	0.006
1/3 rd order	(1- α) ⁿ	0.9851	63.72	130.80	0.9808	31.60	0.11	0.3772	1.88	5x10 ⁻⁵
1/2 nd order	(1- α) ⁿ	0.9858	64.52	158.31	0.9813	36.08	0.30	0.6889	4.53	0.0002
2/3 rd order	(1- α) ⁿ	0.9865	65.33	191.88	0.9815	40.89	0.86	0.7975	7.57	0.0007
2 nd order	(1- α) ⁿ	0.9911	72.03	942.26	0.9782	91.63	2.6x10 ⁴	0.9017	46.55	10.44
Diffusional										
1-D	1/2 α	0.9861	133.89	6.9x10 ⁷	0.9859	58.83	2.7x10 ⁴	0.8457	7.23	0.0003
2-D	[-ln(1- α)] ⁻¹	0.9873	137.02	7.1x10 ⁷	0.9863	73.76	141.28	0.9095	14.74	0.0017
3-D (Jander)	3/2(1- α) ^{2/3} [1-(1- α) ^{1/3}] ⁻¹	0.9885	140.26	3.3x10 ⁷	0.9857	93.40	1636.96	0.9247	27.15	0.0093
3-D (Ginstling-Brounshtein)	3/2[(1- α) ^{-1/3} -1] ⁻¹	0.9877	138.10	2x10 ⁷	0.9862	80.22	116.15	0.9177	18.71	0.0011
Contracting geometry										
Contracting area	(1- α) ^(1-1/n) ; n=2	0.9858	64.52	79.16	0.9813	36.08	0.15	0.6889	4.53	0.0001
Contracting volume	(1- α) ^(1-1/n) ; n=3	0.9865	65.33	63.96	0.9815	40.89	0.29	0.7975	7.57	0.0002
Nucleation										
Avrami-Erofeev	n(1- α)[-ln(1- α)] ^(1-1/n) ; n=2	0.9828	28.68	0.1188	0.9691	19.96	0.01	0.2045	1.44	4.7x10 ⁻⁵
Avrami-Erofeev	n(1- α)[-ln(1- α)] ^(1-1/n) ; n=3	0.9744	15.92	0.0065	0.9406	9.44	0.001	0.7284	n/a	n/a
Avrami-Erofeev	n(1- α)[-ln(1- α)] ^(1-1/n) ; n=4	0.9591	9.53	0.0012	0.8467	4.17	0.0002	0.9376	n/a	n/a

n/a: not available

All things considered, the first order and 3-D Ginstling-Brounshtein kinetic model approaches were the most convenient reaction models for almost all samples. According to Hashimoto et al. [81], first order reaction model is suitable for most of the types of biomass, which also demonstrated in this kinetic study. Moreover, the highest activation energy was calculated from 3-D Ginstling-Brounshtein model among all reaction models due to the some difficulties during diffusion and mass transfers.

The contracting geometry reaction models were also convenient for torrefied, carbonized biochars and untreated biomass samples. Because, the structure shrank due to removal of volatile matters, particularly in Region I. Moreover, burning of biochar which started from surface led to smaller size of particle in Region II.

4. CONCLUSION AND RECOMMENDATIONS

- The main ingredients in biomass are hemicellulose, cellulose and lignin that have varying ratios depending on the structure of biomass. According to macromolecular components analysis, sunflower seed shells had the high holocellulose content, which is the sum of hemicellulose and cellulose composition in biomass, and relatively low lignin content. On the other hand, hazelnut shells had relatively lower content of holocellulose, but higher lignin content in comparison to sunflower seed shells.
- Fixed carbon to volatile matters ratios of both samples were lower than those given for typical coal samples in literatures. That is compatible with Van Krevelen diagram for various solid fuels in Figure 1.2.
- The ratio of macromolecular components found in biomass sample affected the thermal characteristics of biomass species. That is, holocellulose is more reactive compound than lignin; therefore, sunflower seed shells sample showed more thermally reactive characteristic under burning conditions.
- The HHV of produced biochars tended to increase with rising temperature applied during biochar production. The increase in calorific value was very clearly in case of sunflower seed shells samples due to the efficient removal of volatile matters.
- The fuel quality was increased via thermal treatments which increased carbon content and decreased oxygen content in biomass. Furthermore, torrefaction and carbonization led to decline in moisture and volatile matters; along with considerable increases in carbon, fixed carbon and calorific value of biomass.
- With respect to DTA and DSC profiles, it can be mentioned that volatile matters firstly devolatilized and subsequently burned in first region. After burning of volatiles, the biomass turned gradually into porous solid structure to which oxygen diffused to burn it by surface oxidation in a temperature range of second region. Moreover, after end point there was a small region which

meant the decomposition of the ash forming minerals and their phase transitions.

- The rates of the mass losses in the volatile matter transformation and homogenous combustion regions increased considerably under pure oxygen burning condition in comparison to dry air due to the having more reactive characteristics.
- There was a considerable increase in R_{\max} and $\Delta T_{R_{\max}}$ values of both sunflower seed shells and hazelnut shells in case of pure oxygen burning condition. That is to say; the more intensive heat was produced under pure oxygen compared to dry air. This is mainly due to the increase of thermal reactivity during burning with pure oxygen.
- Regarding main samples, the first decomposition region turned into sharp peak under pure oxygen burning which indicates the rapid burning of the volatile matters.
- Some of the volatile matters had been removed during torrefaction; therefore, remained volatiles in biomass were eliminated at higher temperatures in comparison to untreated biomass samples.
- Concerning torrefaction process, it can be obviously said that the extent of R_{\max} data increased, and shifted to the higher temperatures.
- After torrefaction, homogenous reaction was limited due to a dramatic decline in volatile matter content, particularly in sunflower seed shells sample. As a consequence, the burning of torrefied biochar was represented by a sharp peak, and onset and end points shifted to the lower temperatures.
- The highest R_{\max} and $\Delta T_{R_{\max}}$ data were obtained from carbonized sunflower seed shells with pure oxygen burning. In other words; it had the highest calorific value.
- With respect to particle analysis results, holocellulose had the highest specific surface area; whereas, lignin had the smallest which is in good agreement with the low thermal reactivity characteristics. On the other hand, a general trend could not be determined for torrefied and carbonized samples.
- Regarding SEM analysis results, it can be said that holocellulose had cylindrical structure; while, lignin has amorphous shape. Furthermore, some bright regions were available in the torrefied and carbonized samples, which

resulted from inorganic contents. In other words; thermal treatments make the ash forming minerals relatively more concentrated.

- Concerning XRD analysis results, there was a considerable amount of silicon oxides in the forms of silicon dioxide, cristobalite and chbazite in both main samples and their derivatives. It demonstrates that mineral matters are mainly composed of silicon oxides. Furthermore, carbon masks the inorganic substances; therefore, it is difficult to determine mineral phases in torrefied and carbonized samples, particularly in sunflower seed shells.
- The main sample of hazelnut shells contained potassium sulfide leading to problematic depositions such as slagging and fouling in commercial biomass combustion systems. As a consequence, some precautions should be taken and suitable combustion process should be chosen in case of using this material as a biomass source.
- With respect to FTIR analysis results, C-O-C and C-H bond intensities decreased considerably due to the thermal treatments, which demonstrates a decline in oxygen and hydrogen contents in sunflower seed shells samples. On the other hand, intensity of C=C band increased due to the increasing carbon content.
- The holocellulose in hazelnut shells had C-O-C bands due to containing weak ether bonds, which have higher thermal reactivity characteristic. Furthermore, bands below 500 cm^{-1} show minerals which became more apparent in hazelnut shells in comparison to sunflower seed shells due to high ash content.
- It can be obviously said that the temperature of torrefaction and carbonization did not suffice for hazelnut shells to improve the carbon content. Accordingly, the intensity of C=C bands did not increase in torrefied and carbonized samples.
- As regards biomass kinetic analysis result, homogenous burning and pyrolysis took place in Region I for all samples. After pyrolysis, char burning and heterogeneous reaction accounted for Region II in both burning conditions.
- It can be said that first order and 3-D Ginstling-Brounshtein were the most convenient reaction models for almost all samples. The activation energy was calculated higher from 3-D Ginstling-Brounshtein in comparison to first order

reaction model. Since, there were some difficulties in diffusion and mass transfers resulted in a much more energy requirement.

- Moreover, contracting geometry models were also fitted well for both biomass samples due to shrinking structure in Region I and making into smaller particles during burning of biochar in Region II.
- The activation energy increased in torrefied and carbonized samples in comparison to untreated samples due to the high amount of carbon composition.
- As regards sunflower seed shells, calculated activation energy from pure oxygen burning condition was higher than dry air. In contrast, the lowest activation energies were calculated from pure oxygen burning condition for torrefied and carbonized samples. This may be explained by the fact that these samples had higher ash content in comparison to main sample resulted in a high reactivity characteristic. In other words, inorganics may play catalytic or inhibiting role during the thermal processes that affect the activation energy. On the other hand, this trend could not be applied to hazelnut shells samples.
- The performed treatments were not enough for hazelnut shells; therefore, higher temperatures should be taken into account during the thermal treatment of this material. However, in that case loss of the organic part owing to severe conditions will be inevitable. Alternatively, a new reactor configuration that provides rapid heating can be tried. In this way, the desired level of devolatilization may be provided without causing serious losses in the calorific value of biomass.

REFERENCES

- [1] **World Energy Council**, 2013. World energy resources, 2013 survey. Retrieved on 24th February 2014 from http://www.worldenergy.org/wp-content/uploads/2013/09/Complete_WER_2013_Survey.pdf
- [2] **Sieminski, A.**, 2013. International energy outlook 2013, U.S. energy Information Administration. Retrieved on 24th February 2014 from http://www.eia.gov/pressroom/presentations/sieminski_07252013.pdf.
- [3] **Vakkilainen, E., Kuparinen, K. and Heinimö, J.**, 2013. Large industrial users of biomass, IEA Bioenergy Task 40: Sustainable Bioenergy Trade.
- [4] **Müller, S., Marmion, A. and Beerepoot, M.**, 2011. IEA Renewable energy markets and prospects by region. Retrieved on 24th February 2014 from http://www.iea.org/publications/freepublications/publication/Renew_Regions.pdf.
- [5] **McKendry, P.**, 2002. Energy production from biomass (part 1): overview of biomass, *Bioresource Technology*, **83**, 37–46.
- [6] **The United Nations Framework Convention on Climate Change (UNFCCC)**, 2005. Grid-connected electricity generation using biomass from newly developed dedicated plantations, approved baseline and monitoring methodology AM0042. Retrieved on 24th February 2014 from http://cdm.unfccc.int/EB/027/eb27_repan03.pdf.
- [7] **Mishra, S.R.**, 2004. Photosynthesis in Plants, Discovery Publishing House, India, New Delhi.
- [8] **Klass, D.L.**, 1998. Biomass for Renewable Energy, Fuels and Chemicals, Academic Press, California.
- [9] **Ali, M.**, 2013. Climate Change Impact on Plant Biomass Growth, Springer, New York.
- [10] **Basu, P.**, 2013. Biomass, Gasification, Pyrolysis and Torrefaction Practical Design and Theory, Elsevier, San Diego.
- [11] **Koçar, G. and Civaş, N.**, 2013. An overview of biofuels from energy crops: Current status and future prospects, *Renewable and Sustainable Energy Reviews*, **28**, 900–916.
- [12] **Chartier, P., Beenackers, A.A.C.M. and Grassi, G.**, 1995. Biomass for Energy Environment Agriculture and Industry, Volume 1 8th E.C. Conference, Commission of the European Communities, Elsevier, Vienna.
- [13] **Strezow, V., Evans, T.J. and Nelson, P.F.**, 2006. Biomass and Bioenergy: New Research. In Brenes, M.D. (Ed.), *Carbonization of biomass fuels* (pp. 91-123). Nova Science Publishers Inc., New York.

- [14] **McKendry, P.**, 2002. Energy production from biomass (part 2): Conversion technologies, *Bioresource Technology*, **83**, 47–54.
- [15] **Nordin, A., Pommer, L., Nordwaeger, M. and Olofsson, I.**, 2013. Technologies for Converting Biomass to Useful Energy Combustion, Gasification, Pyrolysis, Torrefaction and Fermentation. In Dahlquist, E. (Ed.), *Biomass conversion through torrefaction* (pp. 217-240). CRC Press, London.
- [16] **Jenkins, B.M., Baxter, L.L., Miles Jr., T.R. and Miles, T.R.**, 1998. Combustion properties of biomass, *Fuel Processing Technology*, **54**, 17–46.
- [17] **White, L.P. and Plaskett, L.G.**, 1981. Biomass as Fuel, Academic Press Inc., London.
- [18] **Ryu, C., Yang, Y.B., Khor, A., Yates, N.E., Sharifi, V.N. and Swithenbank J.**, 2006. Effect of fuel properties on biomass combustion: Part I. Experiments—fuel type, equivalence ratio and particle size, *Fuel*, **85**, 1039–1046.
- [19] **Du, S., Yang, H., Qian, K., Wang, X. and Chen, H.**, 2014. Fusion and transformation properties of the inorganic components in biomass ash, *Fuel*, **117**, 1281-1287.
- [20] **Huber, G.W., Iborra, S. and Corma, A.**, 2006. Synthesis of transportation fuels from biomass: chemistry, catalysts, and engineering, *Chemical Reviews*, **106**, 4044–4098.
- [21] **Kamide, K.**, 2005. Cellulose and Cellulose Derivatives Molecular Characterization and its Applications, Elsevier, Amsterdam.
- [22] **French, A.D.**, 2012. Combining computational chemistry and crystallography for a better understanding of the structure of cellulose. In Horton, D. (Ed.) *Advances in Carbohydrate Chemistry and Biochemistry* (Vol. 67, pp. 1-277). Elsevier, San Diego.
- [23] **Krässig, H.A.**, 1993. Cellulose Structure, Accessibility and Reactivity, Gordon and Breach Science Publishers, Amsterdam.
- [24] **Sengupta, D. and Pike, R.W.**, 2013. Chemicals from Biomass Integrating Bioprocesses into Chemical Production Complexes for Sustainable Development, CRC Press Taylor, Florida.
- [25] **Hon, D.N.S.**, 1996. Chemical Modification of Lignocellulosic Materials, Marcel Dekker, Inc., New York.
- [26] **Castro-Montaya, A. J. and Jimenez-Gutierrez, A.**, 2013. Integrated Biorefineries Design, Analysis, and Optimization. In Stuart, P.R. and El-Halwagi, M.M. (Eds.), *Lignocellulosic biomass: A raw material for the future* (pp. 461-468). CRC Press, Florida.
- [27] **Lestander, T.A.**, 2013. Biomass as Energy Source Resources, Systems and Applications. In Dahlquist, E. (Ed.), *Chemical composition of biomass* (pp. 35-56). CRC Press, Leiden.
- [28] **Pinto, P.C.R., da Silva, E.A.B. and Rodrigues, A.E.**, 2012. Biomass Conversion The Interface of Biotechnology, Chemistry and Materials Science. In Baskar, C., Baskar, S. and Dhillon, R.S. (Eds.), *Lignin as source of fine*

chemicals: vanillin and syringaldehyde (pp. 381-412). Springer-Verlag, Berlin, Heidelberg.

- [29] Whetten, R. and Sederoff, R., 1995. Lignin Biosynthesis, *The Plant Cell*, **7**, 1001-1013.
- [30] Boerjan, W., Ralph, J. and Baucher, M., 2003. Lignin biosynthesis, *Annual Review of Plant Biology*, **54**, 519-46.
- [31] Türkiye Elektrik Üretim İletim İstatistikleri (TEİAŞ), 2012. Electricity generation and shares by energy resources. Retrieved on 23rd March 2014 from
http://www.tuik.gov.tr/PreIstatistikTablo.do?istab_id=1578.
- [32] TMMOB Elektrik Mühendisleri Odası, 2014. Türkiye elektrik enerjisi istatistikleri. Retrieved on 23rd March 2014 from
http://www.emo.org.tr/genel/bizden_detay.php?kod=88369.
- [33] Benli, H., 2013. Potential of renewable energy in electrical energy production and sustainable energy development of Turkey: Performance and policies, *Renewable Energy*, **50**, 33-46.
- [34] Toklu, E., 2013. Overview of potential and utilization of renewable energy sources in Turkey, *Renewable Energy*, **50**, 456-463.
- [35] Türkyılmaz, O., 2013. Turkey Energy Outlook April 2013, E-World ICCI 2013 Istanbul. Retrieved on 23rd March 2014 from
http://www.icci.com.tr/2013/sunumlar/OT10_OT10_Oguz_Turkyilmaz.pdf.
- [36] Kotcioğlu, I., 2011. Clean and sustainable energy policies in Turkey, *Renewable and Sustainable Energy Reviews*, **15**, 5111-5119.
- [37] Biyokütle Enerjisi Santralleri Yatırımcıları Derneği (BESYAD), 2009. Biyokütle enerjisi. Retrieved on 23rd February 2014 from
<http://web.ogm.gov.tr/diger/iklim/Dokumanlar/Biyoenerji%20%C3%87al%C4%B1%C5%9Ftay%C4%B1/CalistaySunumlari/Selahattin%20Baysal-BESYAD.pdf>.
- [38] Doğu Karadeniz Kalkınma Ajansı (DOKA), 2013. Fındık Kabuğu, Cürufu, *DOKA Bülten*, **16**, p. 72. Retrieved on 24th February 2014 from
<http://www.doka.org.tr/files/yayin/bulten16/HTML/index.html#/72/zomed>.
- [39] Enerji Piyasası Düzenleme Kurulu (EPDK), 2012. Elektrik piyasası sektör raporu 2011. Retrieved on 23rd February 2014 from
http://www.epdk.gov.tr/documents/elektrik/rapor_yayin/ElektrikPiyasasiRaporu2011.pdf.
- [40] Koç, E. and Şenel, M.C., 2013. Dünyada ve Türkiye’de genel enerji durumu – genel değerlendirme, *Mühendis ve Makina*, **54(639)**, 32-44.
- [41] Karkania, V., Fanara, E. and Zabaniotou, A., 2012. Review of sustainable biomass pellets production - A study for agricultural residues pellets’ market in Greece, *Renewable and Sustainable Energy Reviews*, **16**, 1426- 1436.

- [42] **Richard, T.L., Brownell, D., Ruamsook, K., Liu, J. and Thomchick, E.**, 2012. Handbook of Bioenergy Crop Plants. In Kole, C., Joshi, C.P. and Shonnard, D.R. (Eds.), *Biomass harvest and logistics* (pp. 119-132). CRC Press, Florida.
- [43] **Arshadi, M. and Sellstedt, A.** 2008. Introduction to Chemicals From Biomass. In Clark, J. and Deswarte, F. (Eds.), *Production of energy from biomass*, John Wiley & Sons, Ltd., the UK.
- [44] **Stelte, W., Holm, J.K., Sanadi, A.R., Barsberg, S., Ahrenfeldt, J. and Henriksen, U.B.**, 2011. Fuel pellets from biomass: The importance of the pelletizing pressure and its dependency on the processing conditions, *Fuel*, **90**, 3285–3290.
- [45] **Liu, Z., Quek, A. and Balasubramanian, R.**, 2014. Preparation and characterization of fuel pellets from woody biomass, agro-residues and their corresponding hydrochars, *Applied Energy*, **113**, 1315-1322.
- [46] **Duncan, A., Pollard, A. and Fellouah, H.**, 2013. Torrefied, spherical biomass pellets through the use of experimental design, *Applied Energy*, **101**, 237–243.
- [47] **Wang, C., Peng, J., Li, H., Bi, X.T., Legros, R., Lim, C.J. and Sokhansanj, S.**, 2013. Oxidative torrefaction of biomass residues and densification of torrefied sawdust to pellets, *Bioresource Technology*, **127**, 318–325.
- [48] **Pirraglia, A., Gonzalez, R., Saloni, D. and Denig, J.**, 2013. Technical and economic assessment for the production of torrefied ligno-cellulosic biomass pellets in the US, *Energy Conversion and Management*, **66**, 153-164.
- [49] **Luk, H.T., Lam, T.Y.G., Oyedun, A.O., Gebreegziabher, T and Hui, C.W.**, 2013. Drying of biomass for power generation: A case study on power generation from empty fruit bunch, *Energy*, **63**, 205-215.
- [50] **Mahmoud, A., Arlabosse, P. and Fernandez, A.**, 2011. Application of a thermally assisted mechanical dewatering process to biomass, *Biomass and Bioenergy*, **35**, 288-297.
- [51] **Kaliyan, N.**, 2008. Densification of Biomass, ProQuest LLC, Michigan.
- [52] **Fagernäs, L., Brammer, J., Wilen, C., Lauer, M. and Verhoeff, F.**, 2010. Drying of biomass for second generation synfuel production, *Biomass and Bioenergy*, **34**, 1267-1277.
- [53] **Roos, C.J.**, 2008. Biomass drying and dewatering for clean heat & power. Retrieved on 23rd February 2014 from <http://www.northwestchptap.org/NwChpDocs/BiomassDryingAndDewateringForCleanHeatAndPower.pdf>.
- [54] **Arlabosse, P., Blanc, M., Kerfai, S. and Fernandez, A.**, 2011. Production of green juice with an intensive thermo-mechanical fractionation process. Part I: Effects of processing conditions on the dewatering kinetics, *Chemical Engineering Journal*, **168**, 586–592.
- [55] **Van der Stelt, M.J.C., Gerhauser, H., Kiel, J.H.A. and Ptasinski, K.J.**, 2011. Biomass upgrading by torrefaction for the production of biofuels: A review, *Biomass and Bioenergy*, **35**, 3748-3762.

- [56] **Chen, Y., Yang, H., Yang, Q., Hao, E., Zhu, B. and Chen, H.**, 2014. Torrefaction of agriculture straws and its application on biomass pyrolysis poly-generation, *Bioresource Technology*, **156**, 70-77.
- [57] **Tran, K.Q., Luo, X., Seisenbaeva, G. and Jirjis, R.**, 2013. Stump torrefaction for bioenergy application, *Applied Energy*, **112**, 539-546.
- [58] **Batidzirai, B., Mignot, A.P.R., Schakel, W.B., Junginger, H.M. and Faaij, A.P.C.**, 2013. Biomass torrefaction technology: Techno-economic status and future prospects, *Energy*, **62**, 196-214.
- [59] **Sarvaramini, A., Assima, G.P., Beaudoin, G. and Larachi, F.**, 2014. Biomass torrefaction and CO₂ capture using mining wastes – A new approach for reducing greenhouse gas emissions of co-firing plants, *Fuel*, **115**, 749-757.
- [60] **Kurchania, A.K.**, 2012. Biomass Conversion The Interface of Biotechnology, Chemistry and Materials Science. In Baskar, C., Baskar, S. and Dhillon R.S. (Eds.), *Biomass energy* (pp. 91-122), Springer-Verlag, Berlin Heidelberg.
- [61] **Chen, W.H., Cheng, W.Y., Lu, K.M. and huang, Y.P.**, 2011. An evaluation on improvement of pulverized biomass property for solid fuel through torrefaction, *Applied Energy*, **88**, 3636-3644.
- [62] **Sarvaramini, A. and Larachi, F.**, 2014. Integrated biomass torrefaction – Chemical looping combustion as a method to recover torrefaction volatiles energy, *Fuel*, **116**, 158–167.
- [63] **Koppejan, J., Sokhansanj, S., Melin, S. and Madrali, S.**, 2012. IEA Bioenergy Task 32 report Final Report, Status overview of torrefaction technologies. Retrieved on 4th March 2014 from http://www.ieabcc.nl/publications/IEA_Bioenergy_T32_Torrefaction_review.pdf.
- [64] **Sarvaramini, A., Assima, G.P. and Larachi, F.**, 2013. Dry torrefaction of biomass–Torrefied products and torrefaction kinetics using the distributed activation energy model, *Chemical Engineering Journal*, **229**, 498-507.
- [65] **Laird, D.A., Brown, R.C., Amonette, J.E. and Lehmann, J.**, 2009. Review of the pyrolysis platform for coproducing bio-oil and biochar, *Biofuels, Bioproducts & Biorefining*, **3**, 547-562.
- [66] **Bridgwater, A.V. and Bridge, S.A.**, 1991. Biomass Pyrolysis Liquids Upgrading and Utilization. In Bridgwater A.V. and Grassi, G. (Eds.), *A Review of Biomass Pyrolysis and Pyrolysis Technologies* (pp. 11-92). Elsevier Science Publishers LTD, London.
- [67] **Udomsirichakorn, J. and Salam, P.A.**, 2014. Review of hydrogen-enriched gas production from steam gasification of biomass: The prospect of CaO-based chemical looping gasification, *Renewable and Sustainable Energy Reviews*, **30**, 565–579.
- [68] **Higman, C. and van der Burgt, M.**, 2008. Gasification, 2nd Edition, Elsevier, Oxford.

- [69] Emami-Taba, L., Irfan, M.F., Daud, W.M.A.W. and Chakrabarti, H., 2013. Fuel blending effects on the co-gasification of coal and biomass - A review, *Biomass and Bioenergy*, **57**, 249-263.
- [70] Bocci, E., Sisinni, M., Moneti, M., Vecchione, L., Di Carlo, A. and Villarini, M., 2014. State of art of small scale biomass gasification power systems: a review of the different typologies, *Energy Procedia*, **45**, 247–256.
- [71] Nzihou, A., Stanmore, B. and Sharrock, P., 2013. A review of catalysts for the gasification of biomass char, with some reference to coal, *Energy*, **58**, 305-317.
- [72] Strezov, V., Patterson, M., Zymła, V., Fisher, K., Evans, T.J. and Nelson, P.F., 2007. Fundamental aspects of biomass carbonization, *Journal of Analytical and Applied Pyrolysis*, **79**, 91-100.
- [73] Katyal, S., Thambimuthu, K. and Valix, M., 2013. Carbonisation of bagasse in a fixed bed reactor: influence of process variables on char yield and characteristics, *Renewable Energy*, **28**, 713-725.
- [74] Pelaez-Samaniego, M.R., Garcia-Perez, M., Cortez, L.B., Rosillo-Calle, F. and Mesa, J., 2008. Improvements of Brazilian carbonization industry as part of the creation of a global biomass economy, *Renewable and Sustainable Energy Reviews*, **12**, 1063-1086.
- [75] Xiao, L.P., Shi, Z.J., Xu, F. and Sun, R.C., 2012. Hydrothermal carbonization of lignocellulosic biomass, *Bioresource Technology*, **118**, 619-623.
- [76] Wiedner, K., Rumpel, C., Steiner, C., Pozzi, A., Maas, R. and Glaser, B., 2013. Chemical evaluation of chars produced by thermochemical conversion (gasification, pyrolysis and hydrothermal carbonization) of agro-industrial biomass on a commercial scale, *Biomass and Bioenergy*, **59**, 264-278.
- [77] Liou, T.H., 2004. Evolution of chemistry and morphology during the carbonization and combustion of rice husk, *Carbon*, **42**, 785-794.
- [78] Park, S.W., Jang, C.H., Baek, K.R. and Yang, J.K., 2012. Torrefaction and low-temperature carbonization of woody biomass: Evaluation of fuel characteristics of the products, *Energy*, **45**, 676-685.
- [79] Cao, J., Xiao, G., Xu, X., Shen, D. and Jin, B., 2013. Study on carbonization of lignin by TG-FTIR and high-temperature carbonization reactor, *Fuel Processing Technology*, **106**, 41-47.
- [80] Damartzis, T., Vamvuka, V., Sfakiotakis, S. and Zabaniotou, A., 2011. Thermal degradation studies and kinetic modeling of cardoon (*Cynara cardunculus*) pyrolysis using thermogravimetric analysis (TGA), *Bioresource Technology*, **102**, 6230-6238.
- [81] Hashimoto, K., Hasegawa, I., Hayashi, J. and Mae, K., 2011. Correlations of kinetic parameters in biomass pyrolysis with solid residue yield and lignin content, *Fuel*, **90**, 104-112.
- [82] Anca-Couce, A., Berger, A. and Zobel, N., 2014. How to determine consistent biomass pyrolysis kinetics in a parallel reaction scheme, *Fuel*, **123**, 230-240.

- [83] White, J.E., Catallo, W.J. and Legendre, B.L., 2011. Biomass pyrolysis kinetics: A comparative critical review with relevant agricultural residue case studies, *Journal of Analytical and Applied Pyrolysis*, **91**, 1-33.
- [84] Meriçboyu, A., 1992. Sorbent kalsinasyon ve sülfatasyon kinetiğinin incelenmesi, *PhD Thesis*, Istanbul Technical University Institute of Science, Engineering and Technology, Istanbul.
- [85] Ceylan, S. and Topçu, Y., 2014. Pyrolysis kinetics of hazelnut husk using thermogravimetric analysis, *Bioresource Technology*, **156**, 182-188.
- [86] Coats, A.W., Redfern, J.P., 1964. Kinetic parameters from thermogravimetric data, *Nature*, **201**, p.68.
- [87] ASTM-D 1105, 1984. Preparation of Extractive-Free Wood, *Annual Book of ASTM Standards*.
- [88] ASTM D1104-56, 1978 Method of Test for Holocellulose in Wood (Withdrawn 1985).
- [89] Soest, V.P.J., 1963. Use of Detergents in the Analysis of Fibrous Feeds, A Rapid Method for the Determination of Fiber and Lignin, *Journal of A.O.A.C*, Cornell University Press, Ithaca.
- [90] Meszaros, E., Jakab, E. and Vargehyi, G., 2007. TG/MS, Py-GC/MS and THM-GC/MS study of the composition and thermal behavior of extractive components of *Robinia pseudoacacia*, *Journal of Analytical and Applied Pyrolysis*, **79**, 61-70.
- [91] Zhu, Q., Jones, J.M., Williams, A., Thomas, K.M., 1999. The predictions of coal/char combustion rate using an artificial neural network approach, *Fuel*, **78**, 1755-1762.
- [92] Xiao, R., Chen, X., Wang, F. and Yu, G., 2011. The physicochemical properties of different biomass ashes at different ashing temperature, *Renewable Energy*, **36**, 244-249.
- [93] Sharma, R.K., Wooten, J.B., Baliga, V.L. and Hajaligol, M.R., 2001. Characterization of chars from biomass-derived materials: pectin chars, *Fuel*, **80**, 1825-1836.
- [94] El-Hendawy, A.N.A., 2006. Variation in the FTIR spectra of a biomass under impregnation, carbonization and oxidation conditions, *Journal of Analytical and Applied Pyrolysis*, **75**, 159-166.
- [95] Fu, P., Hu, S., Xiang, J., Li, P., Huang, D., Jiang, L., Zhang, A. and Zhang, J., 2010. FTIR study of pyrolysis products evolving from typical agricultural residues, *Journal of Analytical and Applied Pyrolysis*, **88**, 117-123.
- [96] Moore, J.W., Stanitski, C.L. and Jurs, P.C., 2010. Principles of Chemistry: The Molecular Science, Brooks/Cole, USA, California.

CURRICULUM VITAE



Name Surname: Ezgi BİLGİÇ

Place and Date of Birth: Istanbul / 28.02.1989

Address: Beylikduzu / Istanbul

E-Mail: bilgic.ezgi@gmail.com

B.Sc.: Istanbul Technical University – Chemical Engineering

Istanbul Technical University – Molecular Biology and Genetics

(Double Major B.Sc.)

M.Sc.: Istanbul Technical University – Chemical Engineering